Intra and Intermolecular Interactions of K-Ras4B: From Structure to Function

BY

TANMAY SANJEEV CHAVAN
Bachelor of Pharmacy, University of Pune, 2010

THESIS

Submitted as a partial fulfillment of the requirements for the degree of Doctor of Philosophy in Medicinal Chemistry in the Graduate College of the University of Illinois at Chicago, 2014

Chicago, Illinois

Defense Committee:

Vadim Gaponenko, Chair and Advisor

Bernard D. Santarsiero

Douglas D. Thomas

Michael E. Johnson

R. John Solaro, Physiology and Biophysics

ACKNOWLEDGEMENTS

The most important person for the successful completion of my research studies is my advisor, Dr Vadim Gaponenko. Despite having minimum experience in the field of protein chemistry, Vadim accepted me as a student and mentored me. He has been the biggest source of motivation and inspiration throughout my graduate studies and I thank him for everything.

I would like to thank my committee members: Dr. Michael Johnson, Dr. Bernard Santarsiero, Dr. Douglas Thomas and Dr. John Solaro, all of whom have played crucial roles in helping me in my scientific endeavor.

I would also like to thank our collaborators from NIH: Dr Nadya Tarasova and Dr Ruth Nussinov. Nadya and Ruth have helped develop my project by contributing their binding experiments and computational studies.

I am indebted to the past and current lab members of the Gaponenko Lab. Sherwin Abraham worked extensively on the project before me to establish many of the basic protocols. Erika Guerrero helped me learn many of the biochemical techniques and protein purification procedures. Youngshim Lee taught me NMR and fluorescence spectroscopy. Sherwin, Erika and Youngshim have helped me immensely and I will always be grateful to them. I thank Otto Meyer, Malgorzata Dobosz-Bartoszek, Luke Chisholm and Finn Mannerings for their help at various stages of my project. I also thank Boris Garnier and Ben Hitchinson who have helped me with insightful discussions and constructive criticism. They have greatly improved my presentation skills and critical thinking ability. All of these people have not just been helpful lab mates but also amazing friends throughout my grad school journey.

I thank Dr Ben Ramirez and Dr Gerd Prehna who have taken great care of the Structural Biology Centre where I did many of my experiments. I also thank Dr Bob Lee's lab from the UIC Research Resources Centre who have provided us with peptides and carried out mass spec for us. Many thanks to the Gettins and Simonovic Labs for sharing equipment and reagents.

Dr Sanjay Kshirsagar and Dr Santosh Gandhi, my mentors from India, have helped lay the foundations of my career in science and I will always be grateful to them.

There are numerous friends from the US and India whose names would be impossible to list here without unintentional omissions. Undoubtedly, they have helped me shape into the person I am today and I will forever be indebted to them.

Last, but definitely not the least, I would like to express my gratitude to my parents and all my family members who have stood by me through the ups and downs in life. It is impossible to put in words all the things they have done for me.

TSC

CONTRIBUTION OF AUTHORS

Chapter 1 is an introduction that helps in understanding of the subsequent chapters and highlights the importance of the research carried out by me. Chapter 2 is an unpublished (but submitted) work carried out in collaboration with Dr Tarasova's and Dr Nussinov's group from NIH. Our lab was the main driver of this research study. Dr Tarasova's group performed binding experiments (Figures 2.3 and 2.4). Dr Nussinov's group performed the molecular dynamics simulations (Figures 2.6, 2.7 and 2.8). My experiments provide the strongest empirical evidence for the conclusions mentioned in the chapter. Chapter 3 is a published manuscript (Chavan TS, Abraham S, & Gaponenko V (2013) ; *Molecules* 18(6):7103-7119) of which I am the primary author. All the experiments were performed by myself. Sherwin Abraham generated Figure 3.4A and wrote a small section of the manuscript. My advisor, Dr. Gaponenko and I are responsible for writing this paper. Chapter 4 is an unpublished (but submitted) review written entirely by myself and my advisor. Chapter 5 is also an unpublished (but submitted) work carried out in collaboration with the same collaborators from NIH. Dr Tarasova's group generated Figures 5.1 and 5.3, Dr Nussinov's group generated Figures 5.2 and 5.5. The experiments carried out by me are the most crucial in this study since the data points directly to the dimer interface which is also the basis for the MD simulation-based predictions. Chapter 6 is a manuscript published as a book chapter (Chavan TS, Meyer JO, Chisholm L, Dobosz-Bartoszek M, & Gaponenko V (2014); *Methods in molecular biology* 1120:19-32). James Meyer generated Figure 6.3. Others have helped in optimizing the protein purification procedure. Myself and James Meyer were responsible for writing the manuscript.

TABLE OF CONTENTS

TABLE OF CONTENTS (continued)

TABLE OF CONTENTS (continued)

LIST OF FIGURES

LIST OF FIGURES (Continued)

LIST OF FIGURES (Continued)

LIST OF TABLES

LIST OF ABBREVIATIONS

Error! Not a valid link.

SUMMARY

Ras proteins are small GTPases that act as signal transducers between cell surface receptors and intracellular signaling cascades. According to the existing paradigm, Ras proteins get activated upon growth factor stimulation of tyrosine kinase receptors which recruit GRB2-SOS complex to the membrane. SOS activates Ras by converting it to Ras-GTP. Ras-GTP binds several downstream effectors that are responsible for activation of multiple cellular processes.

Ras proteins consist of four isoforms – H-Ras, N-Ras, K-Ras4A and K-Ras4B. They contain highly homologous catalytic domains, and flexible C-terminal hypervariable regions (HVRs) that differ across Ras isoforms. All the important post-translational modifications occur on the HVR. Since Ras proteins have an almost identical catalytic domain, the HVR is thought to functionally distinguish the Ras isoforms. Ras is mutated in 30% of human tumors. Amongst them, K-Ras4B is most frequently mutated isoform. In my thesis I focus on identifying unique structural features of K-Ras4B that can be explored for development of isoform specific inhibitors of Ras. I investigate how the HVR of K-Ras4B regulates its activity through intra and intermolecular interactions, how it establishes specific protein-protein binding, and how K-Ras dimerization occurs.

Structurally, K-Ras4B has a unique HVR which contains a polylysine patch and only one lipid modification unlike other Ras isoforms. We examined the role of the HVR in the structure of full-length K-Ras4B and how it modulates the protein function. We found that the HVR impacts the catalytic domain of K-Ras4B-GDP by interacting with the Switch I and effector binding region. The interaction is almost 100-fold tighter with the GDP-bound than the GTP-bound protein. HVR binding interferes with Ras-Raf interaction and membrane binding. The data

indicate that contrary to previously suggested models of K-Ras4B signaling, HVR plays essential roles in regulation of K-Ras4B signaling.

Thereafter, we show that GTP-bound, but not GDP-bound K-Ras4B, a highly oncogenic splice variant of the K-Ras isoform, can form stable homodimers. We observe two dimer interfaces. Remarkably, a highly populated dimer interface is at the Switch I and effector binding regions overlapping Raf's, and additional effectors' binding surfaces; a second interface overlaps other effectors' binding site. Raf's activation requires side-to-side dimerization. Our results reveal how GTP-bound monomers can simultaneously dimerize and interact with Raf, thereby unveiling Raf's regulation. The unexpected nucleotide-dependent dimerization modes can resolve nanoclustering and cluster reorganization concomitant with Raf's activation.

CaM binds specifically to K-Ras4B of all the other Ras proteins and influences its downstream activity in a calcium dependent manner. We recently identified the HVR domain as the site responsible for binding affinity and specificity of CaM to K-Ras4B. In order to study a more relevant binding we introduced post-translational modifications in the HVR domain. We discovered that farnesylation of HVR increases its affinity to the CaM. Moreover, the binding mode of farnesylated HVR is different from that of the unmodified HVR.

Lastly, we successfully synthesized and characterized fully post-translationally modified K-Ras4B. We carried this out using a transpeptidase enzyme, sortase, which ligates the catalytic domain of K-Ras4B to the post-translationally modified HVR. The modified K-Ras4B protein produced using this procedure possesses GTPase activity, effector binding capacity and associates with the membrane phospholipids.

These results can aid further studies on delineating the mechanisms of K-Ras4B interactions. Since HVR has been an important element in determining the differential activation of K-Ras4B, we need to find its involvement in binding to other effectors. Our observations also warrant detailed studies of HVR interactions in different Ras proteins that can uncover additional approaches for modulating their overactivation. These mechanisms of Ras regulation can be exploited in the future to design strategies to combat Ras overactivation.

1 INTRODUCTION

1.1 Cancer and Ras discovery

The discovery of oncogenes and their role in human cancer owes a lot to the study of oncogenic retroviruses. In 1911, Dr Peyton Rous discovered the Rous Sarcoma Virus when he found that a cell-free tumor extract from a fowl could transmit a sarcoma to other fowl (1, 2). The *src* oncogene could only be identified later in the 1960s which then became a model for other retroviral oncogenes (3). Since then, the progress made in the field of cancer biology has led us to our current vision of cancer that is driving the therapeutic advances towards the remedies for it. The fundamental characteristics of these retroviral oncogenes were discovered beginning with *src*.

Similarly, *RAS* genes were also identified as retroviral oncogenes that were found accountable for the oncogenic properties of RNA viruses (4). The first indication of the oncogenic properties of Ras can be traced back to a discovery by Jennifer Harvey in1964. An "unidentified virus" isolated from leukemic rats was thought to be responsible for causing tumors when injected in new-born mice (5). This virus later came to be known as Harvey-MSV (Ha-MSV). Shortly afterwards in 1967, Kirsten and Mayer identified yet another virus (Ki-MSV) isolated from mice that was responsible for causing lymphomas in Wister-Furth rats (6). Similar discoveries followed thereafter where virus strains were isolated and were found responsible for propagation of malignant properties (7, 8) .

However, Edward Scolnick et al introduced a change in this existing concept of oncogenic retroviruses in 1973. They determined that these viruses were in fact carrying nucleotide sequences derived from the rat cells (9). Similarly, in 1976, Stehelin et al. made a pivotal

discovery in which they claimed that oncogenic form of *SRC* was derived from the normal *SRC* (10). These findings transformed the cancer model to one where a mutated cellular gene was held responsible for cancer rather than linking it to an external agent like a virus. By 1979 Scolnick's group had pointed out that the oncoprotein transformed by these Kirsten and Harvey virus strains had a molecular weight of 21kDa and hence named it p21 (11, 12). Further they showed that these p21 oncoproteins bind to guanine nucleotides (13) and localize to the plasma membrane in the transformed cells (14). Eventually in 1981, it was identified that p21 oncogenes from Harvey and Kirsten viruses originated from normal vertebrate genes and the DNA sequences homologous to Ha-MSV transforming region in the normal rat DNA were definitively identified in this study (15, 16). This normal gene was shown to induce tumorigenic transformation in mammalian cells (17). Moreover, the wild type form of p21 differed from the mutant form with the latter lacking its GTPase activity (18).

These discoveries of mutationally active *RAS* genes in cancer cell lines demanded a focus on researching Ras structure and biochemistry that remains to this day. Our current knowledge of Ras proteins comes as a result of an extensive and complex advancement contributed by genetic and biological sciences.

Today we know that there are three *ras* genes that encode for four Ras isoforms: H-Ras, N-Ras, K-Ras4A and K-Ras4B. K-Ras undergoes alternative splicing in the fourth exon leading to the production of two splice variants – K-Ras4A and K-Ras4B (19). The abundance of K-Ras4A in tissue is much lower as compared to K-Ras4B (20). These Ras isoforms are GTPases that contain a common structural arrangement. They transmit extracellular stimuli to the intracellular signaling cascades by interacting with a host of effector proteins. These structural and functional aspects are detailed hereafter.

1.2 The Architecture of Ras proteins

Ras GTPases are structurally made up of an N-terminal catalytic domain and a C-terminal hypervariable region (HVR). The catalytic domain, also known as the G-domain, consists of 166 to170 amino acids. This region is homologus across all Ras isoforms. The HVR consists roughly of the C-terminal 20 to 23 amino acids. This region also varies the most across all isoforms with the percentage sequence homology being about 15%. In the overall structure of Ras proteins, the catalytic domain is very rigid and contains 95% sequence homology and 100% resemblance within the structural motifs. The HVR is a highly flexible region and has been the limiting factor in crystallizing the full length form of Ras. Hence, most of the structural information that we have about these proteins is the result of nuclear magnetic resonance experiments and structural data on the catalytic domains (21-24).

1.2.1 Catalytic domain of Ras

All guanine nucleotide binding proteins contain a canonical G-domain structure that allows these proteins to switch between the off and on states that bind GDP and GTP respectively. The catalytic domain of Ras isoforms contain six β-strands lined by five α-helices. There are 10 loops connecting these β-strands and α-helices. These structural elements form an αβα sandwich which is classified as a Rossman fold (25). The loop connecting β1 and α1 is known as the P-loop or the phosphate binding loop. The loop connecting α1 and β2 forms the majority of switch I region whereas the loop connecting the β3 and α2 forms the majority of switch II region. The "Switch Regions" are named so due to their participation in binding to GDP or GTP that allows the conformation to "switch" from active to inactive. The effector binding lobe of Ras extends from the N-terminus upto the 86^{th} residue and is 100% conserved across isoforms (26, 27). The switch

regions and the P-loop are the major effector binding regions in this lobe. The latter half of the catalytic domain is referred to as the allosteric lobe since it bears the allosteric site in addition to membrane interaction sites (28). The allosteric lobe exhibits 90% homology within the Ras family (27). Thus, all differences in the catalytic domain across isoforms arise from the allosteric half of the catalytic domain. The structural details of the catalytic domain are shown in Figure 1.1.

1.2.2 Hypervariable Region of Ras

The HVR of Ras proteins is 20 to 23 amino acids long. It contains a C-terminal CAAX motif (where C is cysteine, A is an aliphatic amino acid and X can be any amino acid) when it is translated which acts as a signal for post-translational modifications (29). Post-translational modifications include carboxymethylation and covalent attachment of an isoprenoid group to the cysteine alongwith the proteolysis of AAX residues. The HVR of Ras proteins is highly unstructured. Of all Ras isoforms, the HVR of K-Ras4B is unique since it contains a polylysine region in addition to the CAAX motif. As much as 50% of the amino acids present in the HVR of K-Ras4B are lysines which gives it a positive charge. The sequences of HVR for the Ras isoforms are shown in Figure 1.2.

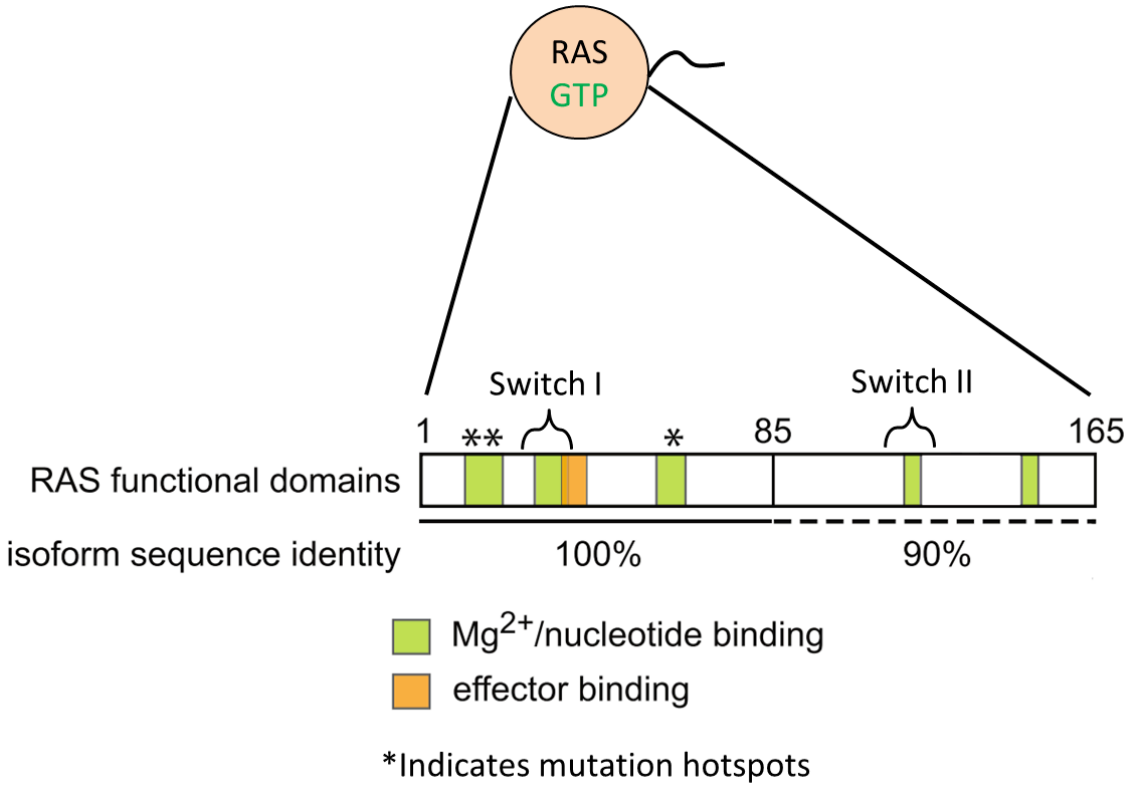

Figure 1.1: Catalytic domain of Ras.
The catalytic domain of Ras proteins contains the Switch regions and the effector binding regions. Mutational hotspots also occur in this region. The first 85 residues constitute the effector binding lobe and share a 100% sequence identity across isoforms whereas the terminal 80 residues constitute the allosteric lobe and share a 90 % sequence identity.

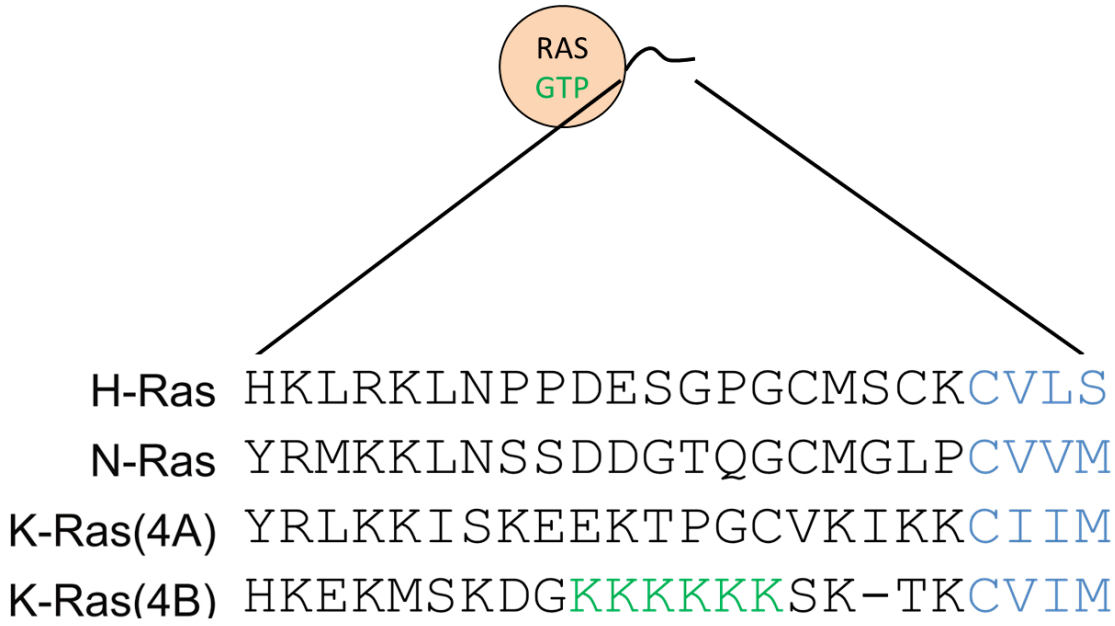

Figure 1.2: The hypervariable region of Ras.
The hypervariable region shares about 15% homology across isoforms. This region also contains the CAAX box at the C-terminus. K-Ras4B contains an additional polylysine region in its HVR.

1.2.3 Post-translational modifications in Ras proteins

The CAAX motifs on Ras dictate the post-translational modifications which occur on the endomembranes and the plasma membrane. First, a prenyl group is attached to the CAAX cysteine through a stable irreversible thioether linkage. This process is carried out by the enzyme farnesyl transferase (30, 31). In an event of inhibition of farnesylation (such as the presence of farnesyl transferase inhibitors), K-Ras and N-Ras get prenylated through geranygeranyl transferase which substitutes the farnesyl for geranylgeranyl group. This is also a reason for the failure of farnesyl transferase inhibitors as a potential therapy for cancers caused by Ras overactivation (32). In addition to the CAAX cysteine, K-Ras4A and N-Ras contain one more cysteine whereas H-Ras has two more. These additional cysteines undergo palmitoylation which has been known to be a reversible process (33). The palmitoylation is carried out by palmitoyl transferase enzyme (PTase) which is present on the endoplasmic reticulum or golgi endomembranes.

The terminal three residues in the CAAX motif of Ras proteins are cleaved by Ras-converting enzyme I (Rce I). Rce I also resides in the endomembranes of ER (34). Finally, Ras proteins get carboxylmethylated by Isoprenylcysteine-carboxyl-methyltransferase (ICMT) at the endomembranes of ER (35-37). It is believed that the carboxyl methylation is a reversible modification (38, 39). Addition of lipid and carboxyl methyl groups renders hydrophobicity to the Ras proteins thus allowing them to localize to the plasma membrane. The presence of different lipid groups present on the HVR allow these proteins to localize differentially on membrane microdomains (40). In K-Ras4B, the polylysine patch plays an important role in membrane targeting which is mediated by electrostatic interactions (41-44). These post-translational modifications are schematically shown in Figure 1.3.

The palmitoylation-depalmitoylation cycle of K-Ras4A, N-Ras and H-Ras proteins allows them to shuttle between the plasma membrane and the endomembranes of golgi and ER (45). Depalmitoylation is carried out by acyl protein thioesterases at the plasma membrane (46). K-Ras4B, on the other hand, has an alternative cycling mechanism. K-Ras4B undergoes phosphorylation at a serine residue (S181) on its HVR. The phosphorylation is mediated by the family of protein kinase C (PKC) enzymes. This phosphorylation has been believed to cause dissociation of K-Ras4B from the plasma membrane (43, 47, 48). However, this view has been challenged recently by a study which claims that the majority of phosphorylated K-Ras4B stays at the membrane. In this study, phosphorylation was found to change the distribution of K-Ras4B between different microdomains in the plasma membrane (49).

Until now, these were the most studied Ras post-translational modifications. However, in recent research studies several other new post-translational modifications have been identified. Ras proteins get acetylated on K104 (50). This modification did not alter the cellular localization of Ras but affected the efficiency of nucleotide exchange by hindering the interaction of Ras with GEFs (50).

Ras isoforms have a highly conserved cysteine at position 118. This cysteine undergoes s-nitrosylation upon reacting with nitric oxide (51). This modification was shown to enhance the guanine nucleotide exchange (52) but the physiological relevance of this modification is yet to be determined.

Glucosylation and ADP-ribosylation of Ras is found to occur in cells containing excess bacterial virulence factors (53). *Pseudomonas aeruginosa* contains Exoenzyme S (ExoS) which adds an APD-ribosyl group to arginines on position 41 and 128 causing inefficient guanine nucleotide

exchange (54). Similarly, *Clostridium difficile* contains a monoglucosyltransferase which glucosylates Ras on threonine 35 which inhibits MAPK signaling through Ras (55).

Ras was also shown to undergo S-glutathionylation in presence of reactive oxygen species at the C118 (56). This post-translational modification was found responsible for an increase in the activity of Ras through Akt and p38.

New data suggests that Ras also undergoes ubiquitination (57). Endosomally localized E3 ligase Rabex5 mono- and di-ubiquitinates H-Ras and N-Ras (58). β-transducin repeat containing protein (β-TrCP) is responsible for proteasome dependent degradation of H-Ras through polyubiquitination (59). Ubiquitin ligases for K-Ras remain unknown.

Ubiquitination, at K117 and K147, promotes endosomal association in case of H-Ras (57, 60, 61). K-Ras on the other hand does not change its localization pattern upon ubiquitination. In K-Ras, ubiquitination at K147 inhibits GTP hydrolysis by obstructing its interaction with GAPs and causes selective downstream activation (61, 62). All of these less common post-translational modifications of Ras are detailed in Figure 1.4.

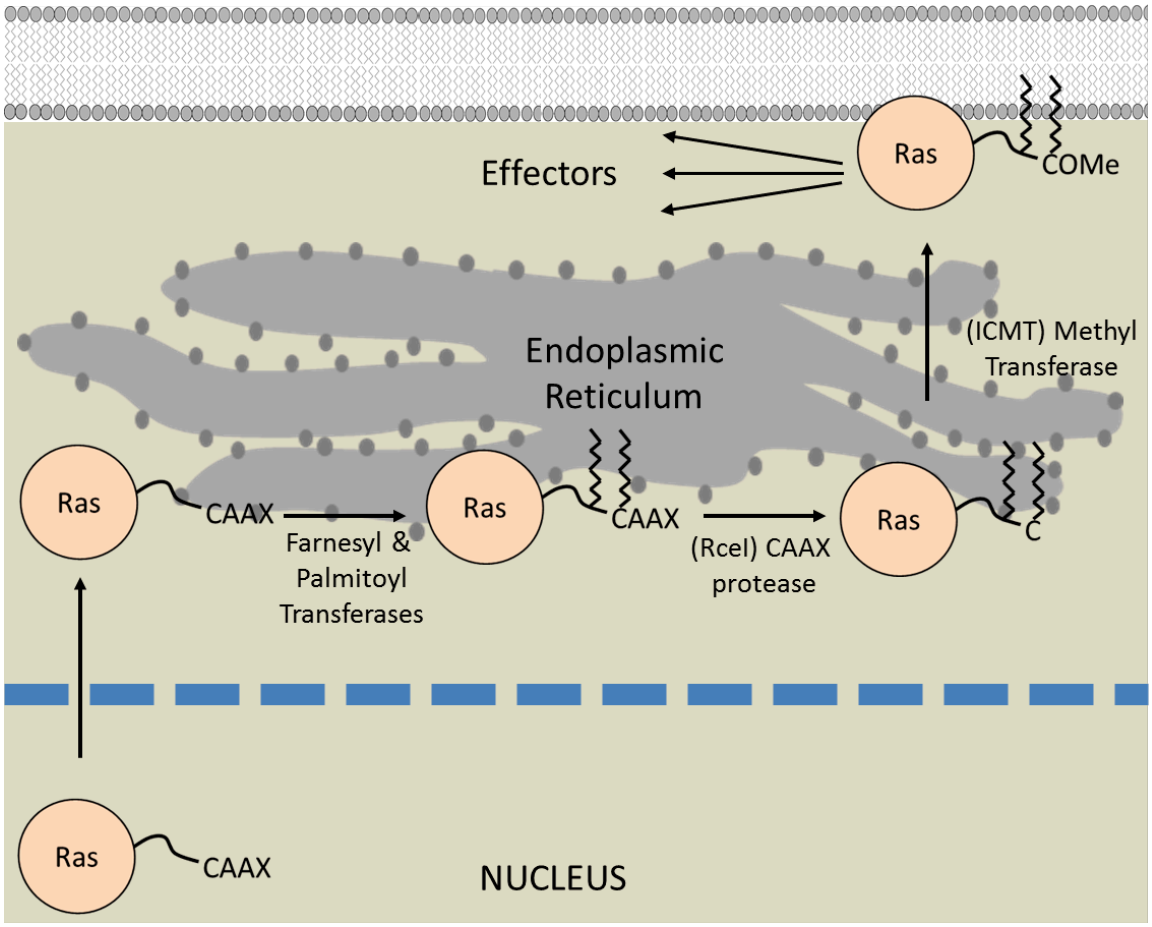

Figure 1.3: Post-translational modifications in Ras.
Ras proteins undergo lipidation, AAX proteolysis and carboxyl methylation to be post-translationally modified.

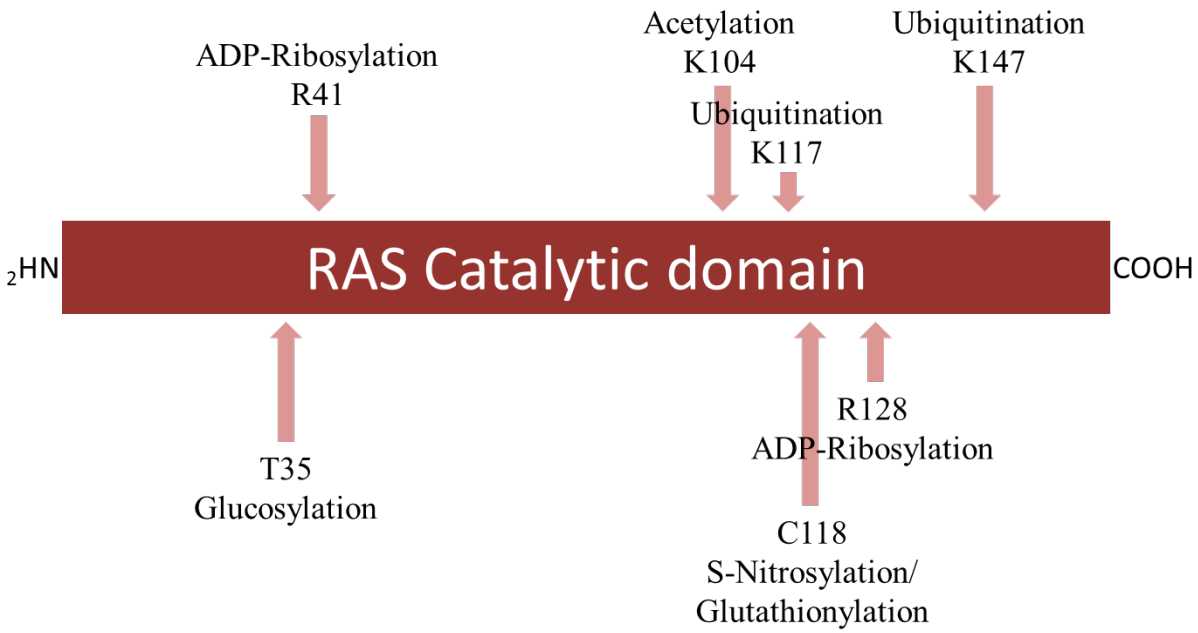

Figure 1.4: Additional post-translational modifications in Ras.
Ras proteins undergo additional post-translational modifications that are less known. The position and kind of modification is shown in this figure.

1.3 Cellular function and mechanism of Ras proteins

According to the existing paradigm, when a growth factor binds to tyrosine kinase receptor (RTK) on the membrane, it causes autophosphorylation of specific tyrosines on the receptor that are responsible for its activation. Upon activation of the receptor, an adaptor protein, growth factor receptor bound 2 (GRB2), is recruited to the intracellular portion of the receptor. The SH2 domain binds tyrosine kinases. At the same time, the SH3 domain of GRB2 is constitutively bound to Son of Sevenless (SOS) which also localizes with GRB2 to the membrane (53). SOS is a Guanine Exchange Factor (GEF). The inactive GDP-loaded Ras binds to GEFs like SOS, which activate Ras by displacing the switch I region, thus disfavoring the GDP binding and allowing GTP, which is more abundant in the cell than GDP, to bind in its place (63). GTP binds to the catalytic domain with a higher affinity as compared to the GDP (64). The GTP loading step switches Ras into its active state which then binds to various effectors like Raf (65), RalGDS (66), PI3K (67), Tiam (68) and NORE1A (69). These effectors signal to activate multiple cellular processes. Effector binding is responsible for stabilizing the switch loops (70-72). The attenuation of these signaling pathways occurs upon hydrolysis of GTP to GDP which is accelerated by GTPase Activating Proteins (GAPs) (73). Although Ras is capable of intrinsic hydrolysis (74), the rate of this reaction is believed to be too slow for being biologically relevant (75). GAPs increase the hydrolysis rate of Ras by 10^5 times (53). The schematic representation of Ras activation is shown in Figure 1.5. The effectors that Ras binds upon activation and their downstream effects are detailed in Figure 1.6.

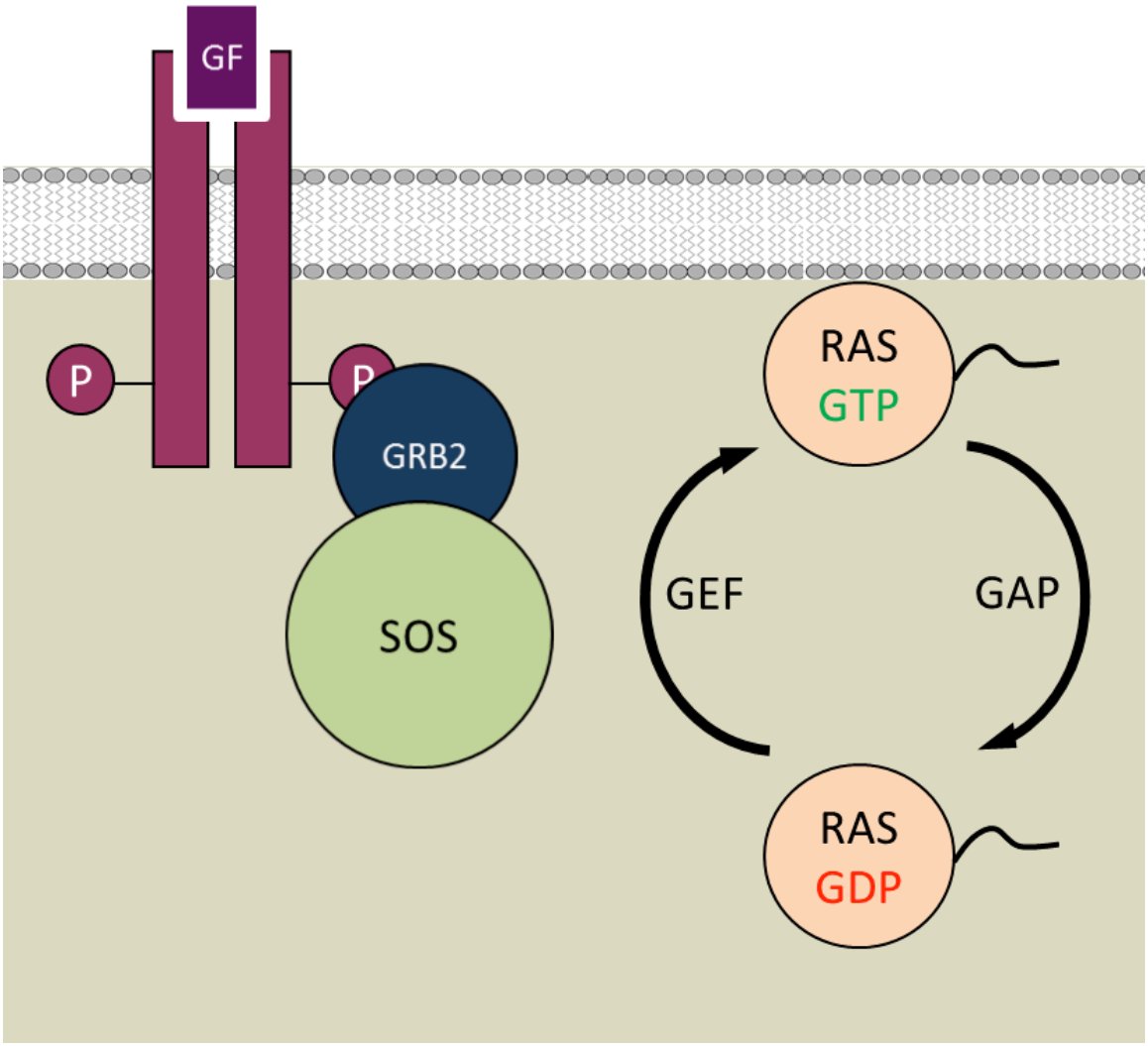

Figure 1.5: Activation of Ras.
When a growth factor (GF) binds to its receptor, it recruits GRB2 and SOS to the membrane. SOS is a guanine exchange factor (GEF) which binds to Ras-GDP and converts it to Ras-GTP. GTPase activating proteins (GAPs) convert Ras-GTP back into its GDP loaded form. The balance between GEFs and GAPs determines the active amount of Ras present in cells.

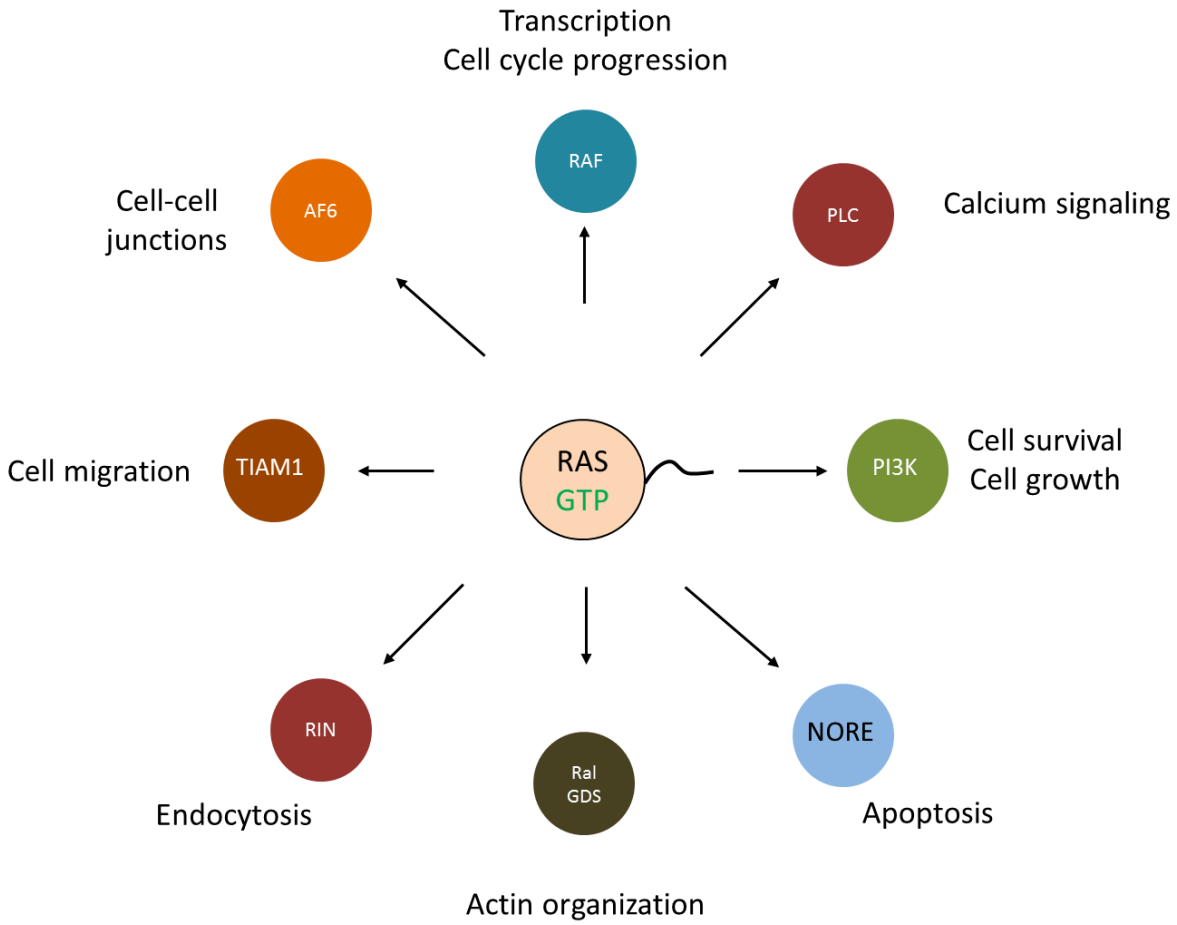

Figure 1.6: Examples of Ras effectors.
Active Ras proteins bind to more than 10 known effectors which produce various cellular effects.

It has to be noted that although Ras-GDP is considered inactive, an interesting discovery reports the binding of a transcriptional factor, Aiolos, only to Ras-GDP and not to Ras-GTP which allows the expression of an anti-apoptotic protein BCL-2 (76). Moreover, Raf has been shown to bind to Ras-GDP with a hundred fold lower affinity (77).

Although Ras effectors possess a Ras binding domain (RBD) it has been shown that regions outside RBD can also participate in Ras binding. For example, the cysteine rich domain (CRD) in Raf participates in Ras binding in addition to its RBD (78). Moreover, the effector binding domain present on Ras can differ depending on which effector it binds. For example, switch II region is involved in binding to phosphoinositide-3-kinase (PI3K) but not to Raf (79).

The downstream signaling effectors of Ras encompass a wide array of cellular effects ranging from cell growth, cell survival and cell proliferation to cell migration, endocytosis and apoptosis (80-83). Deregulation of many of these cellular signaling roles is a hallmark of cancer (84). There are more than 20 known downstream effectors of Ras discovered till date.

1.3.1 Raf kinases

Raf family of serine threonine kinases are the best characterized effectors of Ras proteins. These comprise of A-Raf, B-Raf and c-Raf (or Raf-1). These kinases regulate the mitogen activated protein kinase (MAP kinase or MAPK) cascade (85-87). Raf kinases get recruited to the membrane following Ras activation. Raf activation occurs through the interaction of Raf RBD and the Raf CRD with Ras (78, 88). Raf dimerization is also required for MAPK signaling (89, 90). Raf (homo and hetero) dimers have been observed at the plasma membrane and implicated in downstream signaling (91, 92). Disruption of Raf dimers abrogates Ras-Raf interaction and hence its signaling (93, 94). Overall, Raf activation involves the interplay of many cofactors and

modifications, like phosphorylation, which is not yet completely understood (68). Activation of Raf intiates a signaling cascade by activating MEK1 and MEK2 which consequently activate extracellular signal-regulated kinase 1 and 2 (ERK1 and ERK2). ERK proteins are responsible for the activation of a variety of transcription factors like Elk-1, MNK1, MNK2, etc. that result in cellular functions (68).

1.3.2 Phosphoinositide 3- kinases

Phosphoinositide 3- kinases are a family of enzymes which derive their name due to their action of phosphorylating inositide rings of phosphatidylinositols. This is necessary for the production of mitogenic phosphoinositol lipids. There are three classes of PI3Ks – Class I, II and III. Of these, class I PI3Ks bind Ras proteins. Class I PI3Ks are heterodimeric enzymes composed of a catalytic subunit and a regulatory subunit. The interaction of PI3K with Ras is mediated through an RBD present on the catalytic or p110 subunit of PI3K (95). PI3K activation it produces a secondary messenger lipid, phosphatidylinositol (3, 4, 5) triphosphosphate (PIP3) which is important in activation of Akt (96-98). Akt is involved in regulating apoptosis through the production of Bad and Caspase 9 (99).

1.3.4 MEKK1

Another serine threonine kinase, mitogen-activated protein kinase kinase kinase (MEKK1), is known to interact with Ras-GTP (100). MEKK1 is involved in regulating stress-activated protein kinases and mitogen-activated protein kinases(100). Apart from direct interaction with Ras, MEKK1 is believed to provide a platform for the interplay of other Ras effector pathways by allowing a crosstalk between ERK and Raf (101). MEKK1 deregulates ERK, JNK and p38 pathways to induce apoptosis as well (102).

1.3.5 Calmodulin

Yet another important and newly discovered regulator of Ras is a calcium-modulated protein calmodulin (CaM). CaM binds only to K-Ras4B, but not to H-Ras, N-Ras or K-Ras4A, and influences its downstream activity in a calcium dependent manner (103). This binding has been shown in cell types including fibroblasts (103), platelets, the MCF-7 breast cancer cell line (104), and Hela cells (105). We recently identified the HVR as the site responsible for the binding affinity and specificity of CaM to K-Ras4B (106). The importance of the polylysine region and farnesyl moiety for K-Ras4B-CaM binding has been suggested by Lopez-Alcala et al, 2008 (107). The structure of CaM contains two lobes comprising the N and C terminal domains, which are connected by a linker region. Binding of CaM to its binding partners induces a conformational change in CaM. Importantly, CaM has recently emerged as a key regulator of K-Ras4B in response to platelet derived growth factor (PDGF) signaling (108). K-Ras4B-CaM interactions also regulate cell cycle progression through the ERK2 pathway (109). Furthermore, CaM can prevent Ras activation by PKC in fibroblasts (110). In response to glutamate, CaM causes reversible intracellular translocation of K-Ras4B in hippocampal neurons (105).

1.4 Mutational implications of Ras Proteins

As elaborated previously, there is a variety of effectors Ras proteins interact with to produce a plethora of downstream cellular effects. Hence, it is not surprising to notice that any mutational changes in these proteins can lead to a disease as serious as cancer (4). Apart from cancer, K-Ras4B mutations are also implicated in developmental disorders like Noonan syndrome (111, 112) and cardiofaciocutaneuos syndrome (CFC) (113). Moreover, H-Ras has been mutated in costello syndrome (114, 115).

Activating *Ras* mutations are found in about 30% of human cancers (68). These mutations interfere with the GTPase activity of the Ras proteins. Thus, Ras cannot be inactivated and becomes constitutively active. Interestingly, identified mutations are concentrated on amino acids 12, 13, and 61 for all ras family members. However, the incidence of mutations at these sites is not the same for all family members, and varies according to the tissue and tumor type. Mutations affecting Glycine 12 (G12) and Glycine 13 (G13) are more prevalent in oncogenic K-Ras (86% and 13%, respectively). In H-Ras, mutations of Glycine 12 (G12) and Glutamic acid 61 (Q61) residues are more common (about 54% and 34.5%, respectively). N-Ras, on the other hand, has a different distribution pattern; Q61 has the highest mutation rate (about 60% of total *N-ras* mutations) (116, 117). Analysis of tumor samples has revealed that each specific mutated Ras isoform associates with particular types of tumors. Mutations in colon, lung and pancreatic cancers are present only in the *K-ras* gene. In cancers of the urinary tract and bladder, *H-Ras* is the most frequently mutated Ras isoform. Mutations are primarily in the *N-ras* gene in leukemia. In thyroid carcinomas, all three *ras* genes carry mutations (118-120).

Ras GTPases contribute to a variety of cancer-driving processes. It promotes cellular proliferation, suppresses apoptosis and modulates the tumor microenvironment. Active Ras upregulates the transcription of growth factors such as transforming growth factor-α and amphiregulin and alters the expression of growth factor receptors (121-123). Oncogenic HRASG12V enhances cell proliferation through upregulation of integrins (124, 125).

Programmed-cell death (apoptosis) is an important defense mechanism against malignancy. Suppression of apoptosis causes the accumulation of cells, which in turn promotes tumor formation and metastasis. Ras represses cell death through disturbing the homeostatic balance between pro-apoptotic and anti-apoptotic signals. Raf activation by Ras leads to downregulation

of the pro-apoptotic transcriptional repressor, prostate apoptosis response 4 (PAR4) (126, 127), and the upregulation of the anti-apoptotic proteins, BCL-2 and apoptosis repressor with caspase recruitment domain (ARC) (128, 129). Most anticancer drugs act by activating the endogenous apoptotic program. Thus, disruption of the normal apoptotic program or activation of antiapoptotic pathways may be the reason of developing a resistance to treatment therapies (130).

Ras superfamily of GTPases has also been implicated in the progression of human cancers. They promote metastasis through regulation of cytoskeletal architecture. Rho induces the organization of actin stress fibers, Rac is responsible for lamellipodia formation, and Cdc42 induces filopodia (131, 132). Ras can activate myosin light chain (MLC) kinase (MLCK) via MAPK, which in turn phosphorylates and activates MLC and increases cell motility (133). Apart from their direct effects on the cytoskeletal organization, Ras family members can change the expression of genes associated with metastasis. Among these are several types of protease that are responsible for degradation of extracellular matrix (ECM) components (134).

Cancer cells require energy and building blocks for the synthesis of proteins, lipids, RNA and DNA to maintain their high proliferative rates. These unique metabolic needs were first described by Otto Warburg and are characterized by an increase in glucose uptake and metabolic reprogramming towards aerobic glycolysis (135, 136). Oncogenic *RAS* promotes this glycolytic shift via MAPK- and PI3K-dependent upregulation of hypoxia-inducible factor 1α (HIF1α). It also enhances the transcription of the glucose transporter GLUT1, thus, increases the ability of cells to take up glucose (137-139). It causes an increase in the levels of glycolytic enzymes, such as hexokinase, phosphofructokinase (139, 140). Taken together these data reveal that, oncogenic *RAS* plays a role in metabolic reactions that use glucose as an anabolic substrate to generate building materials for cellular proliferation (141).

1.5 Importance of K-Ras4B

All of the research in my thesis relates to the K-Ras4B isoform. We decided to focus on K-Ras4B because K-Ras mutations account for more than 85% of all Ras mutations in cancer. Mutations in K-Ras4B occur in up to 90% of pancreatic cancers (142, 143), 57% of colorectal cancers (144) and 50% of lung cancers (68, 145, 146). These cancer types have the highest mortality rates. Moreover, K-Ras4B is also indispensible for embryonic development (147, 148) and deletion of K-Ras in mouse embryos results in lethal cardiac, neurological, hematopoetic and liver defects (149).

Table I: Prevalence of K-Ras mutations in selected human cancers (68).

Tumor Type	Frequency of Mutations
Pancreatic	72-90%
Colorectal	32-57%
Lung	15-50%
Endometrium	5-50%
Gall bladder	14-38%
Multiple myeloma	16-33%
Testicular	9-12%

K-Ras4B also contains certain unique structural features. For example, it is the only Ras protein having a single lipid post-translational modification. Other Ras isoforms acquire 2 (N-Ras and K-Ras4A) or 3 (H-Ras) lipid moieties upon post-translational modification. Likewise, K-Ras4B contains a polylysine patch on its HVR which is not observed in other Ras proteins. These unique structural features afford some unique binding partners to K-Ras4B like CaM, Sur8 and RassF2 (150, 151).

Although much of the evidence highlights the differences in HVR, it is unclear as to why human cancers contain mostly *K-Ras* mutations, and significantly less *N-Ras* and *H-Ras* mutations. Despite its unique and crucial nature, no effective targeting strategies against K-Ras exist till date. Different approaches have been tested to inhibit K-Ras signaling. These include but are not limited to the use of antisense oligonucleotides (152, 153), and inhibitors against Ras modifying enzymes (154-156) and downstream effectors (157-159). None of these strategies have been particularly useful due to various shortcomings. K-Ras targeting strategies that reverse the cellular signals initiated by K-Ras overactivation and at the same time do not cause toxicity to the normal cellular signaling pathways will be an important step towards treatment of K-Ras driven cancers. Developing such isoform specific treatment requires thorough knowledge of the differential signaling pathways of Ras proteins and the molecular interfaces involved in these interactions. In my thesis I focus on identifying unique structural features of K-Ras that can be explored for development of isoform specific inhibitors of Ras. I investigate how the HVR of K-Ras regulates K-Ras activity through intra and intermolecular interactions, how it establishes specific protein-protein binding, and how K-Ras dimerization occurs.

2 HIGH AFFINITY INTERACTION OF K-RAS4B HVR WITH THE ACTIVE SITE

2.1 Introduction

Ras proteins belong to a large family of GTPases that play an important role in the transmission of extracellular stimuli to intracellular signaling cascades. The most well studied of these are the MAP kinase and Akt/mTOR pathways. Ras molecules regulate essential cellular functions cell survival, proliferation, motility, and cytoskeletal organization through their downstream pathways (68, 160). Ras proteins cycle between GTP-bound active and GDP-bound inactive states. Ras proteins contain the N-terminal catalytic domain that binds GTP or GDP and the C-terminal hypervariable region (HVR). Effector recruitment occurs in the GTP-bound state. HVR undergoes a series of post-translational modifications with lipids and a methyl group that influence Ras activity. These modifications are essential for membrane localization and protein-protein interactions.

The catalytic domains of Ras proteins share a 95% homology. The structural elements in the catalytic domain are completely conserved across all the isoforms (26, 27, 161). On the other hand, the HVRs are only about 15% homologus. Apart from distinct HVRs, Ras proteins are also differentially post-translationally modified in their HVRs (162). As a result, the differences in the binding of Ras proteins to their binding partners, or the membrane, could be attributed to their HVRs and the different post-translational modifications (163). Recent studies clearly demonstrate that all Ras isoform function in a unique way in normal physiological processes and in pathogenesis (164, 165).

The important members of Ras family include H-Ras, N-Ras, K-Ras4A and K-Ras4B. Activating mutations in Ras genes are found in nearly 30% of all human cancers (68). Of these,

K-Ras mutations predominate, accounting for more than 85%. *KRAS* is frequently mutated in cancers of epithelial origin, including lung, colorectal, and pancreatic malignancies (166, 167). Mutations in K-Ras4B occur in up to 90% of pancreatic cancers (142, 143), 57% of colorectal cancers (144) and 50% of lung cancers (68, 145, 146). These oncogenic mutations in K-Ras4B impair GTP hydrolysis (168) and lead to constitutive activation of signaling (73, 169). Moreover, mutations in K-Ras are also associated with Noonan syndrome, which is a developmental disorder (111, 112). K-Ras4B is also indispensible for embryonic development (147, 148) and deletion of K-Ras in mouse embryos results in lethal cardiac, neurological, hematopoetic and liver defects (149).

The two alternative K-Ras mRNA splice variants, K-Ras4A, and K-Ras4B, differ in their 25 amino acid long C-terminal sequences, HVR, where the fourth exon of K-Ras4B encodes a lysine-rich region (41, 170). The positively charged HVR and the post-translational modifications target K-Ras4B to the plasma membrane where it initiates signaling events. X-ray and NMR structural studies point to highly flexible C-terminal tail. Crystal structures are only available for the catalytic domain.

K-Ras4B is a ubiquitous p21 GTPase that controls cell survival and proliferation (171). Despite the central role of K-Ras4B in oncogenesis and widespread efforts to develop Ras-directed anti-cancer therapeutics (172-175), no selective, specific inhibitor of K-Ras4B is available for clinical use (176-178). This is primarily because its catalytic domain lacks pockets for high affinity small molecule binders (179, 180).

The function of K-Ras in cancer has been studied extensively. However, development of compounds inhibiting K-Ras function directly proved to be a challenging task. We have found

that an unstructured C-terminal fragment, the HVR interacts with the active site of K-Ras with high affinity. Importantly, the identified interaction surface is shared with many known K-Ras effectors suggesting a role for HVR in K-Ras signaling. High affinity binding of short HVR peptide analogs to the protein surface indicates that it can be targeted by synthetic molecules. This suggests a new way of inhibiting the function of the frequently activated oncoprotein for therapy of many tumor types.

Our studies indicate that a β-strand populated K-Ras4B HVR conformation interacts with the catalytic domain extensively when the catalytic domain is GDP-loaded. However, when the GTP replaces GDP, the HVR has a minimal interaction with the G-domain, indicating that the HVR is sequestered by the K-Ras4B catalytic domain in the GDP-bound state and released in the GTP-bound state. Remarkably, the interaction surface we identified by NMR and modeling overlaps significantly those involved in effector, Raf and PI3K binding. Further, the interaction mode is similar, involving extension of the Ras β-sheet motif. Our data indicate that HVR interaction is important in regulation of Ras function and that synthetic analogues of HVR can function as regulators of Ras activity.

2.2 Materials and Methods

2.2.1 Protein preparation:

Protein preparation was carried out according to our previously published protocol (181). K-Ras4B cDNA (full length and catalytic domain) from Invitrogen was cloned into the pET42a vector. The restriction sites used were NdeI and XhoI. A His-tag was introduced to aid protein purification. The plasmid was transformed into BL21AI cells and the cells were grown in M9 medium (182) containing 0.4 M NaCl with shaking at 250 rpm. The cells were grown at 37 °C

until their OD_{600} reached 0.6. Then, the expression of K-Ras4B was induced with 0.2 mM IPTG, 0.2% arabinose and 2% ethanol. The cells were grown thereon for 24 hrs at 18 °C with shaking at 250 rpm. The cells were harvested by centrifuging and the pellets were stored at -80 °C. The pellets were thawed at room temperature before lysis. Lysis was carried out using the B-PER bacterial extraction reagent (Pierce) with addition of 10 mM $MgCl_2$, 50 μg/mL DNaseI, 2 mM phenylmethanesulfonyl fluoride (PMSF), 1–2 tablets of EDTA-free complete (Roche), and 10 mg of lysozyme. Pellets were kept in the lysis buffer with shaking at 200 rpm for 40 min at room temperature. The lysate was centrifuged at 14000g at 4 °C and the supernatant was collected. For extracting the protein from the insoluble fraction, the pellets were resuspended in 10 mM Tris-HCl pH 7.6, 20 mM Na-citrate, 50 mM KCl, 5 mM $MgCl_2$, 0.1 mM GDP, and 2 mM β-mercaptoethanol. The protein pellets were kept in this buffer with shaking at 200 rpm for 40 min at room temperature. The suspension was centrifuged similarly to the first lysate and the supernatant was collected. The cell debris was discarded. The first and second extraction fractions were dialyzed separately against 1X binding buffer (Novagen) containing 10% glycerol for approximately 12 hrs. Both supernatants were incubated with the His-Bind resin for 3 hrs. Washing was done with the His-Bind Wash buffer and elution was carried out using a gradient from 30 mM to 1 M imidazole. The purity of the protein was assessed using an SDS-PAGE gel and mass spectrometry. Pure fractions were dialyzed against 25 mM Tris-HCl, pH 7.6, 150 mM NaCl, 5% glycerol, 10 mM $MgCl_2$, 1 mM EDTA, and 1mM β-mercaptoethanol. For nucleotide loading into the protein, 20 μL of 0.5 M EDTA per 1 mL of protein solution was added and GTP-γ-S or GDP was added to a final concentration of 1 mM. This mixture was incubated at 30 °C for 30 min. The reaction was stopped by adding 100 mM $MgCl_2$. The buffer was changed to include the Tris-citrate buffer (50 mM Tris-citrate, pH 6.5, 50 mM NaCl, 5 mM $MgCl_2$, 0.01 mM

GDP, and 10 mM β-mercaptoethanol). The GTPase hydrolysis assay was carried out to confirm activity of protein.

2.2.2 **Peptide synthesis**:

The peptides were synthesized on a Liberty Microwave peptide synthesizer (CEM Corporation) using Fmoc chemistry. To avoid oxidation, Met residues in the sequence of HVR have been substituted by isosteric norleucine. The peptides were cleaved from the resin and deprotected with a mixture of 90.0% (v/v) trifluoroacetic acid (TFA) with 2.5% water, 2.5% triisopropyl-silane, and 5% thioanisol. The resin and deprotection mixture were pre-chilled to -5 °C and reacted for 15 minutes at -5 °C with stirring. The reaction was allowed to continue at room temperature for 1 hr and 45 min. The resin was filtered off and the product was precipitated with cold diethyl ether. The resin was washed with neat TFA. Peptide suspended in diethyl ether was centrifuged at -20 °C and the precipitate was washed with diethyl ether four more times and left to dry in a vacuum overnight. The dried crude peptide was dissolved in DMSO and purified on a preparative (25 mm × 250 mm) Atlantis C18 reverse phase column (Agilent Technologies) in a 90 min gradient of 0.1% (v/v) trifluoroacetic acid in water and 0.1% trifluoroacetic acid in acetonitrile, with a 10 mL/min flow rate. The fractions containing peptides were analyzed on Agilent 1100 LC/MS spectrometer with the use of a Zorbax 300SB-C3 Poroshell column and a gradient of 5% acetic acid in water and acetonitrile. Fractions that were more than 95% pure were combined and freeze dried (183). For generation of palmitoylated peptide, Fmoc-Lys (ε-DDE) was coupled manually to PAL AM resin. The DDE group was removed by incubation with imidazole/ hydroxylamine mixture as described. Ten-fold molar excess of palmitic acid was dissolved in methylene chloride/N-methylpyrrolidone mixture (1:1), mixed with equimolar amounts of HCTU and diisopropylethylamine and added to the resin. After overnight incubation,

non-reacted amino groups were blocked with acetic anhydride; the resin was washed with N-methylpyrrolidone, methylene chloride and dried under the hood. The rest of the peptide synthesis was performed on the synthesizer as described above. These methods were carried out as per Patent Publication Number: US20140135276 A1.

2.2.3 K-Ras labeling with fluorescein:

1.6 mg fluoresceine maleimide (Santa Cruz) was dissolved in 25 µL DMSO. 5 µL were diluted in 10 µL buffer. The resulting solution was slowly added to 400 µL of 75 µM GDP or GTP-γ-S-loaded K-Ras solution in 100 mM HEPES buffer pH 6.5 containing 5 mM $MgCl_2$, 50 mM NaCl and 0.5 M BCEP. Mixtures were incubated overnight at 4 °C and filtered through NAP-5 column (GE) equilibrated with the reaction buffer. LC/MS showed no traces of the maleimide and complete labeling of intact K-Ras. The preparation contained a small impurity having +78 molecular mas, that corresponded to the β-mercaptoethanol adduct that was present in the starting protein. The adduct was invisible in the subsequent biophysical experiments and thus had no effect on the data.

2.2.4 Microscale Thermophoresis (MST):

For the MST studies we have prepared 16 2-fold serial dilutions of peptides starting from 30 µM. Titration series have been prepared that contained 15 µL of 80 nM fluorescein-labeled K-Ras and 15 µL of peptides solution of varying concentrations. Final buffer composition included 20 mM HEPES pH 7.0, 1 mM $MgCl_2$, 0.5 mM TCEP-HCl, 0.5 mM NaN_3, and 10 µM either GDP or γ-S-GTP ("Ras" buffer) and 0.05% Tween-20 for non-lipidated HVR analogue. Lipidated HVR analog kR-4B-1 was dissolved in Ras buffer containing nanodiscs composed of 95% 1,2-dipalmitoyl-sn-glycero-3-phosphocholine (DPPC) and 5% 1,2-dihexadecanoyl-sn-glycero-3-

phosphoethanolamine (DPPE). Nanodiscs have been prepared as described (181). All measurements were taken using capillaries on Monolith NT.115 instrument (NanoTemper Technologies GmbH, Germany) which uses 60% IR-laser power and LED excitation source with $\lambda = 470$ nm. The software, NanoTemper Analysis 1.2.20, was used for fitting the data and for the determination of the K_D values.

2.2.5 NMR experiments:

900 Mhz and 600 Mhz Bruker Avance Spectrometers equipped with a cryogenic probe were used for measuring ^{1}H-^{15}N HSQC NMR spectra. The proteins were dissolved in 50 mM Tris-citrate, pH 6.5, 50 mM NaCl, 5 mM $MgCl_2$, 10 mM β-mercaptoethanol, 10 mM $CaCl_2$, and 10% $^{2}H_2O$ for conducting the experiments. All experiments were carried out at 25 °C. NMRPipe software (184) was used for processing and analyzing the data. The chemical shift assignments were taken from the BMRB database (http://www.bmrb.wisc.edu) using the 17785 and 18529 BMRB ID numbers. The assignments for the HVR were made using HNCA, HNCACB, and CBCACOHN experiments. Lysine to alanine mutants were used to resolve ambiguities in lysine assignments in the HVR. The experiments on GTP-γ-S-loaded K-Ras4B were carried out as soon as possible after loading with the GTP-γ-S nucleotide isoforms in order to ensure that the nucleotide was not hydrolyzed. The mean chemical shift difference was calculated using the following formula.

$$\Delta\delta_{NH} = \sqrt{\frac{(\Delta\delta H)^2 + (\Delta\delta N)^2 / 25}{2}}$$

Chemical shift perturbations higher than the sum of the average and one standard deviation were considered statistically significant. The concentrations of proteins used in each experiment are mentioned in the figure legends.

2.2.6 Molecular dynamics (MD) simulations:

Two Ras crystal structures (PDB codes: 4EPT and 3GFT) were used to model the full-length K-Ras4B protein. The former is GDP-loaded with a point mutation C118S. The latter is GNP (a GTP analogue)-loaded, with a point mutation Q61H. We extracted the coordinates from both crystal structures and replaced the mutants with the wild-type residues. GNP was converted to GTP. The coordinates of Mg^{2+} at the active site were also extracted. Then, we constructed an HVR chain and covalently connected it to H166 with the CHARMM program (185). Interactive molecular dynamics (IMD) (186) on a molecular visualization program (VMD) (187) with the NAMD (188) code were used to relocate the HVR onto the catalytic domain based on the NMR CSP results and to pre-equilibrate the proteins for 5 ns. Four different initial configurations for each GDP- and GTP-bound state of K-Ras4B were generated. The initial configurations of the K-Ras4B proteins were solvated by the modified TIP3P water model (189) and gradually relaxed with the proteins held rigid. The unit cell dimension is 120 $Å^3$ containing almost 180,000 atoms. The systems also contain 50 Na^+, and 5 Mg^{2+}, and 61 Cl^- for the GDP-bound K-Ras4B, but 60 Cl^- were added to the GTP-bound protein systems. A series of minimization and dynamics cycles were performed with the harmonically restrained proteins. The harmonic restraints were then gradually reduced with the full Ewald electrostatics calculation and a constant temperature (Nose'-Hoover) thermostat/barostat at 310K. For production runs for 100 ns, the NAMD code (188) were employed on the Biowulf cluster at the NIH. Averages were taken after 30 ns,

discarding initial transient trajectories. Analysis was performed with the CHARMM programming package (185, 190).

2.2.7 Raf-1 RBD assay:

Raf-1 Ras binding domain (RBD) assay was carried out according to the protocol published by Chavan et al (191) using Raf-1 RBD agarose beads from Millipore. The assay was done on GDP and GTP-bound forms of K-Ras4B in its full length and truncated versions. The respective protein samples were incubated with RafRBD agarose resin for 45 minutes at room temperature with intermittent mixing. The beads were then washed with HEPES buffer containing 25mM HEPES, 150mM NaCl, 5mM $MgCl_2$, 10mM β-merceptoethanol and 5% glycerol atleast two times. Western blot was performed on the pulled down protein and probed for K-Ras4B using an anti-Ras antibody. ImageJ software was used for quantifying the Western blots. Ratio of measured band intensities of K-Ras4B$_{1-166}$ pulled down with Raf-1 RBD beads to K-Ras$_{1-166}$ alone was normalized to a 100%. The full length protein band intensities were treated in a manner similar to those of K-Ras$_{1-166}$.

2.2.8 Nanodiscs and Surface Plasmon Resonance experiments:

The stabilized lipid bilayers called nanodiscs were assembled according to published protocols (192, 193). First, membrane scaffold protein (MSP1D1) was expressed as a 6X His fusion in BL21DE3-Star cell and purified to homogeneity using Ni^{2+}-His-bind resin (Novagen). Pure fractions of MSP1D1 were pooled and dialyzed against storage buffer (20 mM Tris-HCl pH 7.4, 0.1 M NaCl, 0.5 mM EDTA and 0.1% NaN_3). The protein concentration was adjusted to around 0.4 mM using an Amicon ultracentrifugal filter device. DPPC phospholipids were utilized for making the nanodiscs. We also used phosphatidylethanolamine based lipids for the purpose of

immobilization. The mixture was subsequently dried at room temperature using an Eppendorf Vacufuge and resuspended in storage buffer containing 2-fold molar excess of sodium cholate. MSP1D1 was added to the phospholipid mixture. The protein and phospholipid mixture was stored at 37 °C for 1 hr. The concentration of sodium cholate in solution was reduced by 5-fold dilution in storage buffer. The sample was dialyzed extensively against the storage buffer to remove all traces of sodium cholate. Prior to immobilization on SPR sensor chips the phospholipid nanodiscs were dialyzed against 20 mM HEPES pH 7.6 and 0.1 M NaCl. The immobilization was carried out on one flowcell of the CM5 sensor chip (Biacore) using EDC and NHS to obtain a maximum 6000 RU using the immobilization wizard on the Biacore T100 control software. Ethanolamine was immobilized on the control flowcell of the same sensor chip for referencing purposes. Before each run, the running buffer was applied to the sensor chip for equilibration. The affinity wizard was used for binding and dissociation tests. All experiments were performed at 25 ºC with a flow rate of 10 μL/min and a contact time of 240 s. The regeneration time and dissociation time were set to 30 s and 240 s, respectively. A solution of 2 M NaCl was used to regenerate the sensor chips. After successive rounds of association and dissociation the response was adjusted to baseline using the regeneration procedure. Microsoft Excel was used to analyze the sensorgrams.

2.3 Results

2.3.1 Interaction of the HVR with the catalytic domain of K-Ras4B.

We previously found that the interaction of calmodulin with the HVR of K-Ras4B is inhibited upon GDP binding (106). This observation led us to hypothesize that the catalytic domain of K-Ras4B-GDP might sequester the HVR, making it unavailable for protein-protein interactions. To

test the hypothesis that HVR interacts with the rest of K-Ras4B and nucleotide binding plays a role in HVR function, we compared the ^{1}H-^{15}N HSQC spectra of K-Ras4B and K-Ras4B$_{1-166}$ in the GDP- and GTP-bound states (Figure 2.1). NMR was used, since attempts to crystallize full-length K-Ras4B were unsuccessful. Spectral comparison revealed residues with significant chemical shift perturbations (CSPs) caused by HVR. The residues were mapped on the crystal structures of GDP- and GTP-bound K-Ras catalytic domains (Figure 2.1 A, B, C and D). Most of the changes occur in the Switch I and effector binding regions, β2, and in the C-terminal helix, α5 (Figure 2.2A and B; the Ras domain and functional sites are shown in Figure 1.1). This suggests that in the GDP-bound state, the C-terminal HVR interacts extensively with the catalytic domain. Conversely, when K-Ras4B is GTP-γ-S bound, only very few changes are observed in the Switch I and effector binding regions (I36) and in the adjacent N-terminal portion (S17 and A18) (Figure 2.2).

A

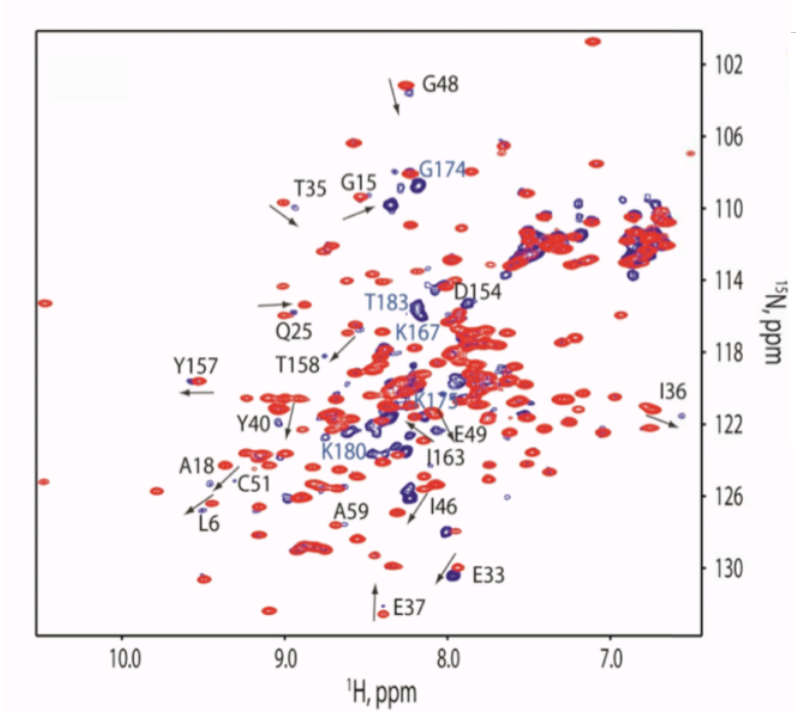
G48
G174
T35
G15
T183
D154
Q25
K167
Y157
T158
I36
Y40
E49
K180
I163
A18
C51
A59
I46
L6
E33
E37
102
106
110
114
118
122
126
130
15N, ppm
10.0
9.0
8.0
7.0
1H, ppm

B

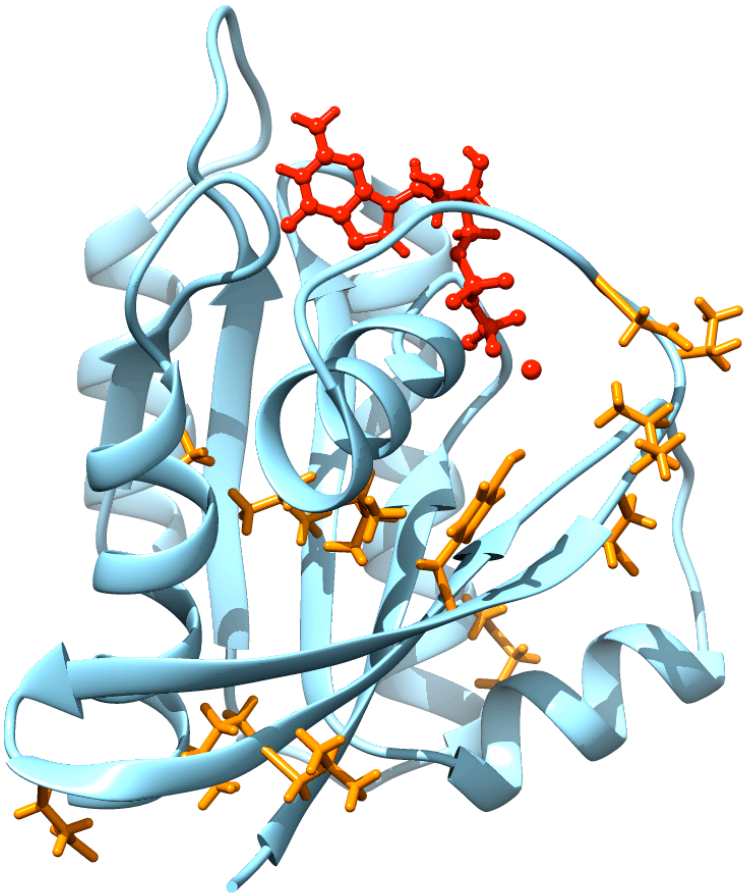

C

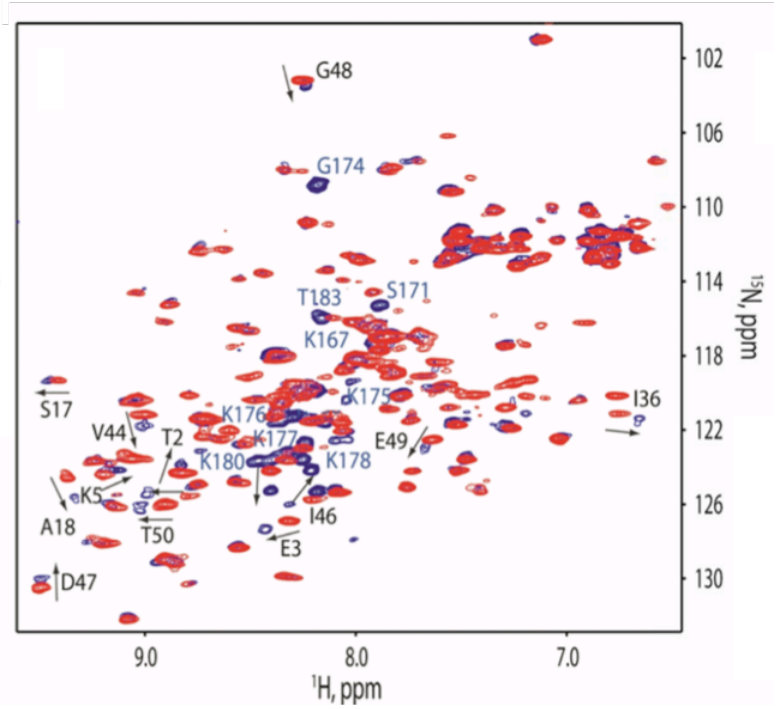
G48
G174
T183
S171
K167
K175
I36
S17
K176
V44
T2
K177
E49
K180
K178
K5
I46
A18
T50
E3
D47
102
106
110
114
118
122
126
130
^{15}N, ppm
9.0
8.0
7.0
^{1}H, ppm

D

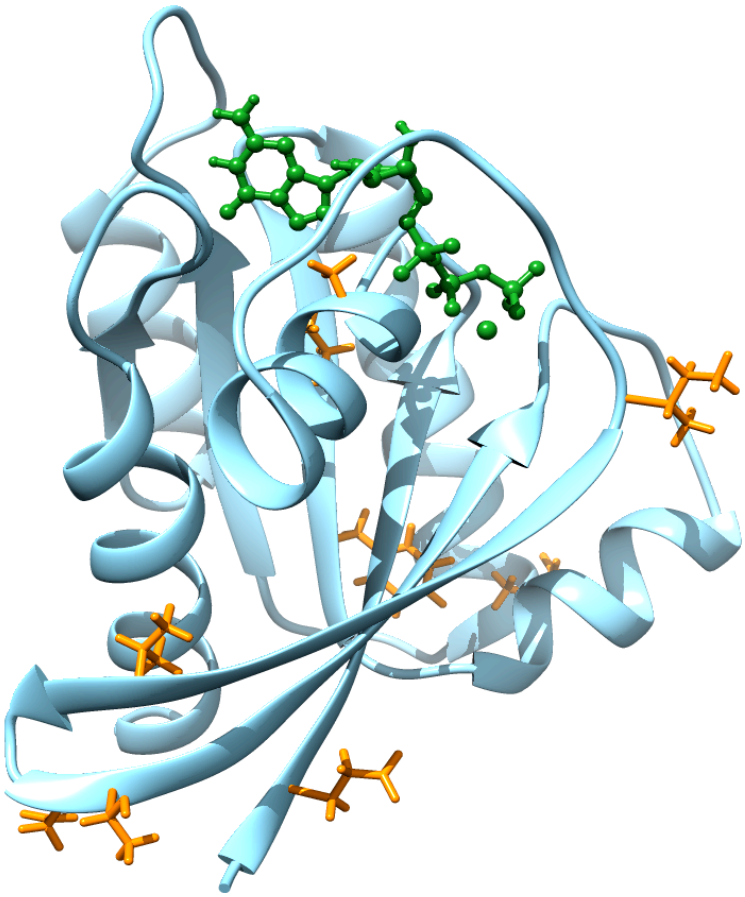

Figure 2.1: NMR chemical shift perturbations of residues induced by the HVR on the catalytic domain of K-Ras4B.
Superimpositions of ^{1}H-^{15}N HSQC spectra of (A) full-length K-Ras4B (blue, 0.78 mM) and truncated K-Ras4B$_{1-166}$ (red, 1 mM) in the GDP-bound states, and (B) mapping of the perturbed residues on the structure of the GDP-bound K-Ras4B catalytic domain. Superimpositions of ^{1}H-^{15}N HSQC spectra of (C) full-length K-Ras4B (blue, 0.5 mM) and truncated K-Ras4B$_{1-166}$ (red, 0.4 mM) in the GTP-γ-S-bound states, and (D) mapping of the perturbed residues on the catalytic domain structure of GTP-bound K-Ras4B. Examples of chemical shift perturbations are marked with arrows and resonance assignments. New resonances in the spectrum of full-length K-Ras4B represent the HVR and are shown in blue. These experiments were performed using a 900 Mhz Bruker Avance Spectrophotometer.

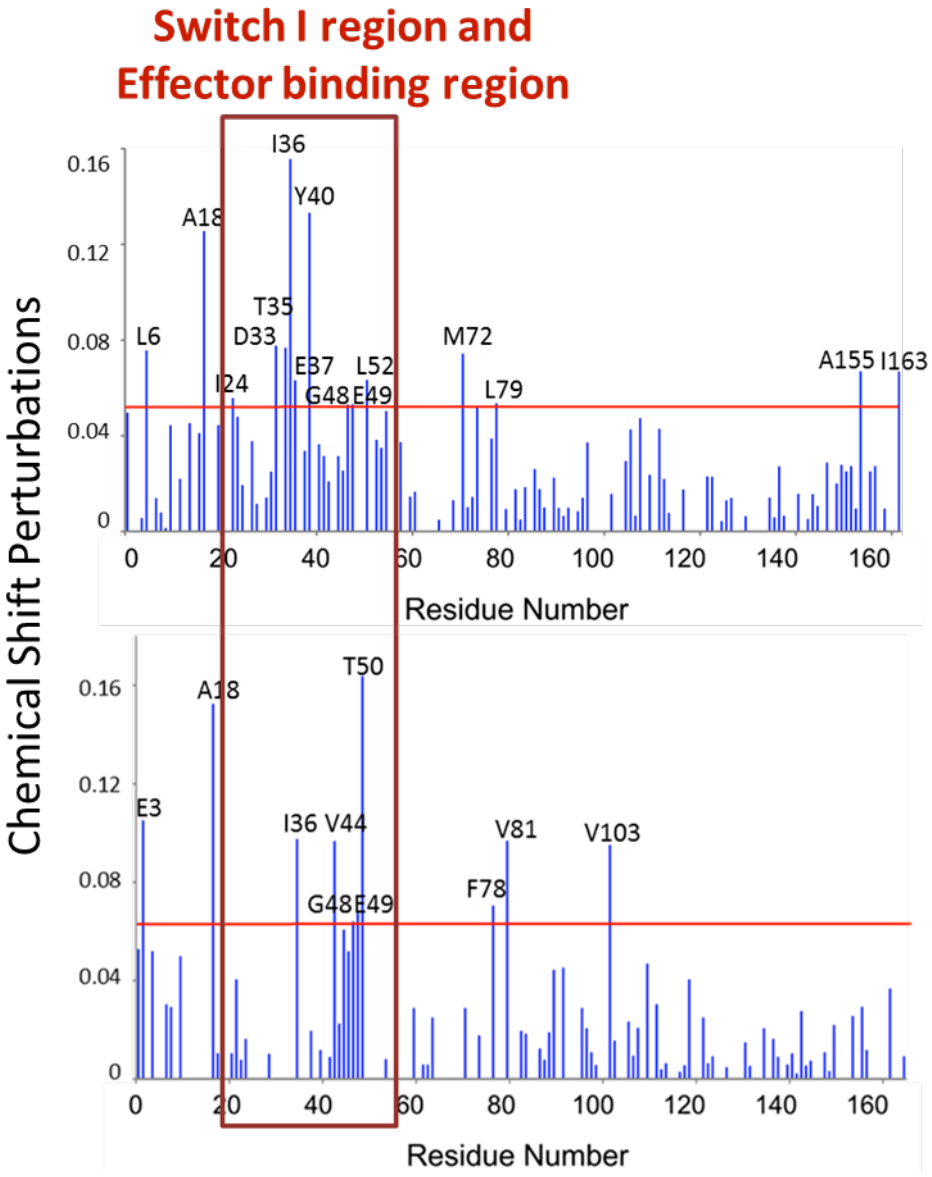

Figure 2.2: Residual chemical shifts obtained after the overlay of ^{15}N HSQC NMR spectra of truncated and full-length K-Ras4B in its GDP and GTP loaded states.
Overlay of full length K-Ras4B-GDP and that of K-Ras4B$_{1-166}$-GDP is shown in the upper panel. Overlay of full length K-Ras4B-GTP-γ-s and that of K-Ras4B$_{1-166}$-GTP-γ-s is shown in the lower panel. The horizontal line in the graphs shows the sum of average CSP and standard deviation. Residues that show zero chemical shift difference on the graph were the ones that were not assigned due to resonance overlap.

2.3.2 K-Ras4B HVR analogs interact with K-Ras$_{1-166}$ with high affinity.

To establish if the hypothesis that the HVR interacts with the catalytic domain was correct, we carried out binding studies of the HVR with the catalytic domain using microscale thermophoresis. We generated a K-Ras4B HVR synthetic analog (Ac-KEKL$_N$SKDGKKKKKKSKTK-NH$_2$). Microscale Thermophoresis (MST) (194, 195) revealed that the peptide interacts better with GDP- than with GTP-γ-S-bound K-Ras$_{1-166}$, with dissociation constants, K_D, of 250.0 ± 33.4 nM and 18.6 ± 0.9 μM, respectively (Figure 2.3). The interaction appeared sequence-specific. Substitution of just one residue, D173 with proline (Ac-KEKL$_N$SKPGKKKKKKSKTK-NH$_2$) abolished the interaction. In addition, phosphorylation of Ser181 (Ac-KEKL$_N$SKDGKKKKKKS(PO$_4$)KTK-NH$_2$), a post translational modification known to regulate K-Ras4B activity and its interaction with calmodulin (196, 197) prevents binding of HVR to the catalytic domain as shown in Figure 2.3. To determine if membrane interaction prevents the HVR from binding the G-domain, we performed binding studies for the lipidated K-Ras4B HVR analog (Ac-KEKL$_N$SKDGKKKKKKSKTKK-ε-Pal-NH$_2$) in the presence of membrane-mimicking nanodiscs as shown in Figure 2.4. Membrane anchoring of the HVR analog had no significant effect on its interaction with truncated K-Ras4B$_{1-166}$-GDP (K_D = 230.0 ± 22.1 nM).

To further probe the specificity of this interaction between HVR and the catalytic domain of K-Ras4B-GDP, we added an excess (1.5 molar equivalents) of the HVR peptide to ^{15}N-enriched K-Ras4B$_{1-166}$-GDP. ^{15}N HSQC spectra for K-Ras4B$_{1-166}$-GDP with and without the peptide were compared. The results highlight resonances for D30, Y32, I36 and T158, and four side chains (Figure 2.5 A). The CSPs induced by the HVR in the full-length and truncated proteins concentrate in the same area, namely the Switch I, effector binding region and helix α5.

Moreover, comparison of side-chain resonances in the ε-NH region of the spectra indicates striking similarities between chemical shifts in K-Ras_{1-166}-GDP bound to the HVR peptide and in K-Ras4B-GDP. The similarity of CSPs induced by HVR peptide addition (Figure 2.5 B) and those induced by HVR in the full-length protein (Figure 2.5 C) indicates the specificity of HVR to the catalytic domain of K-Ras4B-GDP. NMR-based structural determination of full-length K-Ras was difficult due to significant resonance line-broadening caused by conformational exchanges.

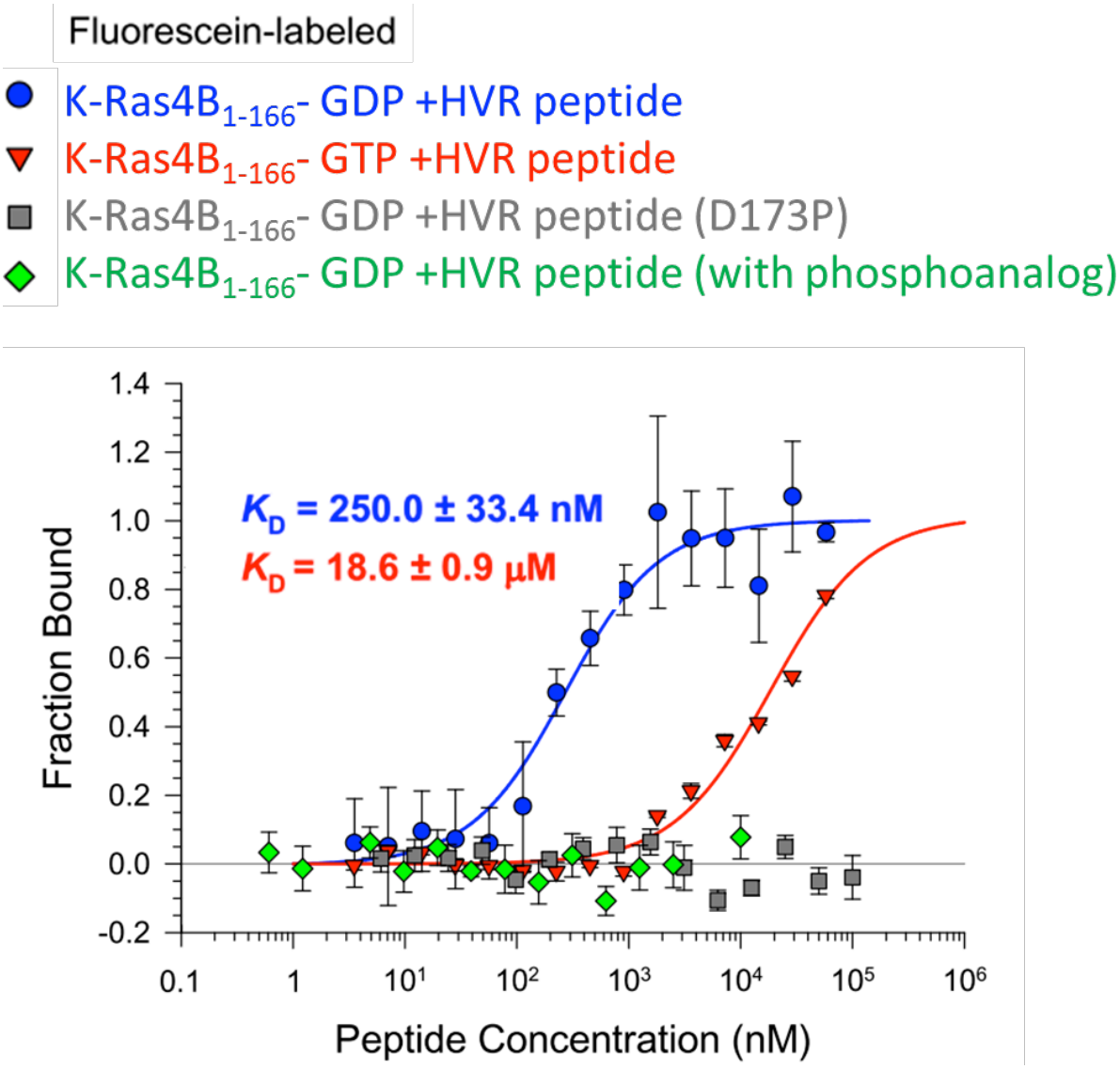

Figure 2.3: K-Ras4B HVR peptides interact with recombinant truncated K-Ras$_{1-166}$.
The interaction was characterized with the help of Microscale Thermophoresis (MST) using recombinant K-Ras$_{1-166}$ that was labeled on Cys118 with fluorescein maleimide. GDP-bound and GTP-γ-S-bound proteins have been titrated with synthetic HVR analog, its variant having D173P substitution, and another variant containing a phosphorylated analog.

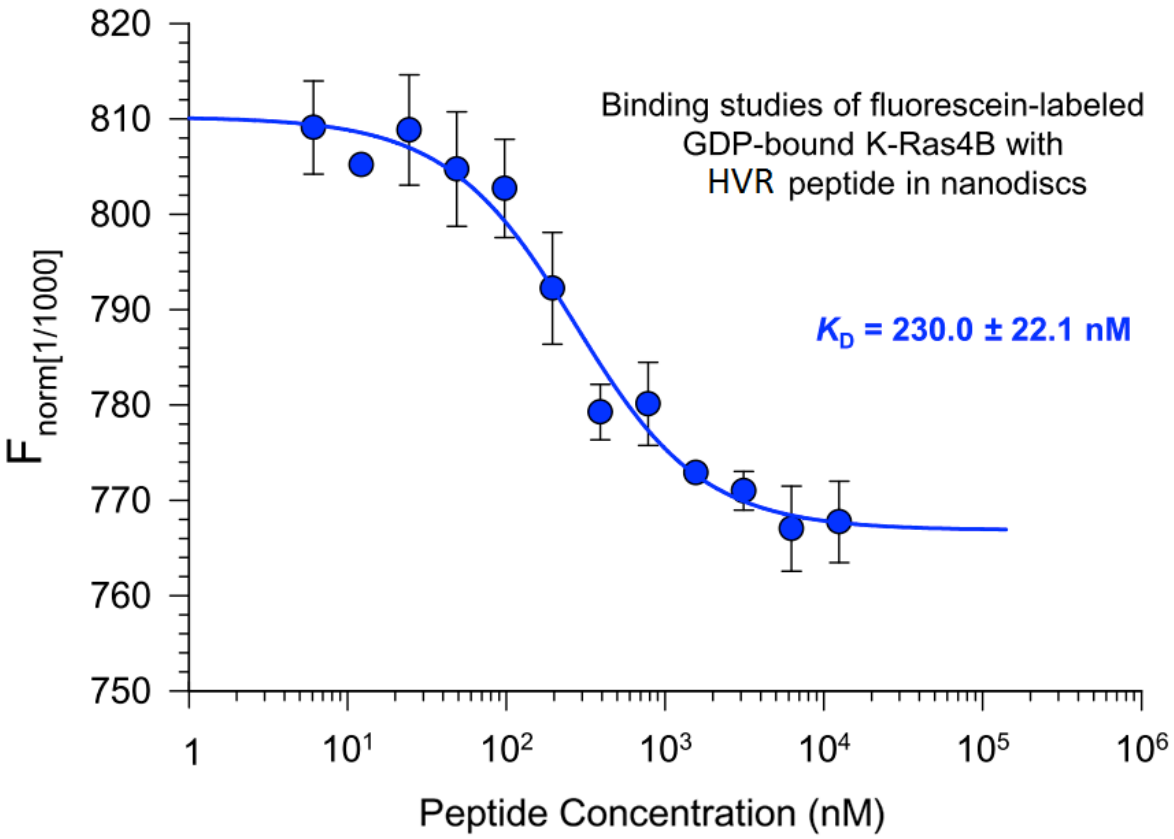

Figure 2.4: Lipidated HVR binds to K-Ras4B-GDP in the presence of membrane nanodiscs.
Palmitoylated HVR analog showed high affinity binding to GDP-loaded K-Ras$_{1\text{-}166}$ in the presence of membrane-mimicking nanodiscs.

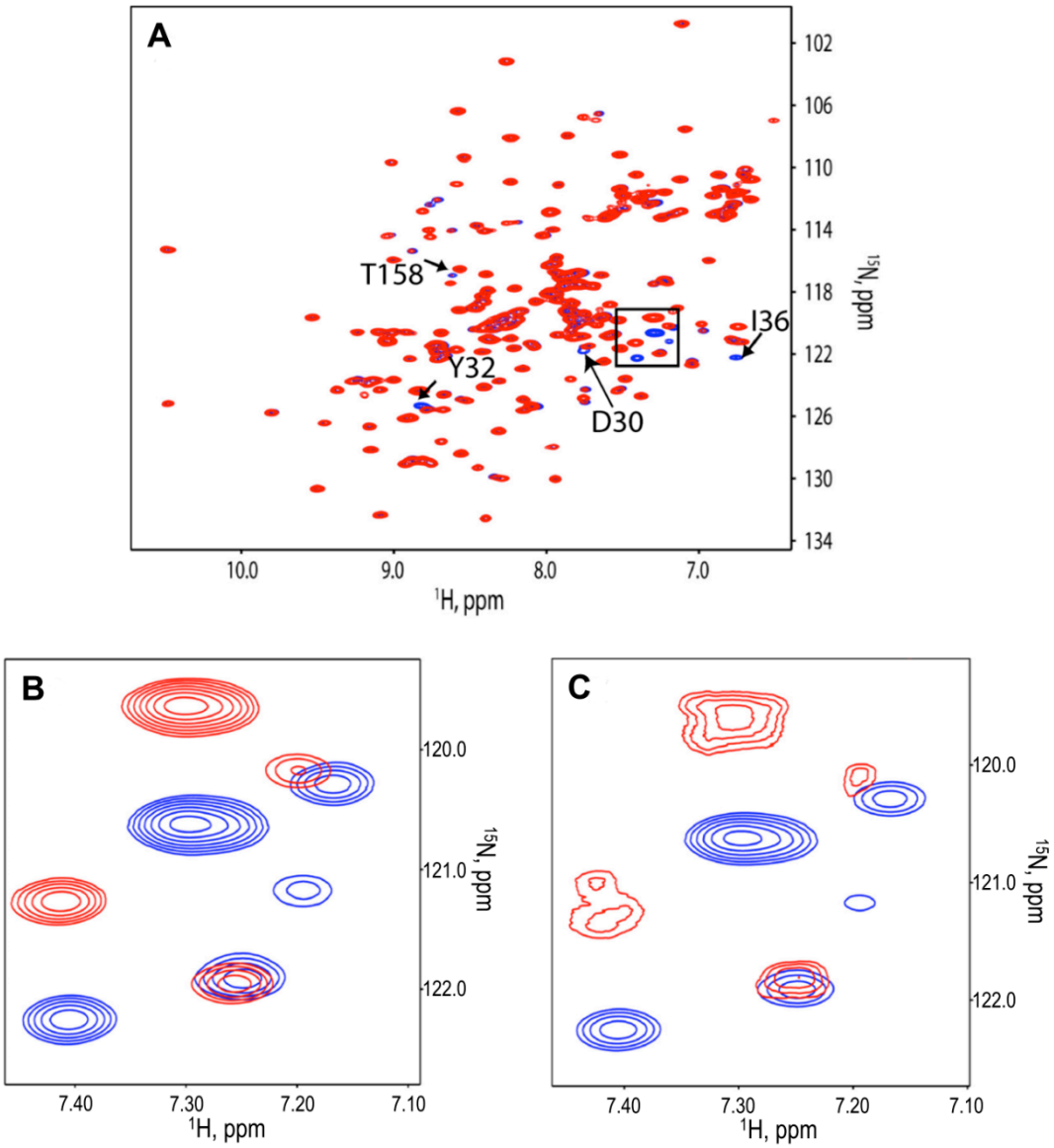

Figure 2.5: Investigation by NMR of interactions of the HVR with the GDP-bound state of the catalytic domain of K-Ras.

(A) A superimposition of ^{15}N HSQC spectra of GDP-bound K-Ras$_{1\text{-}166}$ in the absence (blue) and in the presence of 1.5 molar equivalents of the HVR peptide (red). Examples of chemical shift perturbations are marked by arrows. Zoomed-in ε-NH regions in spectral superimpositions of (B) GDP-bound K-Ras4B$_{1\text{-}166}$ in the absence (blue) and in the presence of 1.5 molar equivalents of the HVR peptide (red) and (C) full-length GDP-bound K-Ras4B (red, 0.4 mM) and GDP-bound K-Ras4B$_{1\text{-}166}$ (blue, 1 mM). These experiments were performed using a 600 Mhz Bruker Avance Spectrophotometer.

2.3.3 MD simulations of the HVR interaction with the catalytic domain.

To obtain structural details of the HVR interaction with the GDP-bound catalytic domain, we performed all-atoms molecular dynamics (MD) simulations (185, 188) on K-Ras4B$_{1-185}$ and K-Ras4B$_{1-166}$ in an aqueous environment. The crystal structures of the GDP- and GTP-bound catalytic domains, which are almost identical (Figure 2.6 A), were used to generate four different initial configurations based on the NMR CSP data (Figure 2.6 B and C). During the initial generation, the HVR chain folded over residues presenting highly perturbed NMR chemical shifts. Four independent simulations for each nucleotide with the full-length as well as truncated Ras proteins as controls were carried out. Three of the four configurations retain the HVR on the catalytic domain of K-Ras4B-GDP, while only one out of four retains the HVR on K-Ras4B-GTP, marginally interacting with the catalytic domain (Figure 2.7 A and B). We calculated the interaction energy of the HVR with the catalytic domain to determine the best candidate for the structural model of folded HVR. The interactions of the HVR with the catalytic domain are mainly driven by electrostatics and reveal stronger attraction in K-Ras4B-GDP as compared to the GTP counterpart (Figure 2.7 C and D). Based on these data, we designated both configurations 3 of K-Ras4B-GDP and K-Ras4B-GTP as the best model conformations of HVR interacting with the catalytic domain. The analysis presented below is for those configurations. The catalytic domain is highly conserved during the simulations, with root-mean-squared deviation (RMSD) less than 1.0Å relative to the starting point for K-Ras4B$_{1-166}$. Not surprisingly, the HVR populates a β-sheet in the GDP-bound state which is not the case for the GTP-bound state (Figure 2.8 A and B). Higher occupancy of a β-strand conformation in the S171- D173 region in the GDP-bound state can be observed. HVR residues S171, K172, and D173 form an antiparallel β-sheet motif, which extends the β-sheet network of residues K42, Q43, and V44.

Especially, D173 forms a salt bridge with K42, stabilizing the HVR β-sheet. Shifts in the HVR β-strand location are possible. This β2-strand is in the effector interaction site, with the HVR antiparallel β-sheet mimicking the common Ras effector-binding motif. Although at $t \sim 30$ ns the lysine cluster (residues 175-180) forms a transient α-helix in the GDP-bound state, it mostly remains unstructured during the GTP-bound state simulations (Figure 2.8 A). To complement the NMR CSPs, we calculated the combined CSPs (198, 199), mapping them over K-Ras4B$_{1\text{-}166}$. In the GDP-bound state, many residues exhibit perturbations, especially in the Switch I and effector binding regions, in agreement with the NMR results (Figure 2.9 A and B). In the GTP-bound state, fewer residues are perturbed, suggesting loose HVR-catalytic domain interaction.

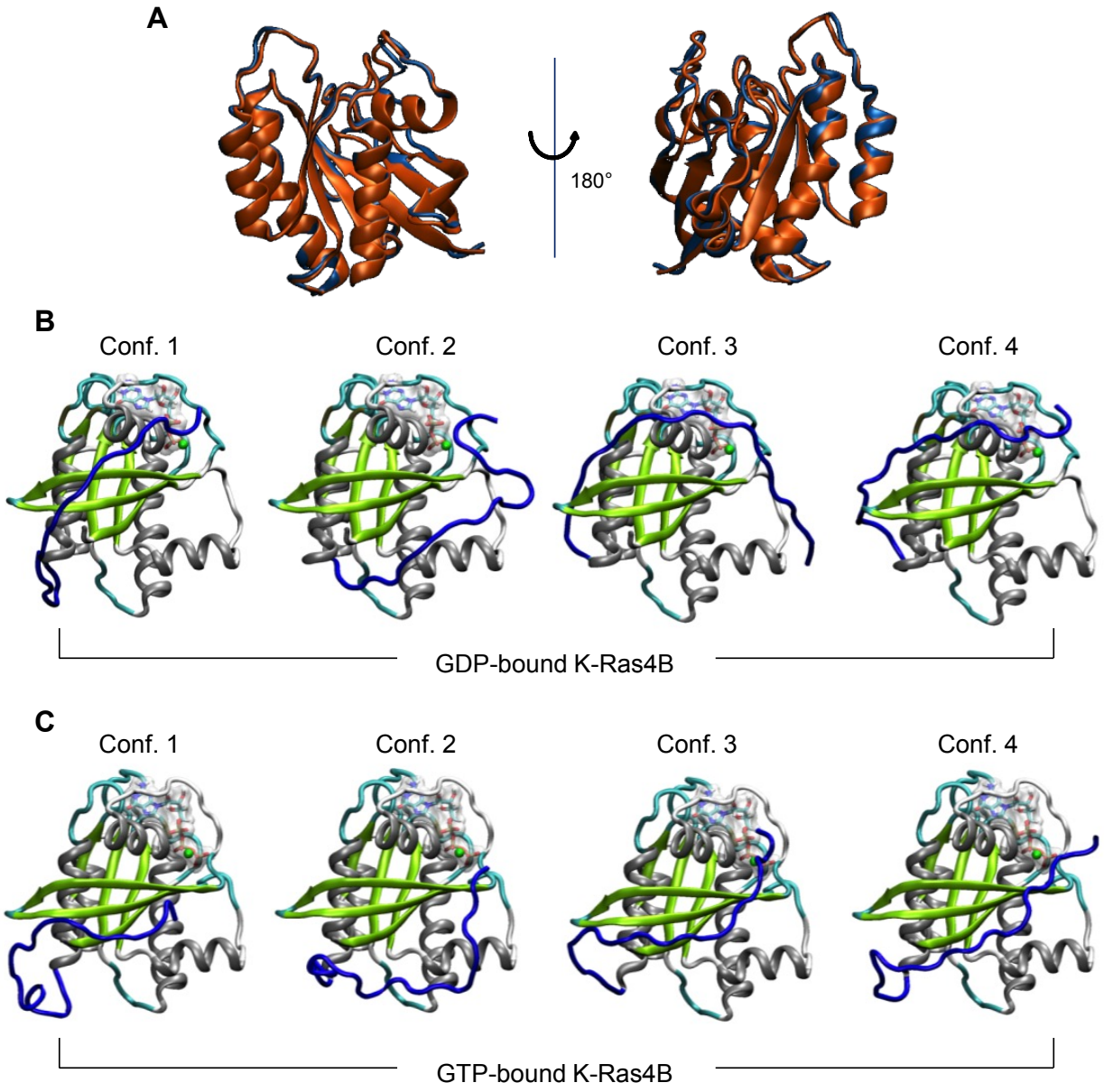

Figure 2.6: The molecular dynamics (MD) simulations based on the crystal structures and NMR data.
(A) Superimposition of the crystal structures for the GDP-bound (PDB code: 4EPT, light blue) and GTP-bound (PDB code: 3GFT, orange) K-Ras4B$_{1\text{-}166}$. For the full-length K-Ras4B with HVR, initial coordinates of the catalytic domain were taken from the Ras crystal structures representing the (B) GDP-bound and (C) GTP-bound states of K-Ras4B. The covalently connected HVRs (HVRs) were modeled and folded onto the catalytic domain using the interactive molecular dynamics (IMD). The initial locations of the HVR were based on the NMR chemical shift perturbations. In the catalytic domain, the α-helix and β-sheet secondary structures are colored gray and yellow, respectively, and the HVR is colored blue.

A GDP-bound K-Ras4B

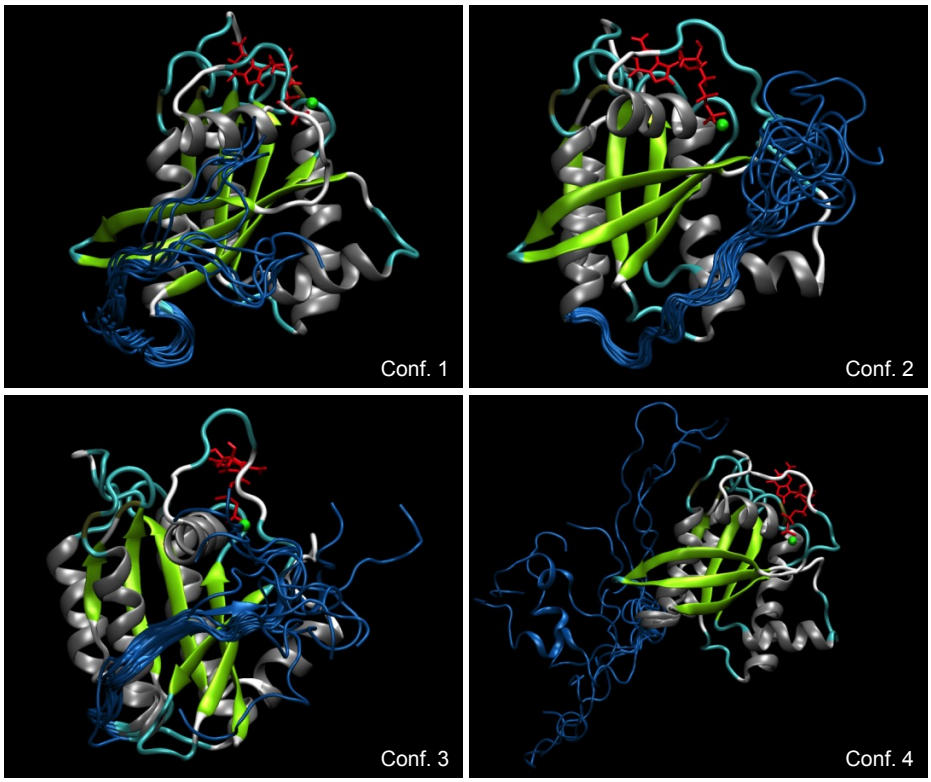

B GTP-bound K-Ras4B

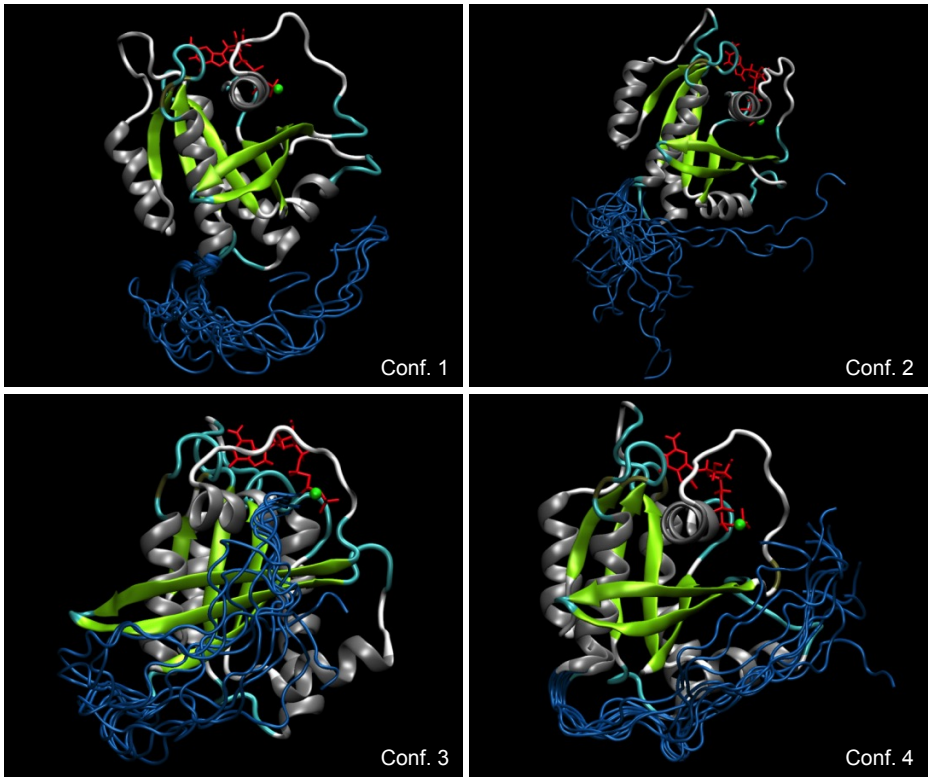

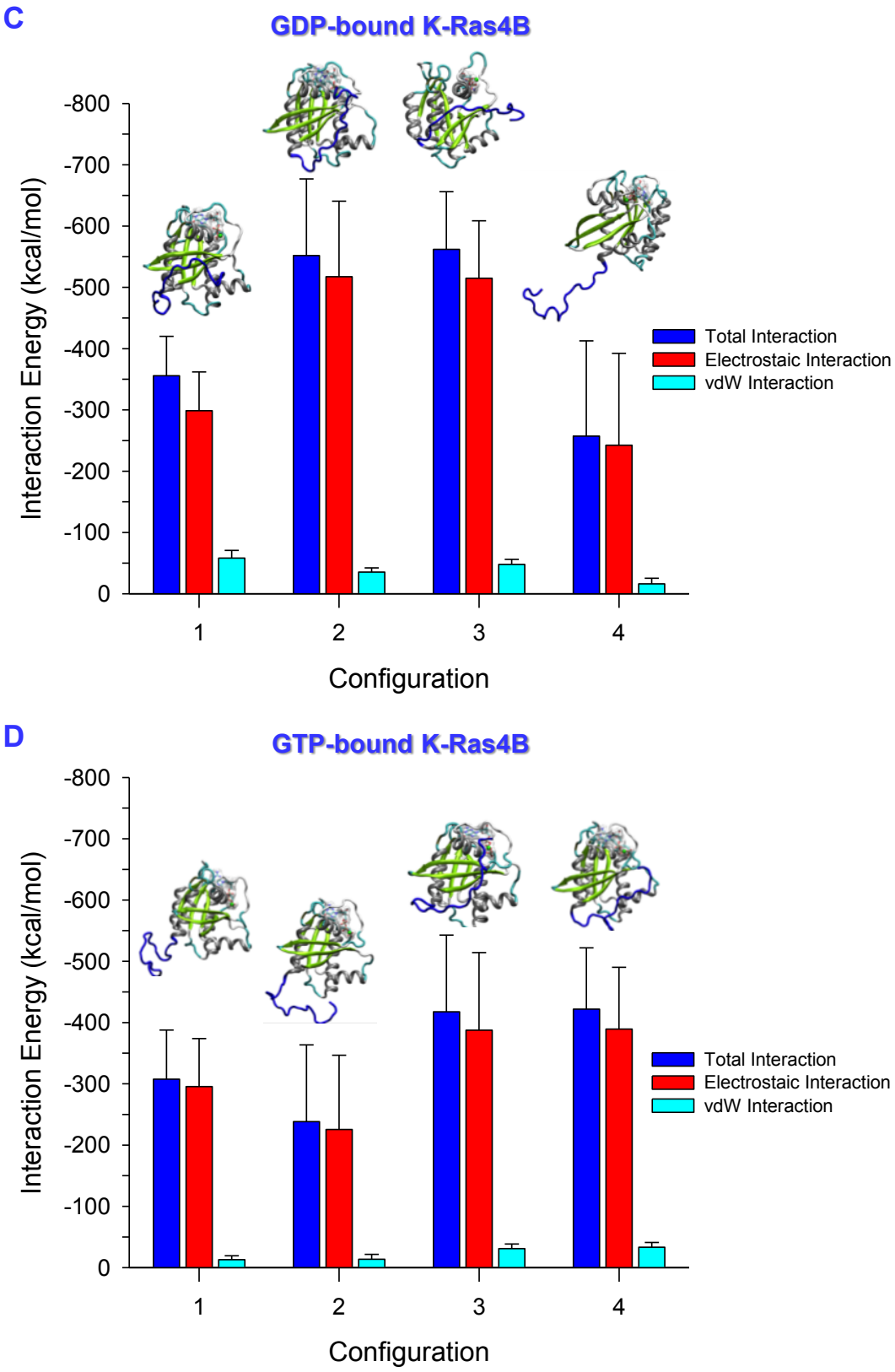
C
GDP-bound K-Ras4B
Interaction Energy (kcal/mol)
-800
-700
-600
-500
-400
-300
-200
-100
0
1
2
3
4
Configuration
Total Interaction
Electrostaic Interaction
vdW Interaction
D
GTP-bound K-Ras4B
Interaction Energy (kcal/mol)
-800
-700
-600
-500
-400
-300
-200
-100
0
1
2
3
4
Configuration
Total Interaction
Electrostaic Interaction
vdW Interaction

Figure 2.7: Structures of full-length K-Ras4B in the aqueous environments.
Ensembles of HVR structures sampled at each 10 ns simulation are shown on the averaged catalytic domain structures of K-Ras4B over 100 ns molecular dynamics (MD) simulations in the (A) GDP-bound and (B) GTP-bound states. In the catalytic domain, the α-helix and β-sheet secondary structures are colored gray and yellow, respectively, and the HVR is colored blue. Averaged total interaction energy (blue bars) of HVR with the catalytic domain, and the contributions from the electrostatic (red bars) and vdW (cyan bars) interactions for four different configurations of K-Ras4B in the (C) GDP-bound and (D) GTP-bound states. Averaged protein structures are embedded on the corresponding configuration bars. Interactions of HVR with the catalytic domain are mainly driven by electrostatics and reveal stronger attraction in GDP-K-Ras4B as compared to the GTP counterpart. Based on these data, we designated configuration 3 K-Ras4B-GDP and configuration 3 K-Ras4B-GTP for the best model conformations of HVR interacting with the catalytic domain.

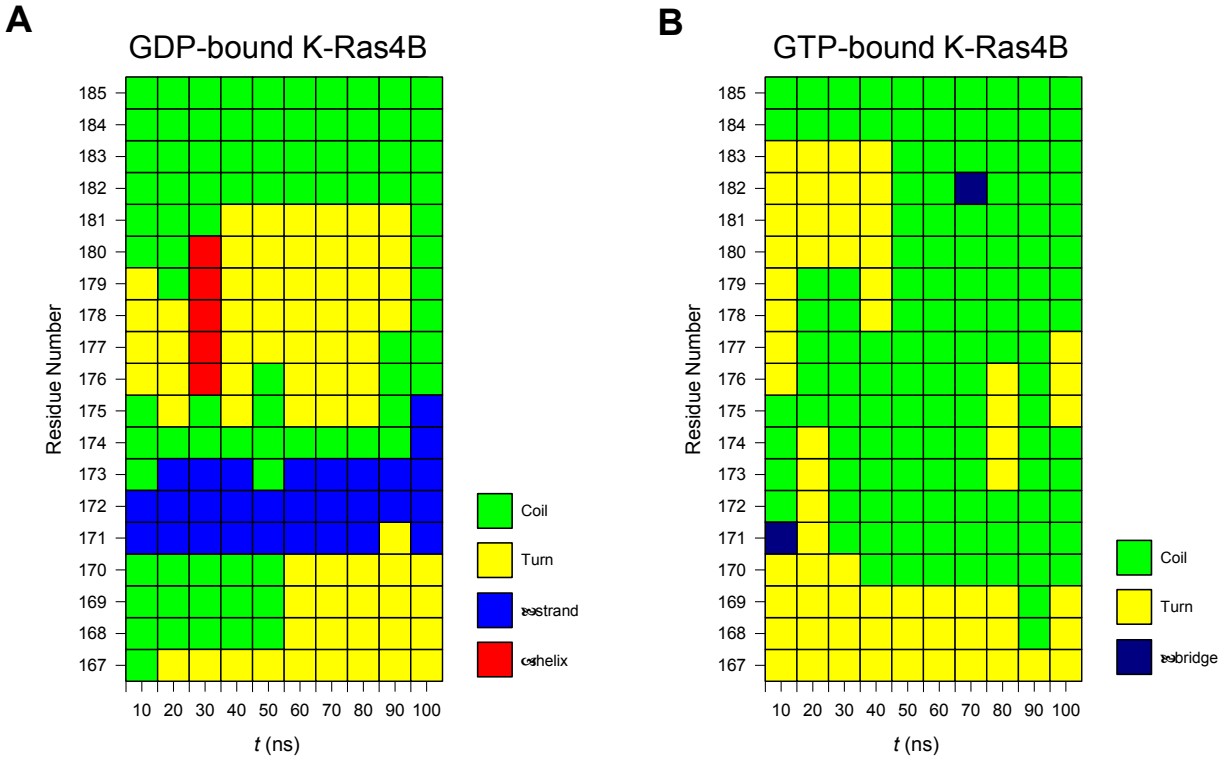

Figure 2.8: Investigation of the secondary structure for the HVR of K-Ras4B.
Descriptions of the HVR secondary structure by STRIDE (200) averaged over each 10 ns interval for (A) GDP-bound (conf. 3) and (B) GTP-bound (conf. 3) K-Ras4B.

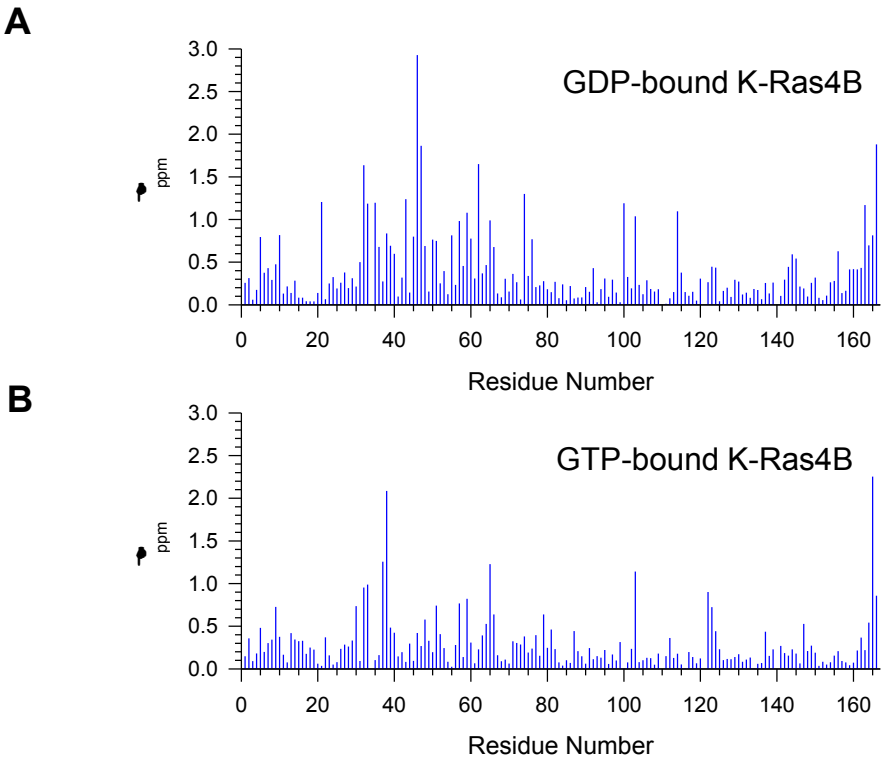

Figure 2.9: Theoretical estimations of the chemical shift perturbations (CSPs) with the NMR CSPs.

ShiftX (201) program was used to calculate ^{1}H, ^{13}C, and ^{15}N chemical shifts. The combined CSPs for the full-length K-Ras4B with respect to K-Ras4B$_{1\text{-}166}$ during the simulations were calculated using the equation (202) $\Delta_{ppm} = \sqrt{(\Delta\delta_{HN})^2 + 6(\Delta\delta_N \alpha_N)^2}$, where α_N is a scaling factor with a value 0.17, for the (A) GDP-bound (conf. 3) and (B) GTP-bound (conf. 3).

2.3.4 The HVR interacts with the catalytic domain of K-Ras4B in the GDP-bound state and released in the GTP-bound state.

To provide further validation for our NMR data and the computations we analyzed the effect of HVR mutations K180A and K182A on the structure of the catalytic domain. We reasoned that any change in the structure of HVR should have an effect on the catalytic domain of K-Ras4B-GDP if the HVR is indeed sequestered by the Switch I region. HVR mutations K180A and K182A caused significant CSPs in the Switch I region of K-Ras4B-GDP. We performed additional ^{15}N HSQC NMR experiments on HVR point mutants, K180A and K182A, in the GDP-bound state. CSPs were obtained by comparing the spectra of the K180A (Figure 2.10 A and B) and K182A (Figure 2.10 C and D) mutants with the spectrum of wild-type K-Ras4B-GDP. We observed significant CSPs in the Switch I region (residues 30-38) and α1 helix (residues 16-26). In both cases, E37 exhibited the highest CSPs, suggesting that these lysine residues are involved in HVR sequestration by the catalytic domain. The K180 and K182 residues are relatively far removed from the HVR attachment to the catalytic domain and are expected to have a reduced effect on HVR sequestration. An HVR mutation in the region closer to the catalytic domain is expected to more significantly perturb the chemical shifts in the catalytic domain than the K180A and K182A mutations. To test this hypothesis, we prepared K-Ras4B$_{1\text{-}188}$-GDP bearing a K175A mutation in the HVR. Comparison of NMR chemical shift differences between the mutant and wild type full-length proteins revealed larger and more numerous CSPs caused by the K175A than those caused by the K180A and K182A mutations (Figure 2.11). These data suggest that the K175A mutation induces a significant disruption of the HVR-catalytic domain interaction. HVR mutations affect the chemical shifts in the GDP-bound catalytic domain. To test the possibility that mutations in the catalytic domain might also alter

chemical shifts in the HVR we compared NMR chemical shifts of the full-length G12D mutant of K-Ras4B-GDP and the wild type GDP-bound protein. The G12D mutation of K-Ras4B occurs most frequently in cancer (203). Our analysis identified statistically significant CSPs in K178 and K179 residues within the HVR (Figure 2.12). This observation suggests that the conformational changes induced by the G12D mutation alter the interaction of HVR with the catalytic domain.

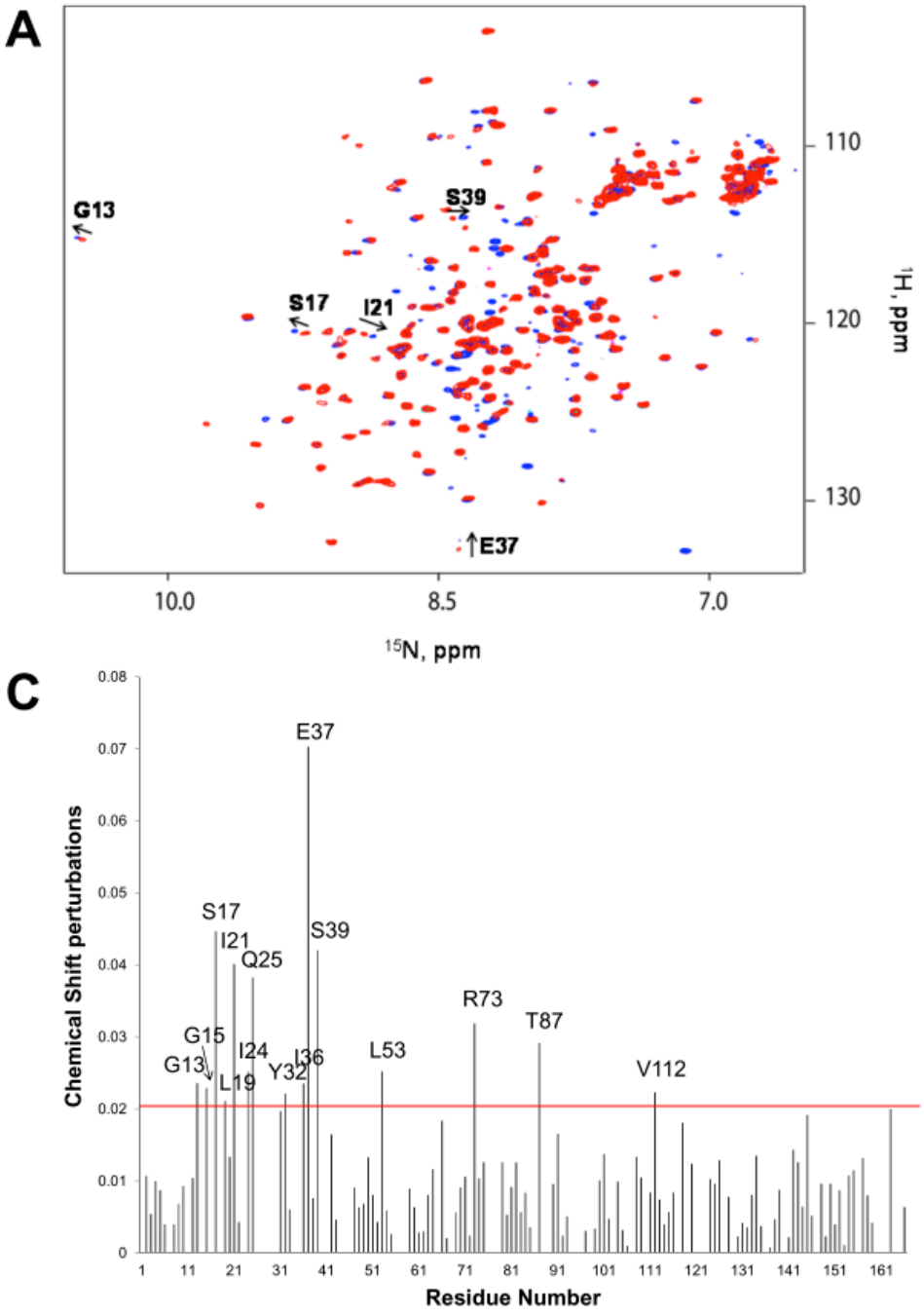
A
G13
S39
S17
I21
E37
110
120
130
^{1}H, ppm
10.0
8.5
7.0
^{15}N, ppm
C
Chemical Shift perturbations
0.08
0.07
0.06
0.05
0.04
0.03
0.02
0.01
0
E37
S17
I21
Q25
S39
R73
T87
G15
G13
I24
I36
L53
Y32
L19
V112
1
11
21
31
41
51
61
71
81
91
101
111
121
131
141
151
161
Residue Number

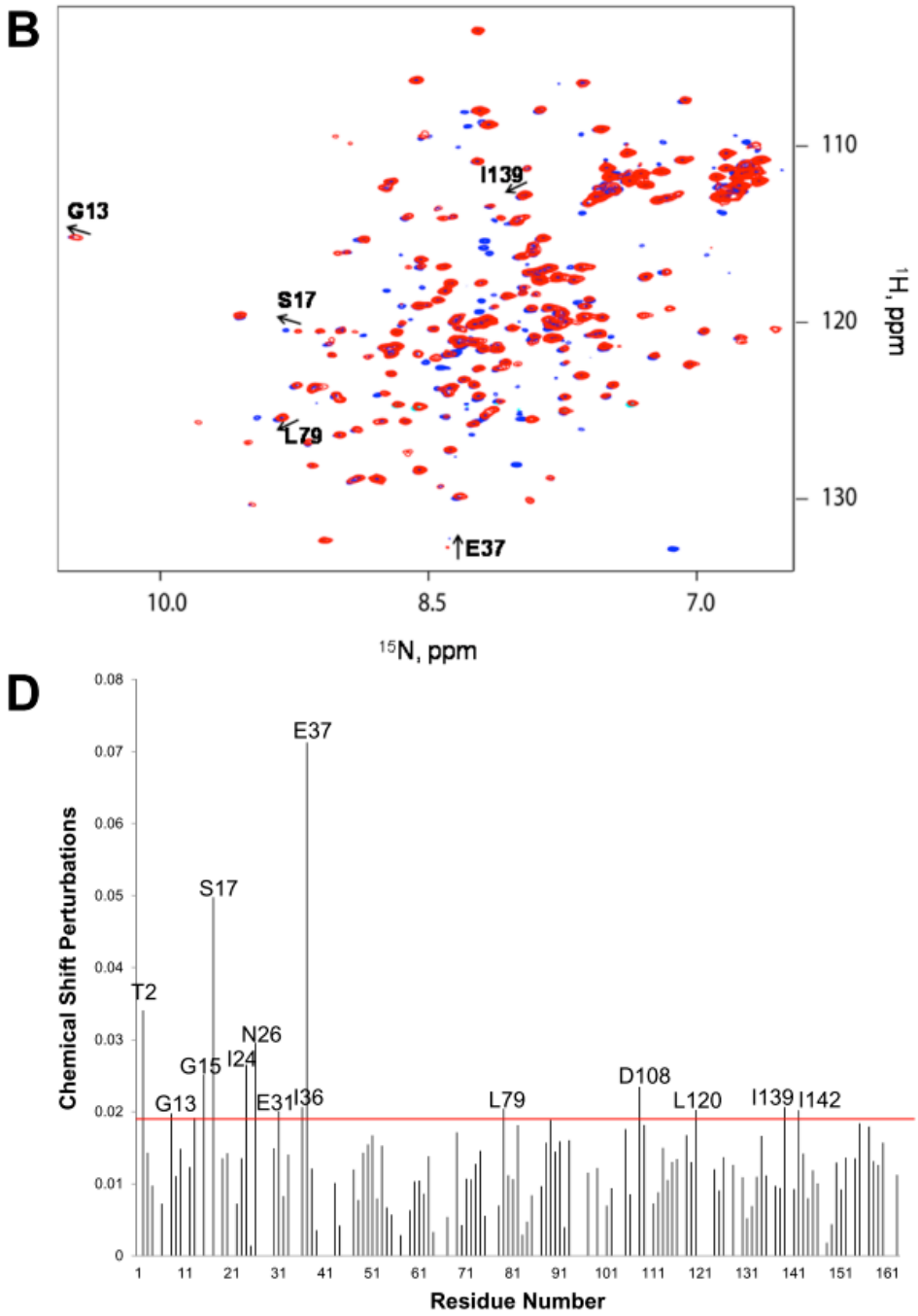

Figure 2.10: Chemical shift perturbations obtained after comparing K-Ras4B-GDP K180A and K182A mutants.

Overlays of ^{15}N-HSQC NMR spectra of full-length, wild-type K-Ras4B-GDP protein (blue) and (A) K180A and (B) K182A mutants of K-Ras4B-GDP (red). The CSPs measured from the spectra for (C) K180A and (D) K182A mutants. Examples of chemical shift changes are marked with arrows. The red horizontal line in the graph shows the sum of average CSP and one standard deviation. The names of residues exhibiting statistically significant (above the line) CSPs are marked.

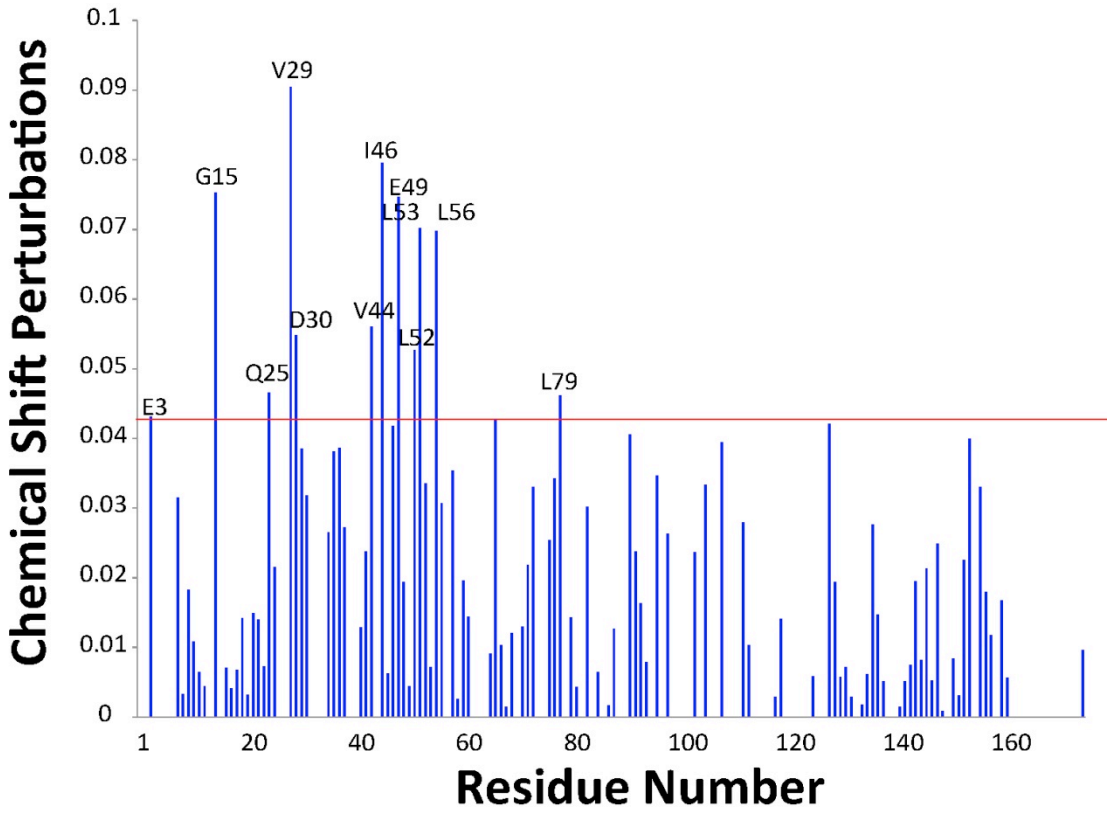

Figure 2.11: Chemical shift perturbations obtained upon overlaying K-Ras4B-GDP K175A and wild-type full length K-Ras4B-GDP.

The red horizontal line in the graph shows the sum of average and one standard deviation. The names of the residues exhibiting statistically significant CSPs are marked.

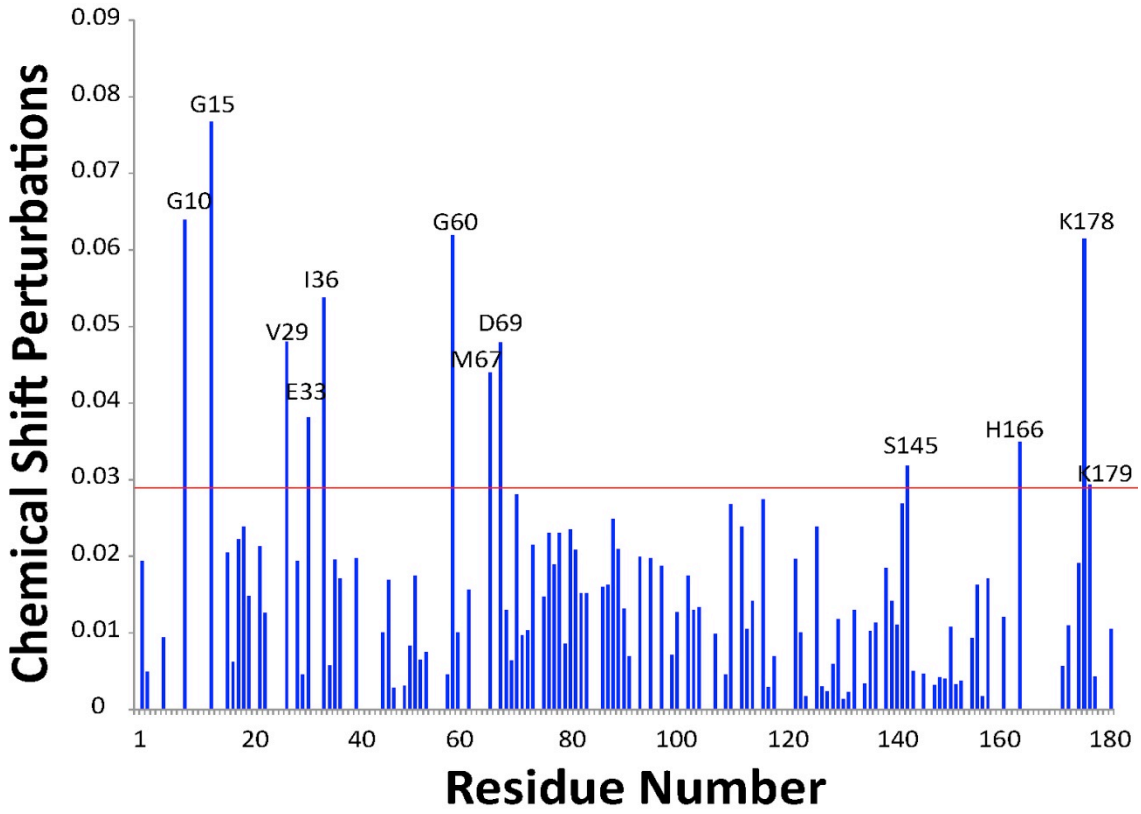

Figure 2.12: Chemical shift perturbations obtained upon overlaying K-Ras4B-GDP G12D and wild-type full length K-Ras4B-GDP.

The red horizontal line in the graph shows the sum of average and one standard deviation. The names of the residues exhibiting statistically significant CSPs are marked.

2.3.5 The interaction of the HVR with the catalytic domain decreases the binding affinity of the GDP-bound form of K-Ras4B to membrane phospholipids.

To test the effect of HVR sequestration in the GDP-bound form on the interaction with the plasma membrane phospholipids we performed a surface plasmon resonance (SPR) membrane binding assay on the GDP and GTP loaded K-Ras4B$_{1\text{-}188}$ (191). Different concentrations of either K-Ras4B$_{1\text{-}188}$-GDP or K-Ras4B$_{1\text{-}188}$-GTP-γ-S were individually titrated onto dipalmitoyl phosphatidyl choline nanodiscs immobilized on a CM5 sensor chip. Non-linear regression fits on the data points revealed that there is almost a 5-fold decrease in affinity for the nanodiscs when the protein is GDP-bound as compared to when it is GTP-γ-S-bound (Figure 2.13). The apparent K_D for K-Ras4B-GDP is 107.2 ± 6 μM, while K-Ras4B-GTP-γ-S has an apparent K_D of 24.0 ± 2 μM for DPPC nanodiscs. These values reflect the HVR-mediated binding to phospholipids. The membrane binding affinity may be higher when K-Ras4B is post-translationally lipidated and carboxymethylated. Our results suggest that the HVR sequestration in the GDP-bound state lowers the membrane binding affinity, while its release in the GTP-bound state allows for tighter association with phospholipids.

2.3.6 The interaction of HVR with the catalytic domain prevents low affinity Raf1 binding to K-Ras4B-GDP and slows down GEF-catalyzed nucleotide exchange.

Ras dependent activation of Raf-1 is initiated when its Ras binding domain (Raf-1 RBD) interacts with the effector region of Ras-GTP with nanomolar affinity. Raf-1 also binds to Ras-GDP with an affinity that is one hundred fold lower than that for Ras-GTP (77). HVR interacts with the catalytic domain through the effector binding site in K-Ras4B-GDP. To investigate the impact of HVR sequestration on Raf-1 interaction we performed the Raf-1 binding assay (191)

with the full-length and truncated forms of K-Ras4B-GTP-γ-S and K-Ras4B-GDP. The comparison of Raf-1 binding was done with K-Ras4B$_{1-166}$-GTP-γ-S against K-Ras4B$_{1-188}$-GTP-γ-S and with K-Ras4B$_{1-166}$-GDP against K-Ras4B$_{1-188}$-GDP (Figure 2.14). Our results demonstrate that full-length K-Ras4B-GDP binds Raf-1 RBD with 55% efficiency when compared to the catalytic domain of K-Ras4B-GDP. At the same time, the GTP-γ-S loaded catalytic domain of K-Ras4B showed slightly weaker binding as compared to the full length protein (127%).

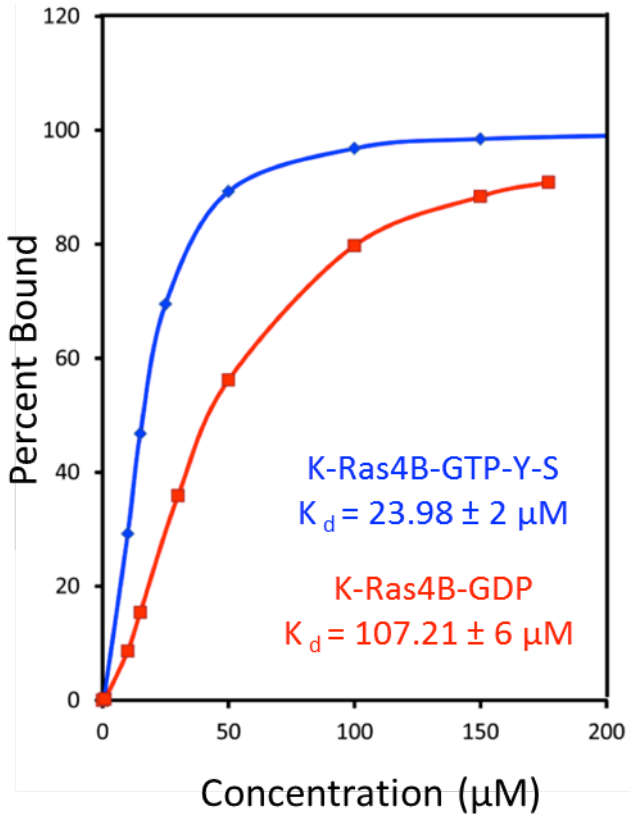

Figure 2.13: K-Ras4B-GTP-γ-S has a higher affinity for phospholipid bilayers than K-Ras4B-GDP.

Equilibrium dissociation constants were determined for K-Ras4B$_{1\text{-}188}$-GTP-γ-S and K-Ras4B$_{1\text{-}188}$-GDP from SPR titrations on DPPC nanodiscs. Non-linear regression analysis was used to fit the titration data of K-Ras4B$_{1\text{-}188}$-GTP-γ-S (blue) and K-Ras4B$_{1\text{-}188}$-GDP (red) onto DPPC nanodiscs immobilized on the CM5 SPR sensor chip. The K_D values obtained were 24.0 ± 2 µM and 107.2 ± 6 µM for the GTP-γ-S- and GDP-bound proteins respectively. The errors were determined using the "jack-knife" error analysis procedure.

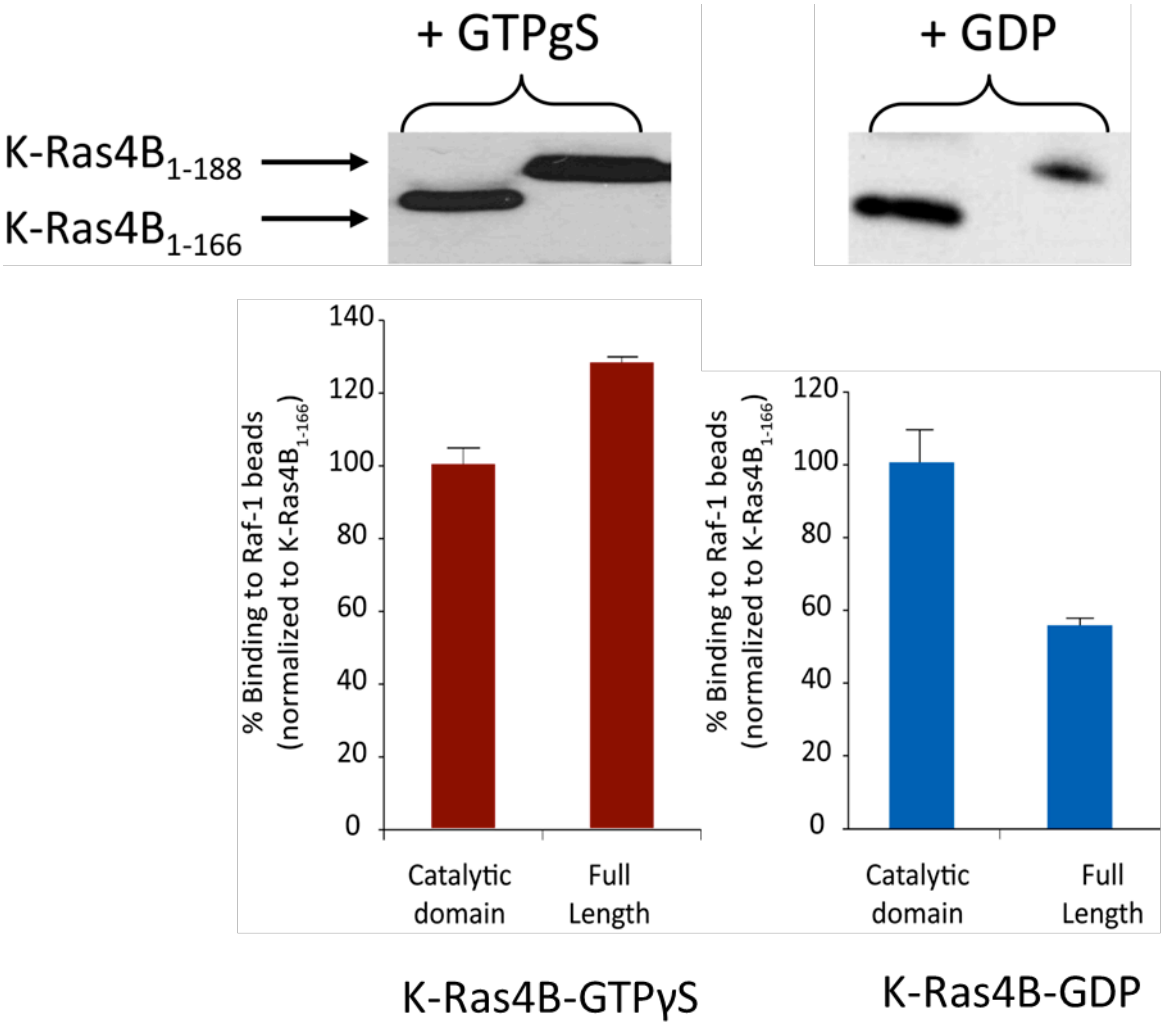

Figure 2.14: HVR binding to the catalytic domain reduces the interaction of Raf-1 Ras binding domain (RBD) with full-length K-Ras4B-GDP.
RBD pull down assay was used to determine the difference in binding of equal amounts of the catalytic domain (G-domain) and full-length versions of K-Ras4B in its GTP- as well as GDP-bound states. Data were normalized to G-domain. Percentage of RBD binding of K-Ras4B$_{1-188}$-GTP-γ-S was 127.8 ± 2% when normalized to K-Ras4B$_{1-166}$-GTP-γ-S binding (100.0 ± 5%). However, the percentage of RBD binding of K-Ras4B$_{1-188}$-GDP was only 55.2 ± 3.1% when compared to K-Ras4B$_{1-166}$-GDP binding (100.0 ± 10%). The Raf-1 RBD assay was carried out on GTP-γ-S- and GDP-loaded forms of the catalytic domain and full-length K-Ras4B. Raf-1 RBD pulldowns on the catalytic domain and full-length K-Ras4B in GTP-γ-S bound is shown in the top left panel. Raf-1 RBD pulldowns on the catalytic domain and full-length K-Ras4B in the GDP-bound state is shown in the top right panel. Statistical analyses for the pulldowns were carried out using ImageJ software and are shown below the respective panels.

2.4 Discussion

In order to successfully complete these experiments we had to produce significant amounts of recombinant K-Ras4B protein. A C-terminal His tag could have affected the interaction of the HVR hence we expressed and purified protein which contained an N-terminal His tag for these experiments. We used a published protocol for expression and purification of K-Ras4B (204). According to the protocol we use a high salt concentration and low induction temperature. These conditions engage osmotic shock response and cold shock response chaperones that assist in proper folding of K-Ras4B thereby increasing the yield of the protein. In the past, use of different physical lysis procedures like French press and sonication was tested by the previous lab members. However, due to aggregation of protein in the inclusion bodies, chemical lysis of cells using B-Per was found to be most efficient. In addition a second extraction is also employed which helps in extracting protein trapped in inclusion bodies. It has been observed that K-Ras4B tends to precipitate when it is not bound to a nucleotide hence the lysis procedures also involve use of nucleotides. Addition of magnesium is also essential since it is responsible for stabilizing the nucleotides bound to the protein. After the purification step, we carry out an additional nucleotide loading step in order to ensure that most protein species in solution contain the same nucleotide. Moreover, we used a slow hydrolyzing GTP analog, GTP-γ-S, in our experiments. This was done because GTP tends to hydrolyze quite rapidly to GDP in solution. Production of labelled protein is easily achieved using this protein purification procedure by replacing ammonium chloride in the medium with labelled ammonium chloride instead.

The HVR of K-Ras4B is a very flexible tail present on the C-terminal end of the protein. We started out asking the question: What role does HVR play in the active and inactive forms of K-Ras4B and why does CaM not bind K-Ras4B-GDP? To answer this, we compared the full length

structure of K-Ras4B with that of its catalytic domain. If the HVR was not affecting the catalytic domain, there would have been no change in the spectral comparison of the catalytic domain in the full length and truncated forms of the protein in both of its nucleotide loaded states. But since we found more prominent chemical shift perturbations in the catalytic domain of GDP loaded protein, we postulated that the HVR was interacting with the catalytic domain and hence decided to probe deeper into this interaction. From the MST data we found out that the HVR was indeed binding tightly with the GDP loaded catalytic domain when compared to its GTP counterpart. Moreover, this interaction was also found to be very specific as demonstrated by the mutant peptides in MST and the peptide titrations in NMR. In addition, the presence of a phosphate on the HVR abolishes this interaction. This observation falls in line with our hypothesis since a phosphate group is known to increase the activity of K-Ras4B (197).

In the simulations for K-Ras4B, although the overall conformation of the catalytic domain is preserved with RMSD less than 1.5Å, there are subtle structural rearrangements in the effector binding lobe, including Switch I, Switch II, helices α1 and α5, and β1-3 strands in K-Ras4B-GDP, and Switch I, Switch II, and helix α1 in K-Ras4B-GTP. Further, large structural differences are observed when the catalytic domains are compared between the full-length GDP- and GTP-bound states, in contrast to the truncated states. These differences are expected to favor HVR binding to the GDP-bound as compared to the GTP-bound Ras. This is in agreement with the MST and NMR data showing that the HVR is sequestered by the catalytic domain in GDP-bound K-Ras4B, but released in the GTP-bound state.

Perturbations of thermal fluctuations during the simulations for K-Ras4B with respect to K-Ras4B$_{1\text{-}166}$ also point to residues in β2, including the effector-binding region and Switch I and II,

as HVR binding sites. Interactions between the HVR and GDP-bound catalytic domain are transient, suggesting that multiple possible modes of interactions are common.

D173 lies in the putative beta strand in the HVR. When D173 is mutated to a proline, it interferes with the HVR binding proving that this region is extremely essential for the interaction. Likewise, K175A mutation lies close to the putative beta strand in the HVR. Since the K175A mutant of the HVR shows chemical shift perturbations when compared to full length wild type protein, it reinforces the idea of the beta strand stabilizing the HVR interaction with the catalytic domain. The NMR experiments with the G12D mutant of K-Ras4B were done to check if mutations in the catalytic domain have an effect on the HVR. The choice of G12D mutant was made because this mutation locks K-Ras4B in an active conformation. Moreover, the mutation is the most frequently occurring K-Ras4B mutation obtained amongst Ras cancer patients. As expected, the active mutation in K-Ras4B had an effect on the HVR interaction. All these studies taken together validate our hypothesis of the HVR interacting with the catalytic domain extensively in its GDP bound state.

We believe that the HVR farnesylation increases the affinity of the HVR to the catalytic domain. Although the NMR experiments and computational analyses were carried out in the absence of lipidation, the binding affinity studies were carried out in the presence of lipidation. These studies also suggest a stable association of the HVR with the catalytic domain.

We also prove the effects of this autoinhibition mechanism by carrying out the membrane binding assay and the Raf-1 binding assay. The HVR domain of K-Ras4B is the primary membrane binding domain. It contains a polylysine region which is believed to bind to the membrane through electrostatic interactions with the phospholipid headgroups. Since the HVR is not sequestered in the full length GTP loaded K-Ras4B, its interaction with the membrane should

be higher. The increased affinity of the K-Ras4B-GTP to proves this theory. Futhermore, in K-Ras4B-GDP the HVR interaction with the catalytic domain occurs through the effector binding region and Switch I region. This could probably be why Raf-1 binds to Ras-GTP with a higher affinity as compared to the GDP loaded form (77). The low affinity binding to Ras-GDP may be relevant in cells because in the full-length Raf-1 protein, the cysteine rich domain also binds Ras in a nucleotide independent manner (205). The result that we obtained showed that Raf-1 bound more efficiently to the truncated version of the GDP loaded protein as opposed to the full length version possibly because the truncated protein did not have an HVR domain to cover its active site. The HVR interaction with the active site can cause Raf-1 to bind full length K-Ras4B less efficiently. All these results taken together demonstrate the autoinhibition mechanism of K-Ras4B and also prove the physiological importance of the mechanism.

The paradigm for Ras function states that resting GDP-bound Ras is activated by GEFs that catalyze GDP exchange for GTP. GTP binding induces a conformational change in the Switch I and Switch II regions that exposes the effector interaction site in Ras. Ras effectors, such as Raf kinase, bind Ras-GTP with a higher affinity than Ras-GDP and this allows initiation of signaling. Signaling proceeds until Ras hydrolyzes GTP to GDP with the help of GAPs. Subsequently, the low affinity effector-Ras-GDP complex dissociates and signaling stops. Sequence properties and post-translational modifications in Ras HVRs regulate Ras-membrane localization (162, 163, 206). Our results suggest that the current model of Ras function is incomplete. We suggest that the role of HVR extends beyond membrane anchoring and Ras-membrane orientation (207).

Autoinhibition by HVR regulates K-Ras4B interactions with the plasma membrane phospholipids. HVR is a major membrane targeting element in Ras GTPases. Its sequestration by the GDP-bound catalytic domain reduces the affinity of K-Ras4B for the lipid bilayers.

Dissociation of K-Ras4B-GDP may be necessary to remove signaling complexes from the membrane to ensure that signaling completely stops after GTP hydrolysis. A similar mechanism is employed by Arf and Rac GTPases to regulate their function at the plasma membrane.

Further, we demonstrate that HVR regulates effector binding to K-Ras4B. It is remarkable that the K-Ras4B$_{1-166}$-HVR β-sheet interface is similar to that of Raf RBD. We speculate that within the HVR ensemble, a preferred β-strand conformer selectively binds to the functional site of the K-Ras4B catalytic domain to extend the β-sheet, a common interface motif. Consistent with this mode of interaction, HVR significantly affects binding of GDP-loaded K-Ras4B to Raf RBD. Markedly less effective binding of Raf RBD to GDP-bound K-Ras4B $_{1-188}$ than to GDP-bound K-Ras4B $_{1-166}$ suggests that the HVR can play an important role in preventing premature signaling from the GDP-bound protein. At the same time, the presence of HVR in full-length K-Ras4B-GTP-γ-S increases interaction efficiency with Raf RBD, implying that there is a possible binding site of HVR in Raf. Thus, HVR in both, the sequestered and released conformations, can regulate signaling through Raf. In a similar manner, HVR in K-Ras4B-GTP is a major binding site for calmodulin (106). However, in the GDP-bound state the HVR is unavailable to interact with calmodulin due to its sequestration by the catalytic domain.

Autoinhibition by HVR can also be relieved by phosphorylation on S181. HVR phosphorylation on Ser181 has a significant impact on K-Ras4B signaling(197). Recent studies have shown that K-Ras4B phosphorylation is responsible for more sustained activation of K-Ras4B. This activity is harder to reverse by GAP catalyzed GTP hydrolysis. In addition, K-Ras4B phosphorylation is essential to drive normal cell proliferation under conditions of low growth factor concentration.

Most of the studies into K-RasB activation mechanisms have focused on the analysis of how GEFs, GAPs and cellular localization are regulated by external and internal signals. The new

data suggest that multiple feedback loops exist that are capable of fine-tuning Ras activity not only through protein-protein interactions but also through intramolecular mechanisms that are rather complex. K-Ras is a potent amplifier of signals transmitted from the cell surface, and is involved in many essential functions including proliferation, survival, and migration. Thus, it is not surprising that K-Ras activity requires tight regulation. Auto-inhibition is frequently utilized by tyrosine and serine/threonine kinases (208, 209) to prevent accidental or excessive activation. Currently, it is difficult to speculate whether the autoinhibition by HVR found in K-Ras4B also occurs in other Ras GTPases. Ras isoforms differ predominantly in HVR regions and these differences may have functional implications (210, 211). In H-Ras, the HVR was found to affect dynamics of the catalytic domain. However, high affinity sequestration was not observed (212). HVRs of other Ras isoforms may also regulate effectors binding and/or GDP/GTP exchange. Domain swapping has shown that H-Ras, but not N-Ras HVR determines the invasive/migratory signaling program in breast tumor cells, which was independent of differences in lipidation between two HVRs (213).

It is also unclear whether the newly discovered autoinhibition mechanism plays a role in K-Ras mediated oncogenesis. Our finding that an oncogenic mutation in K-Ras affects interaction of HVR with the active site allows us to speculate that oncogenic mutations may allosterically modulate HVR-binding affinity (161). The role of HVR in K-Ras4B induced oncogenesis remains controversial, with reports supporting both highly significant and more subtle effects of HVR mutations on K-Ras4B G12V dependent cancer transformation (41, 42). These preliminary observations warrant detailed studies of HVR interactions in different mutants of Ras proteins because they can lead to uncovering additional approaches for modulating their oncogenic activity.

Finally, the high affinity interaction of HVR with the active site of K-Ras4B suggests that targeting this surface with synthetic inhibitors is feasible. Optimization of compounds that bind at the HVR-catalytic domain interface and promote K-Ras4B auto-inhibition is a potentially promising approach for development of potent inhibitors of so-far undruggable Ras (176).

3 INTERACTION MODE OF THE FULLY POST-TRANSLATIONALLY MODIFIED K-RAS4B HVR AND CALMODULIN

3.1 Introduction

In the previous chapter the importance of the hypervariable region (HVR) in the active and inactive states of K-Ras4B was demonstrated. The structural conformation of the HVR was found to be crucial in determining the downstream activity of the protein. In this chapter, I describe how we determined the binding mode of post-translationally modified HVR and calmodulin (CaM).

Ras protein isoforms are extremely similar in their structure but distinct in their functions (164, 165). In that, K-Ras4B has a number of distinct properties. For instance, K-Ras preferentially activates PI3 kinase (214). The differential distribution of Ras proteins in the cell accounts for some functional variation. However, inherent biochemical differences also exist. For example, the scaffold protein Sur8 and the tumor suppressor RassF2 interact only with K-Ras *in vitro* (16, 17). Another K-Ras4B-specific interaction is observed with the calcium-modulated protein, CaM.

CaM binds K-Ras4B and influences its downstream activity in a calcium dependent manner (103). We recently identified the HVR as the site responsible for the binding affinity and specificity of CaM to K-Ras4B (106). The HVR of K-Ras4B is unique among Ras proteins because it contains a polylysine region and a farnesyl group. Other Ras proteins are palmitoylated in addition to farnesylation. The importance of the polylysine region and farnesyl moiety for K-Ras4B-CaM binding has been suggested by Lopez-Alcala et al, 2008 (107).

The structure of CaM contains two lobes comprising the N and C terminal domains, which are connected by a linker region. Binding of CaM to other proteins induces a conformational change

in CaM. Many structural studies of CaM binding to its target enzymes use only CaM binding domains (CBDs) (215-217). CBDs serve as an excellent model for interactions of fully intact enzymes with CaM. Calcium loaded CaM binds and dissociates K-Ras4B from the membrane in breast cancer cell lines (MCF-7). Importantly, CaM has recently emerged as a key regulator of K-Ras4B in response to platelet derived growth factor (PDGF) signaling (108). K-Ras4B-CaM interactions also regulate cell cycle progression through the ERK2 pathway (109). Furthermore, CaM can prevent Ras activation by PKC in fibroblasts (110). In response to glutamate, CaM causes reversible intracellular translocation of K-Ras4B in hippocampal neurons (105).

In this chapter, we investigate binding between the post-translationally lipidated HVR of a human proto-oncogenic GTPase, K-Ras, and CaM. We use a combination of biochemical methods including isothermal titration calorimetry (ITC), dynamic light scattering (DLS), fluorescence, and nuclear magnetic resonance (NMR) to examine this interaction in detail. In order to study a more relevant binding we introduced post-translational modifications in the HVR domain. We discovered that fully post-translationally modified HVR (FM-HVR) aggregates at concentrations higher than 10 μM. In order to study its binding to CaM, protein concentrations lower than 10 μM are desirable. Conventional HSQC NMR is not sufficient to study proteins at such low concentrations. To study binding at a concentration where FM-HVR does not aggregate, the reductive methylation technique was applied to CaM to identify the domains responsible for binding to FM-HVR. Reductive methylation introduces two ^{13}C methyl groups on lysine residues of the protein. The methyl groups in dimethyl-lysines are degenerate and result in one $^{13}CH_3$ signal arising from two carbons and six protons, as compared to one carbon and three protons in aliphatic amino acids. This leads to an intense signal, which can be detected even at low protein concentrations. In addition, increased sensitivity may be related to

superior relaxation properties of methyl groups on lysines that result from their commonly low order parameters (218). This is not possible using conventional ^{15}N and ^{13}C labeling. We detected NMR signals at concentrations as low as 650 nM. When compared to the chemical shift perturbations obtained by carrying out the same experiment at higher concentrations, we observed that the non-specific binding produced a different spectrum. Thus, we have shown that specific binding of FM-HVR is different from the non-specific aggregate binding to CaM and have provided evidence for the use of reductive methylation as a tool to study protein-protein interactions at low micromolar to nanomolar concentrations.

3.2 Materials and Methods

3.2.1 Isothermal Titration Calorimetry (ITC):

Titration isotherms were obtained using VP-ITC microcalorimeter (MicroCal LLC, Northampton, MA) at 25^0C. For the experiments, CaM, FM-HVR and non-modified HVR peptides were dialyzed against 50 mM Tris-citrate pH 6.5, 50 mM NaCl, 5 mM $MgCl_2$, 1 mM TCEP and 10 mM $CaCl_2$. The peptide (FM-HVR or HVR) solution was always taken in the cell of volume 1.4 mL and CaM was always titrated using a syringe in twenty-eight 10 µL injections preceded by one 2 µL injection to account for diffusion artifacts. The reference data was obtained by titrating CaM into buffer. This reference data was subtracted from the actual peptide titration data. Analysis of the data was done using Origin 7.0 software. Fitting was done using the "one set of sites" model or "two sets of sites" model. The other thermodynamic parameters were also obtained using the fitting procedures.

3.2.2 **Particle size analysis**:

For studying aggregation of peptides, dynamic light scattering experiments were performed on a DynaPro-801 molecular sizing instrument. The peptide samples were dialyzed against PBS. The sample volume of 250 µL was used for the experiments. The FM-HVR and HVR peptide concentrations were 250 µM and 1 mM, respectively. Samples were centrifuged at 12000 rpm for 10 minutes before experiments. Analysis of the data was carried out using *Dynamics* software.

3.2.3 **Pyrene Fluorescence experiments**:

In order to determine the critical aggregation concentration we utilized the fluorescent properties of pyrene (219). Pyrene was dissolved in 100% ethanol and then added to different concentrations of peptides. Pyrene concentration in all the samples was 2 µM. The concentrations of the peptides used were 0.5 µM, 1 µM, 5 µM, 10 µM, 50 µM and 100 µM. All dilutions were carried out in phosphate buffered saline (PBS). The excitation scans were recorded between 315 to 360 nm with the emission wavelength set at 393 nm. PTI quantamaster instrument, equipped with double monochromators, was used to record all the fluorescence measurements. We used 1 cm path-length cuvettes for all experiments and the sample volume was 1.2 mL. The slit width of the monochromators was set to 2 nm throughout all experiments.

3.2.4 **Tryptophan Fluorescence experiments**:

Tryptophan fluorescence experiments were performed by titrating the farnesylated and non-farnesylated hypervariable peptide against tryptophan CaM mutant proteins. For this, three tryptophan mutants were prepared which have been reported to be isofunctional and isostructural

with native CaM (220). The synthesis of these CaM mutant proteins was done using the same expression and purification procedure as explained above. For fluorescence measurements, PTI Quantamaster spectrofluorimeter was used which contained monochromators at the emission and excitation sides. The emission spectra were recorded at 290 nm. The slit width for emission and excitation was 4 nm and 0.5 nm respectively. Reference data was obtained by titrating the buffer into CaM and this data was subtracted from the peptide titration data. The change in intensity was plotted against concentration and fitting was done using "one set of sites" model to obtain the related parameters. The error range was calculated using "jack-knife" analysis.

3.2.5 NMR experiments:

The ^{1}H-^{13}C and ^{1}H-^{15}N NMR experiments were carried out on a 900 Mhz Bruker Avance Spectrometer. The spectrometer was equipped with a cryogenic probe. The buffer was 50 mM Tris-citrate pH 6.5, 50 mM NaCl, 5 mM $MgCl_2$, 10 mM β-mercaptoethanol and 10 mM $CaCl_2$ and the experiments were carried out at the temperature of $25^{0}C$. Data analysis was done using NMRPipe. In case of the ^{1}H-^{15}N NMR experiments, the mean chemical shift difference was calculated using the following formula.

$$\Delta\delta_{NH} = \sqrt{\frac{(\Delta\delta H)^2 + (\Delta\delta N)^2 / 25}{2}}$$

Statistically significant chemical shift differences were considered to be the ones higher than the sum of the average and one standard deviation.

3.2.6 Reductive methylation of CaM:

Reductive methylation of CaM was done using the technique described by Means and Feeney, 1968 (221). The procedure for carrying out reductive methylation of CaM has been previously described in our publication (222). After carrying out reductive methylation on CaM, all the water in the buffer was replaced with D_2O in order to minimize water signal.

3.2.7 Protein purification:

The CaM plasmids were transformed into BL21AI cells. The cells were grown in LB media at 37^0C for 15 hours and shaken at a 250 rpm with the use of kanamycin for antibiotic selection. Then the cells were transferred into M9 media with the dilution of 1:20 and grown at 37^0C and 250 rpm until the OD was 0.6-0.8 at 600 nm. Induction was carried out by adding 0.2% arabinose, 2% ethanol and 200 μM IPTG. After 4 hours from induction, cells were harvested by centrifugation at 8000 rpm. The pellets obtained were lysed using 10 mM Tris-HCl, 1 mM $CaCl_2$ and 10 mM β-mercaptoethanol at 60^0C for 1 hour. The lysate was centrifuged again at 18000 rpm for 30 minutes. The pellets from this centrifugation were discarded and the supernatant was loaded onto a phenyl sepharose column pre-equilibrated with 10 mM Tris-HCl, 1 mM $CaCl_2$ and 10 mM β-mercaptoethanol. The same buffer was used for washing the column loaded with supernatant until no more protein was detected by the Coomassie Plus Assay. The elution of the protein was done using 10 mM Tris-HCl, 5 mM EDTA, and 10 mM β-mercaptoethanol. Eluted fractions were assessed for purity using an SDS Page gel. Pure fractions were dialyzed against 50 mM Tris-citrate pH 6.5, 50 mM NaCl, 5 mM $MgCl_2$, 10 mM β-mercaptoethanol and 10 mM $CaCl_2$. The purified protein was concentrated using an Amicon pressurized stir-cell equipped with a filter membrane (Millipore) with a 10,000 Da cut-off whenever needed.

3.2.8 Modification of the HVR:

The HVR peptide with the sequence 'KEKMSKDGKKKKKKSKC' was purchased from the Research Resources Laboratory at UIC. A 68 µL solution of 73.6 mM S-farnesyl-L-cysteine methyl ester in 100% dimethyl sulfoxide (DMSO) was added to 2 mg of no-weigh sulfosuccinimidyl-4-(*N*-maleimidomethyl)cyclohexane-1-carboxylate (sulfo-SMCC) (Thermo Scientific), and mixed thoroughly until all sulfo-SMCC was dissolved. A 50 µL solution of 50% (w/v) N-octyl-β-D-glucopyranoside (Sigma) was added to the above mixture, followed by 381 µL of PBS pH 7.4 and 1 µL of 50 mM di-*tert*-amyl peroxide (DTAP). The reaction mixture was incubated for 1.5 hours and thereafter diluted to the final volume of 8 mL with PBS. The solution was centrifuged at 4,500 rpm for 30 min at 4˚C. The supernatant was discarded and the pellet dissolved in 150 µL of 100% ethanol followed by the addition of 100 µL of 50% (w/v) N-octyl-β-D-glucopyranoside. The above solution was added to 2.0 mg of the HVR peptide dissolved in 750 µL of PBS and incubated at room temperature overnight. The reaction mixture was then applied to a C-18 column and purified by reversed phase high performance liquid chromatography (RP-HPLC). Briefly, the column was equilibrated with 90% Buffer A (0.1% trifluoroacetic acid) and 10% Buffer B (90% acetonitrile) before applying the sample. Thereafter, a linear gradient up to 80% Buffer B was applied. The fractions eluted at 66-68% Buffer B were collected and subjected to mass spectrometric analysis for purity. The pure fractions were pooled and dried using an Eppendorf Microfuge. Since the peptide does not have aromatic residues the yield was estimated using a previously described protocol that takes advantage of the absorbance difference at 215 nm and 225 nm (223). The schematic of the reaction for making FM- HVR is outlined in the supplementary data section (Figure 3.1 A). Mass spectra for both, the modified and the non-modified HVR, are also provided therein (Figure 3.1 B).

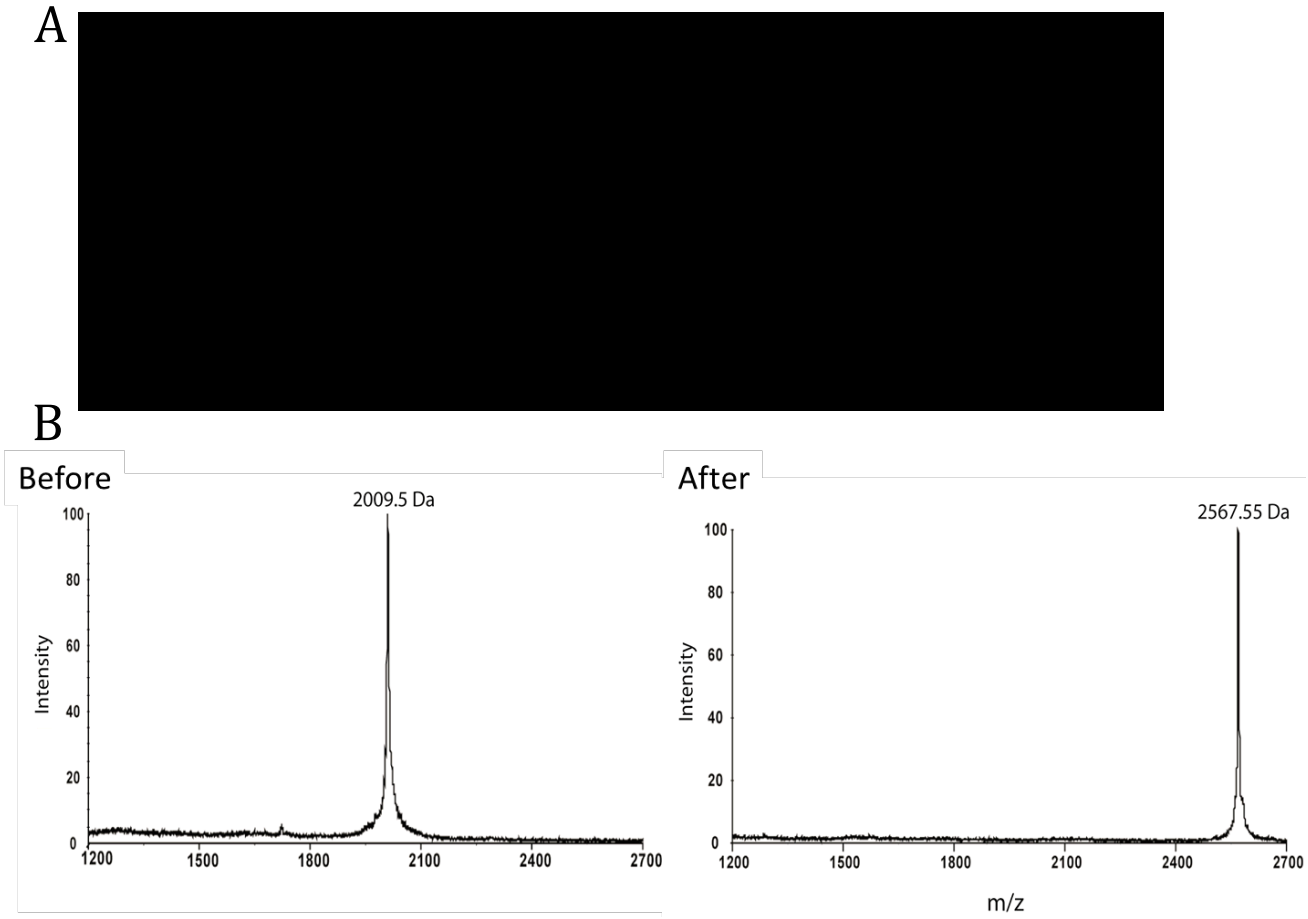

Figure 3.1: Preparation of fully modified HVR.
(A) Reaction scheme for making farnesylated and methylated HVR. (B) Mass spectra obtained before and after modifying the HVR domain of K-Ras.

3.3 Results

3.3.1 ^{15}N HSQC titration of ^{15}N CaM with FM-HVR does not reveal a continuous binding interface.

The conventional method for determination of protein binding interfaces relies on recording ^{15}N HSQC spectra of ligand bound protein at different ligand concentrations. To investigate the binding interface between the FM-HVR peptide and CaM, ^{15}N, ^{1}H NMR spectra of the CaM titrations with the peptide were recorded. A solution of CaM was titrated in FM-HVR such that their final concentrations were 25 μM and 50 μM, respectively. Figure 3.2 A and 3.2 B show an overlay of the titration spectra and a graph of the chemical shift perturbations induced by peptide binding, respectively. Residues (A15, T26, G33, Q41, A57, D64, V121, R126, I130, N137, and F141) in all the three domains show statistically significant chemical shift perturbations. Figure 3.2 C shows the results of chemical shift perturbations mapped on the three-dimensional structure of CaM and highlights the discontinuous binding interface formed by FM-HVR. The fact that several binding sites are observed suggests the presence of non-specific interactions. Moreover, since the concentration of FM-HVR was high, it is possible that the observed binding events are caused by non-specific interactions of the aggregated peptide with CaM.

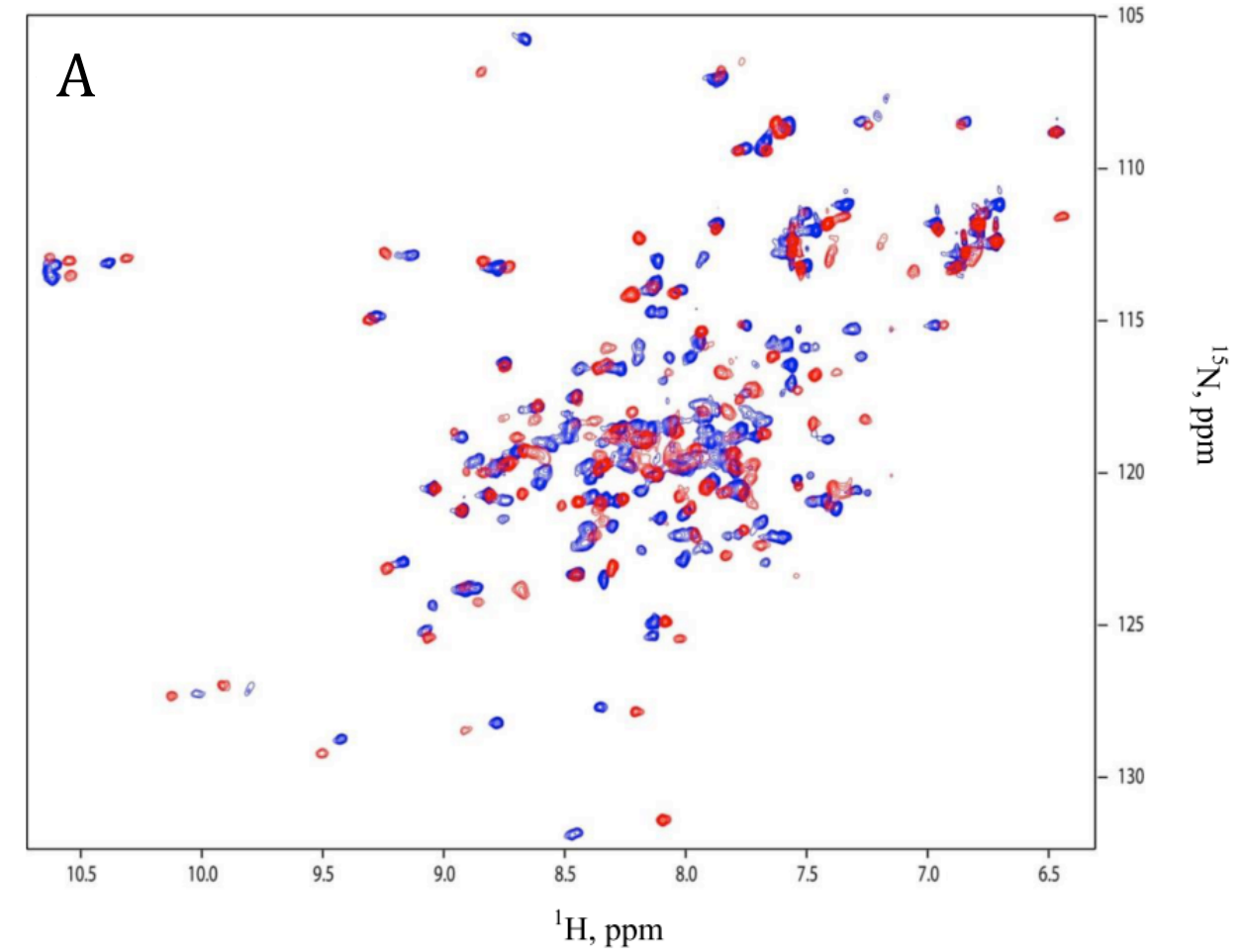
A
105
110
115
120
125
130
^{15}N, ppm
10.5
10.0
9.5
9.0
8.5
8.0
7.5
7.0
6.5
^{1}H, ppm

B

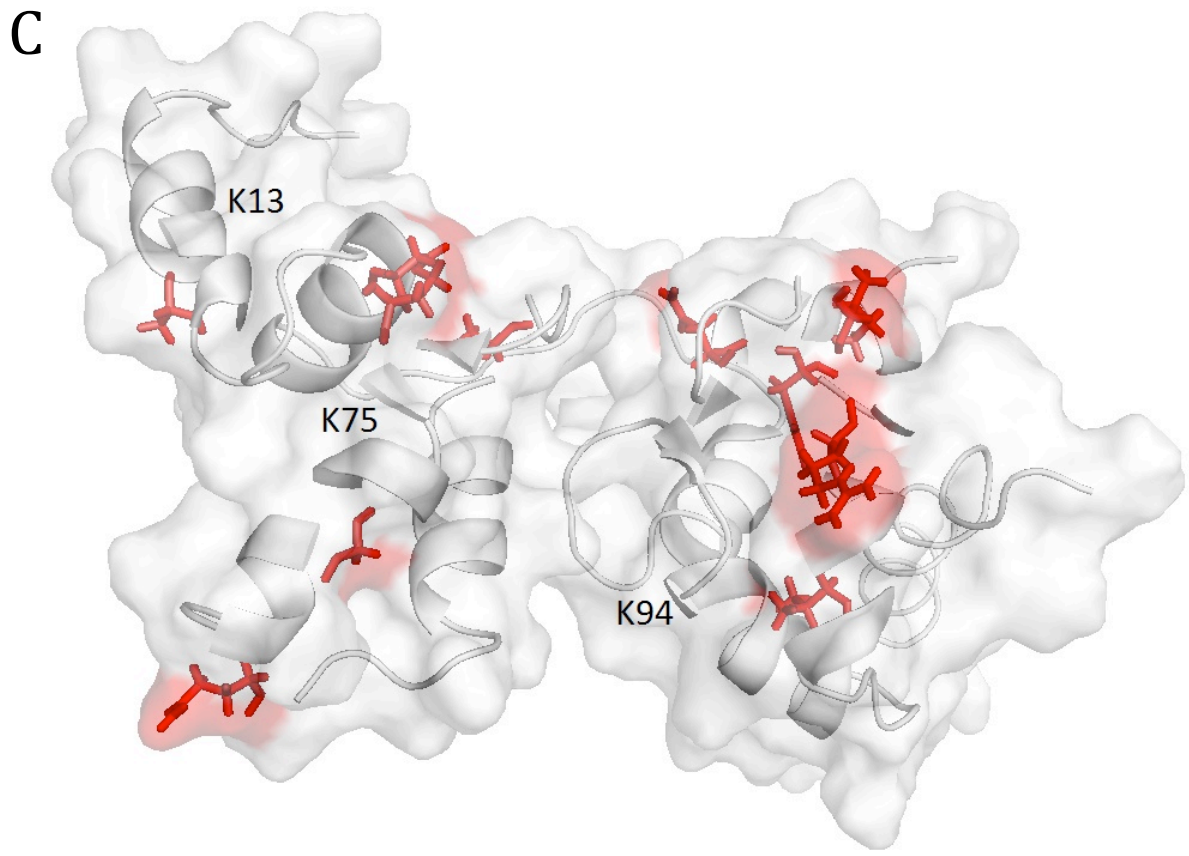

Figure 3.2: Interaction of FM-HVR with CaM at high concentrations.
(A) Overlay of CaM spectrum without (red) and with (blue) the FM-HVR peptide. The final concentrations of CaM and FM-HVR were 25 μM and 50 μM, respectively. (B) Residual chemical shifts obtained after the NMR titration of CaM with FM-HVR peptide. The horizontal line in the graph shows the sum of average chemical shift perturbation and standard deviation. Residues that show zero chemical shift difference on the graph were the ones that were not assigned due to resonance overlap. (C) Statistically significant chemical shift differences were mapped on the structure of CaM (PDB: 1CFF). K13, K75 and K94 have been labeled. We make the use of these residues in reductive methylation to investigate CaM FM-HVR interactions.

3.3.2 Farnesylation and methylation of HVR cause aggregation.

We then tested the possibility that introduction of hydrophobic farnesyl and methyl groups into HVR induces peptide aggregation. We performed dynamic light scattering experiments on 1 mM HVR and 0.25 mM FM-HVR in PBS at room temperature. The measured hydrodynamic radius for HVR was 1.23±0.05 nm, which corresponded to 3.7±0.46 kDa, shown in Figure 3. 3 A. This roughly corresponds to the monomeric form of peptide. However, upon introduction of farnesylation and methylation the hydrodynamic radius of the peptide increased to 8.15±0.46 nm at a 4 times lower concentration as shown in Figure 3.3 B. This hydrodynamic radius corresponded to a particle of 471.92±63.75 kDa in size. Observation of higher order assemblies of FM-HVR allowed us to conclude that post-translational modifications in K-Ras can lead to aggregation through hydrophobic interactions.

To study physiologically relevant binding of the peptide to CaM we need to know the concentration at which HVR aggregates. To accomplish this, we used a small fluorescent molecule, pyrene, which changes its fluorescent properties upon transitioning from the hydrophilic to the hydrophobic environment. We conducted fluorescence experiments with different concentrations of FM-HVR and HVR. All samples contained 2 μM pyrene. Excitation scans were recorded between 315 to 360 nm with the emission wavelength set at 393 nm. There was a significant 3 nm red shift in the excitation peak of pyrene in the presence of increasing concentrations of FM-HVR. This suggested that pyrene transitioned from the hydrophilic to the hydrophobic environment upon addition of FM-HVR. Conversely, the increasing concentrations of unmodified HVR did not induce similar changes in pyrene fluorescence. Example fluorescence spectra obtained from both the peptides are shown in Figure 3. 3 C. Determination

of the critical aggregation concentration was performed by plotting the intensity ratio I_{334}/I_{337} against the logarithm of peptide concentration. The results from our analysis are shown in Figure 3.3 D. The increase in the I_{334}/I_{337} ratio of pyrene fluorescence indicates occurrence of FM-HVR aggregation. The graph suggests that aggregation starts in the FM-HVR only after the concentration of 10 μM whereas in HVR samples no aggregation is observed even at 250 μM. Thus, we conclude that the critical aggregation concentration of FM-HVR is 10 μM or greater. We must also acknowledge that there is a slight decrease in the I_{334}/I_{337} ratio of the FM-HVR peptide between the concentrations of 1 to 10 μM, however we do not know the exact cause for it. FM-HVR exists in the monomeric and multimeric states. In addition, it is possible that there is a transition intermediate between the monomeric and multimeric states of the peptide. This notion is supported by detection of the peptide species presenting a highly polar environment in the FM-HVR concentration range of 5 to 10 μM. However, at higher peptide concentrations, the hydrophobic forces leading to peptide aggregation dominate and cause an increase in the I_{334}/I_{337} ratio of pyrene fluorescence.

A

B

C

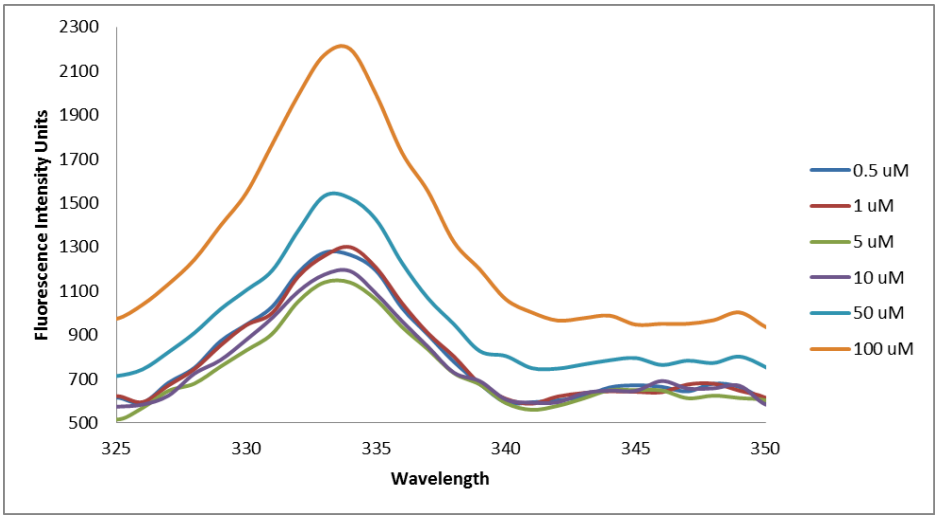
2300
2100
1900
1700
1500
1300
1100
900
700
500
Fluorescence Intensity Units
325
330
335
340
345
350
Wavelength
0.5 uM
1 uM
5 uM
10 uM
50 uM
100 uM

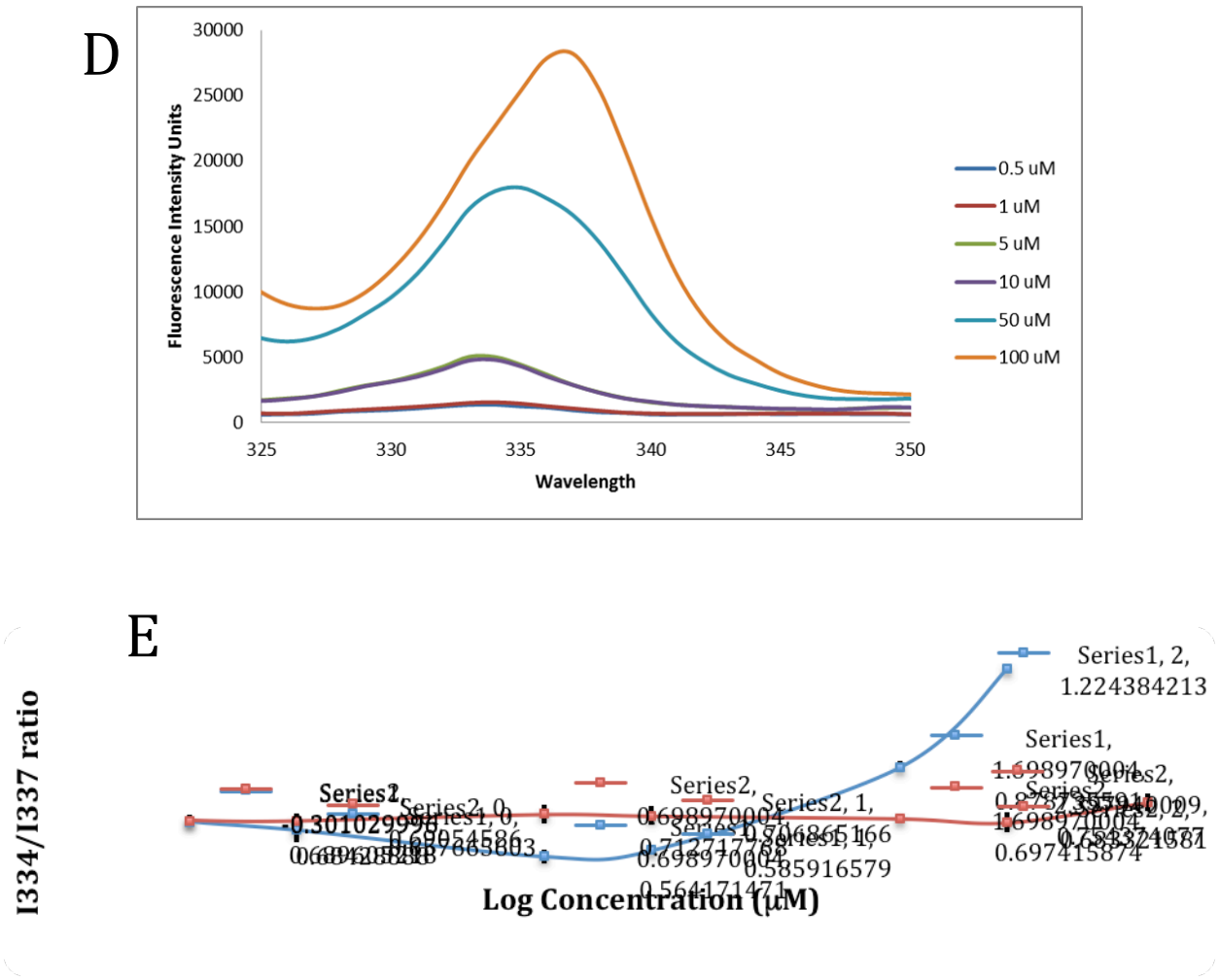

Figure 3.3: FM-HVR aggregates at high concentrations.
(A) Dynamic light scattering of 1mM HVR peptide in PBS at room temperature. (B) Dynamic light scattering of 250 μM FM-HVR peptide in PBS at room temperature. (C) Example fluorescence spectra obtained from different concentrations of HVR and (D) FM-HVR. The legend shows the respective concentrations of the peptides used. All samples contain 2 μM pyrene. (E) The plot of fluorescence intensity ratio (I_{334}/I_{337}) from pyrene excitation spectrum as a function of concentration of modified and non-modified HVR peptides. The FM-HVR peptide, shown in blue, aggregates beyond 10 μM. The HVR peptide, shown in red, does not aggregate.

3.3.3 Farnesylation increases affinity of the HVR for CaM.

To characterize the interaction of either FM-HVR or HVR with CaM, ITC experiments were performed wherein CaM was titrated into either FM-HVR or HVR solutions. The farnesylated peptide was at a concentration which does not promote aggregation and non-specific binding. Titration of 1 mM CaM into 70 μM non-farnesylated HVR, as in Figure 3.4 A, yielded a dissociation constant K_d = 11.2 ± 1.6 μM, ΔH = 0.65 ± 0.1 kcal/mole, and ΔS = 25.1 cal/deg/mole. The data was fitted with the 'one set of binding sites' model. A similar experiment was performed where 33 μM CaM was titrated into 2.9 μM FM-HVR. The data was analyzed using the 'one set of binding sites' model. The curve in Figure 3.4 B shows that FM-HVR binds to CaM with an affinity of 0.35±0.06 μM for CaM. The other fitted parameters for this site are ΔH = -14.88 ± 0.99 kcal/mole and ΔS = -19.81 cal/deg/mole. In short, there is almost a 40-fold increase in affinity for CaM when the HVR peptide is farnesylated and methylated, as compared to the non-modified peptide. This suggests that the post-translational modification of HVR is responsible for the increase in affinity to CaM.

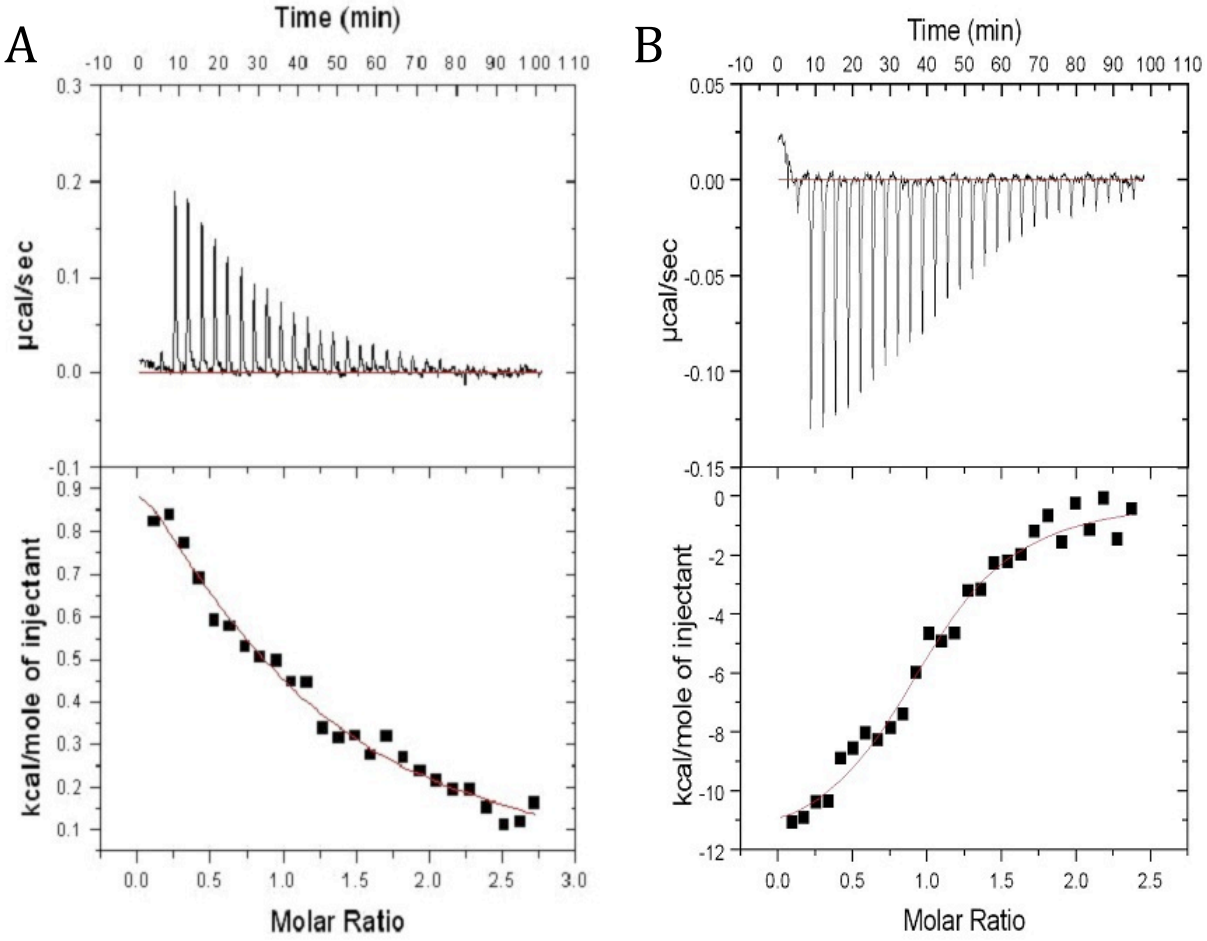

Figure 3.4: Interaction of modified and non-modified HVR with CaM.
Isothermal Titration Calorimetry of (A) 70 µM HVR peptide with 1 mM CaM, and (B) 2.9 µM FM-HVR peptide with 33 µM CaM. The upper panels in (A) and (B) show titration isotherms. The lower panels in (A) and (B) show the fit of the reference-subtracted titration. The "one set of binding sites" model were used in (A) and (B).

3.3.4 All three domains of CaM are involved in binding to farnesylated HVR peptide.

In order to determine the domains of CaM involved in binding to the modified HVR peptide, tryptophan fluorescence experiments were performed using three tryptophan mutants of CaM, namely T27W, S82W and Q137W. The three mutations were created in the three domains of CaM that included the N-terminal domain, linker region and the C-terminal domain. Upon titration, a shift in the absorbance was seen in all the three mutants. The Figure X shows the fluorescence spectra obtained using the T27W CaM mutant. Similar spectra were also obtained for S82W and Q137W. Concentration of CaM was kept constant at 1.5μM while the peptide concentration was varied from 0 to 4μM. The dissociation constants for N-terminal domain, linker region and C-terminal domain were determined using nonlinear regression analysis to 0.014 ± 0.017 μM, 0.19 ± 0.029 μM and 0.08 ± 0.041 μM, respectively (Figure 3.5). This suggests that the N and C terminal domains along with the linker region are involved in binding to the farnesylated HVR.

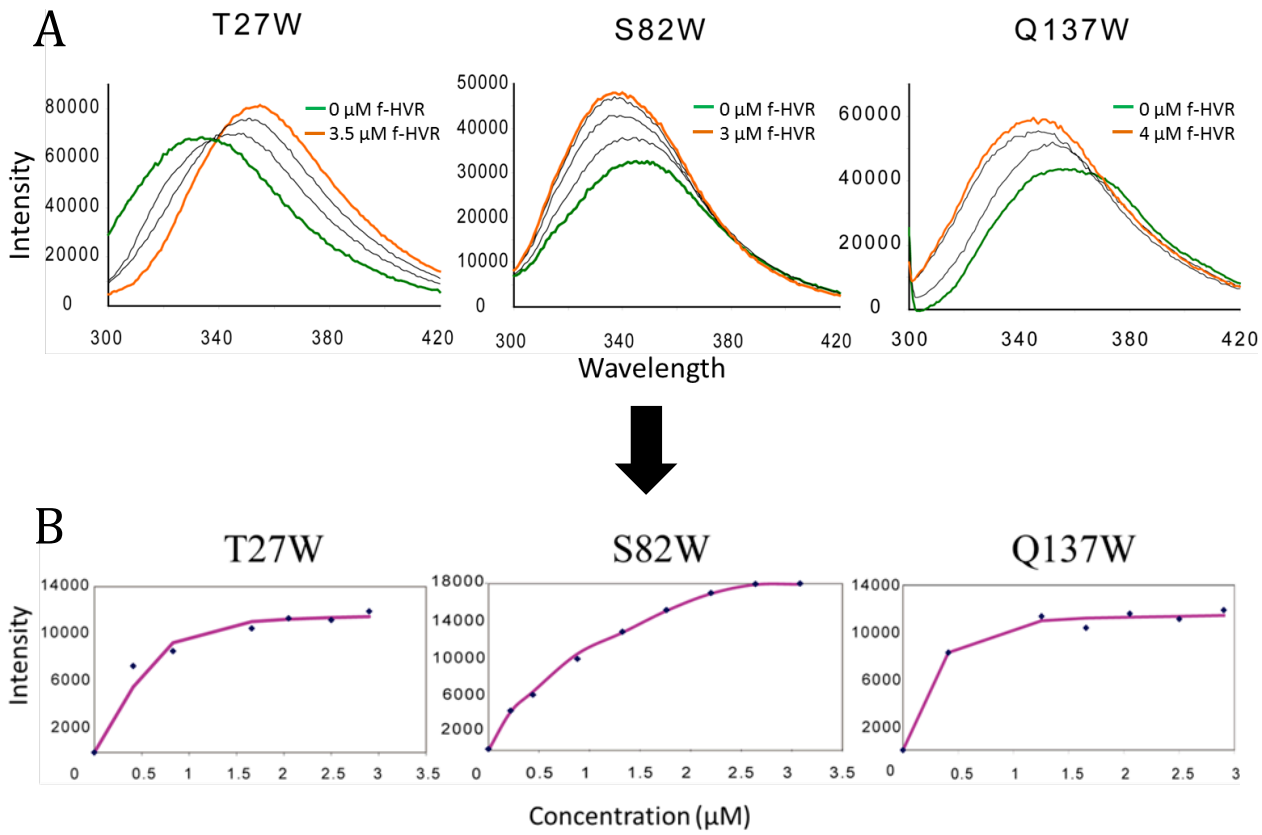

Figure 3.5: Interaction of FM-HVR with CaM mutants.
(A) Fluorescence spectra obtained after titrating T27W, S82W and Q137W CaM mutants with different concentrations of farnesylated HVR peptide (beginning with 0µM to 3µM). Concentration of CaM was kept at 1.5µM. (B) Dissociation constants for N-terminal domain, linker region and C-terminal domain obtained using nonlinear regression analysis. Fitting was done using "one set of binding sites" model.

3.3.5 ^{13}C HSQC of reductively methylated CaM can be performed at nanomolar protein concentration.

To address the problem with non-specific peptide binding to CaM we needed to perform NMR experiments at low protein concentrations. CaM was reductively methylated to increase the sensitivity of NMR signal detection. In order to show that reductively methylated CaM had similar properties to wild-type CaM, we have previously shown that reductive methylation does not affect binding properties of CaM (222). We also carried out ITC titrations to determine the dissociation constants of the two proteins and they were equal as shown in Figures 3.6 A and B. All lysines present in CaM are shown in FigureS6.

We tested the lowest concentration, at which we could achieve reliable signal detection with reductively methylated CaM. We could observe signals with 650 nM reductively methylated CaM at a signal to noise ratio greater than 10 (Figure 3.7). The total time for this experiment was 11 hours. The improved sensitivity allows studying protein-protein or protein-peptide interactions at nanomolar concentrations. Signal assignments for reductively methylated CaM were obtained by site directed mutagenesis (222).

For our experiments, we titrated different concentrations (0 μM, 0.5 μM, 1 μM and 1.5 μM) of FM-HVR into 1 μM CaM. This concentration was chosen because of the NMR time-constraints and the absence of peptide aggregation in the low micromolar range. Titration ratios were 0:1, 0.5:1, 1:1 and 1.5:1 of FM-HVR to CaM. It was found that CaM saturated at 1:1 titration ratio as shown in Figure 3.8 A and B.

The same experiment was carried out using a higher concentration of FM-HVR. CaM concentration in this experiment was 70 μM. FM-HVR concentrations were varied to achieve 0:1, 1:1, 2:1 and 3:1 molar ratios to CaM. This was done to study binding of aggregated FM-

HVR to CaM. Figure 5C shows the respective superimposed spectra obtained before and after titrating the various amounts of FM-HVR. We found that FM-HVR saturated CaM at 2:1 titration ratio as shown in Figure 3.8 B and C. This was significantly different from the low concentration saturation event. Comparison of the chemical shifts in figures 8A and 8C reveals that the conformation of bound CaM is different for different concentrations of the peptide. These experiments suggest that all the three domains of CaM interact with the modified HVR peptide at high and low concentrations. However, the way CaM binds to aggregates of FM-HVR is significantly different from the way it binds to the monomeric peptide. For example, K75 shows a significant upfield shift in the proton dimension in the spectrum of 70 μM CaM titration, while K75 shows a very minor change in the spectrum of 1 μM CaM titration.

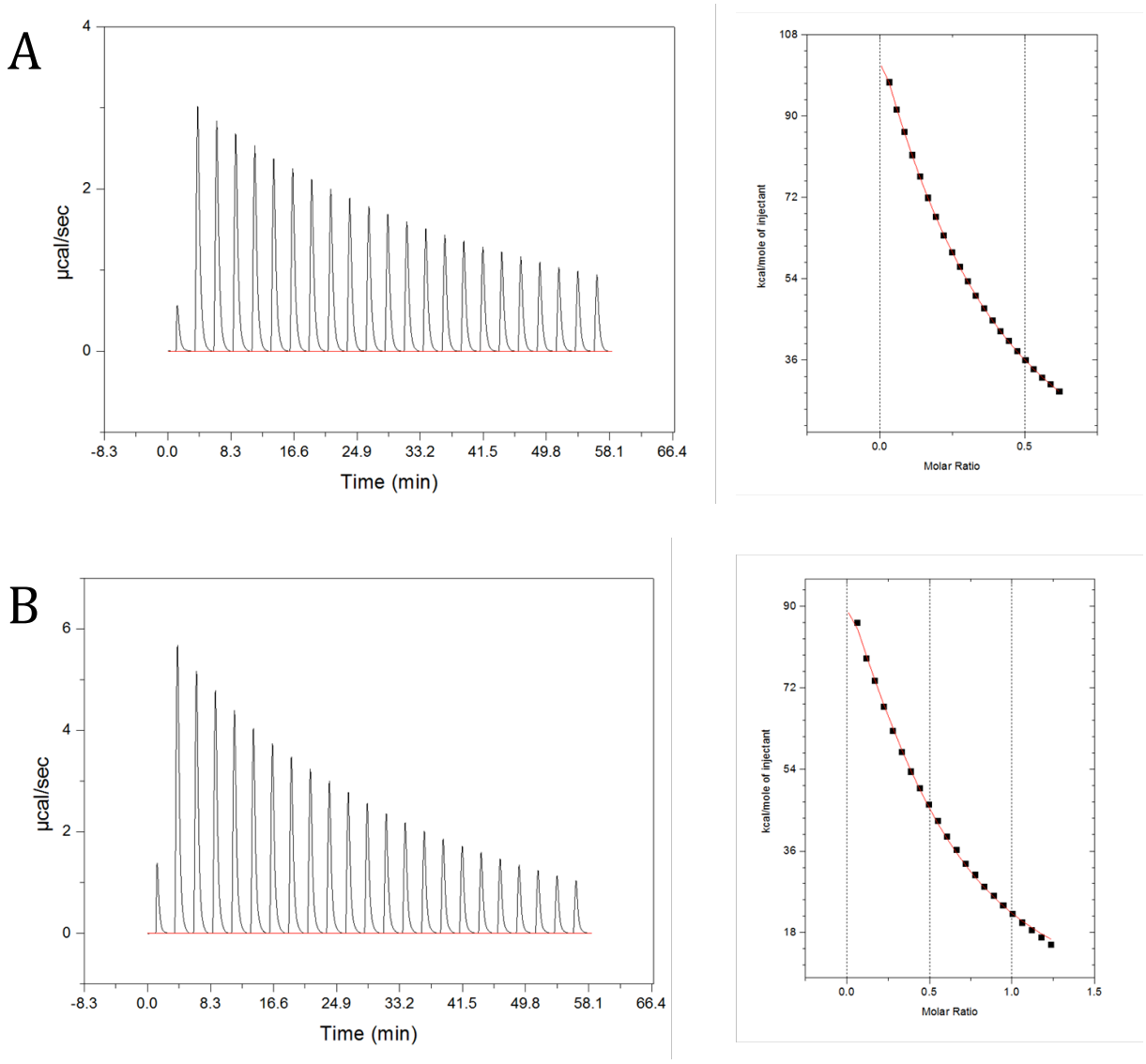

Figure 3.6: Reductive methylation does not change the affinity of CaM with FM-HVR. (A) ITC isotherm obtained upon titrating 100 µM wild type CaM into 20 µM FM-HVR. The dissociation constant was 9.95±0.15 µM. (B) ITC isotherm obtained upon titrating 200 µM reductively methylated CaM into 20 µM FM-HVR. The dissociation constant was 9.42±0.5 µM. The data fitting was done using one set of binding sites model.

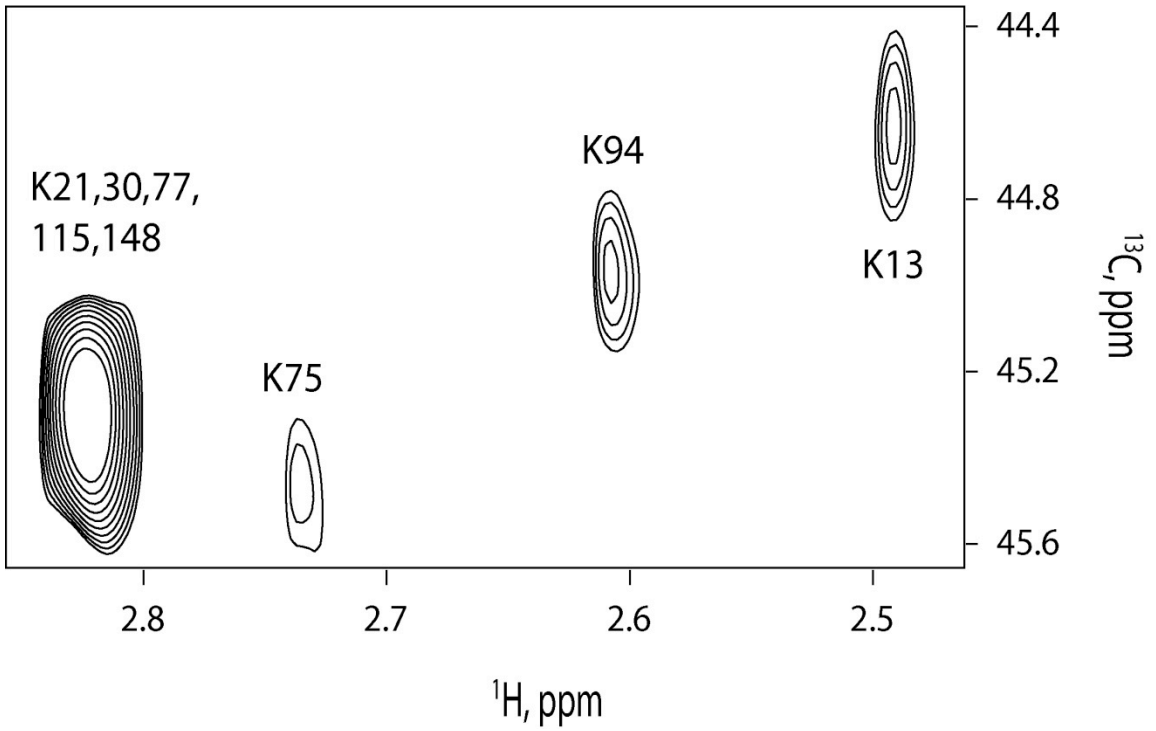

Figure 3.7: NMR spectrum of 650 nM reductively methylated CaM.

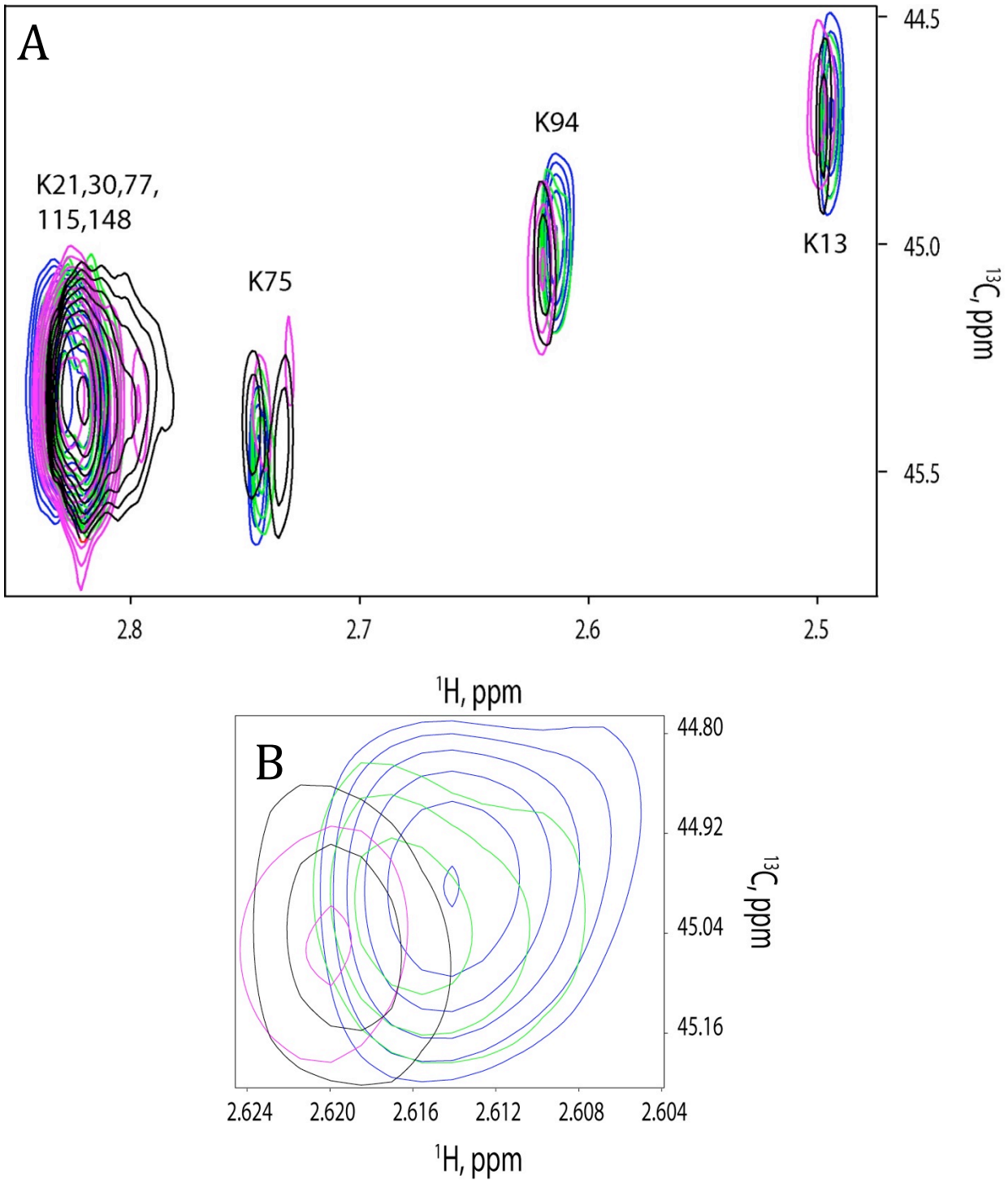
A
K21,30,77,
115,148
K75
K94
K13
44.5
45.0
45.5
^{13}C, ppm
2.8
2.7
2.6
2.5
^{1}H, ppm
B
44.80
44.92
45.04
45.16
^{13}C, ppm
2.624
2.620
2.616
2.612
2.608
2.604
^{1}H, ppm

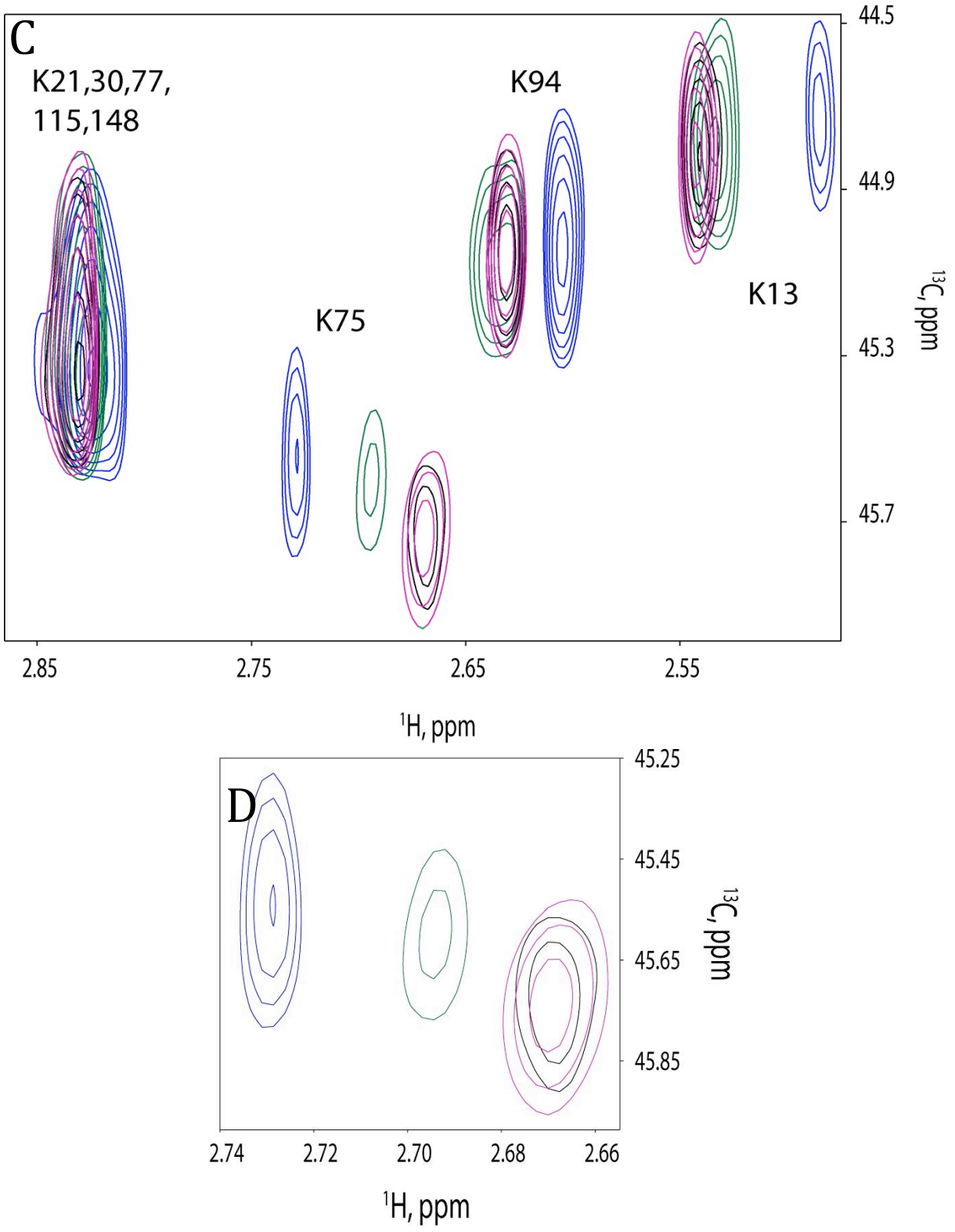
C
K21,30,77,
115,148
K94
K75
K13
44.5
44.9
45.3
45.7
^{13}C, ppm
2.85
2.75
2.65
2.55
^{1}H, ppm
D
45.25
45.45
45.65
45.85
^{13}C, ppm
2.74
2.72
2.70
2.68
2.66
^{1}H, ppm

Figure 3.8: Binding mode of FM-HVR with CaM is different at low and high concentrations.

(A) NMR titration of different concentrations of FM-HVR into 1uM CaM. Titration ratios were 0:1(blue), 0.5:1(green), 1:1(magenta) and 1.5:1(black) of FM-HVR and CaM (B) Magnified view of K94 residue showing saturation at 1:1 FM-HVR to CaM ratio. (C) NMR titration of different concentrations of FM-HVR into 70uM CaM. FM-HVR concentrations were varied to achieve 0:1(blue), 1:1(green), 2:1(magenta) and 3:1(black) molar ratios to CaM.(D) Magnified view of K75 residue showing saturation at 2:1 FM-HVR to CaM ratio.

3.4 Discussion

The expression and purification of CaM, and the production of modified HVR was of crucial importance for the experiments in this chapter. The protocol for carrying out CaM purification is well established and can be performed with relative ease. Lysis is carried out simply by heating the lysate at 60^0C. Given the thermal stability of CaM, it is able to withstand the high temperature unlike other proteins. Phenyl sepharose beads are used for eluting CaM. In addition, His tags are not required for purifying the protein since it is eluted based on the changes in its surface hydrophobicity upon contacting EDTA. EDTA chelates the calcium ions sequestered by CaM. This causes the N- and C-terminal domains of CaM to collapse and changes its surface hydrophobicity causing it to displace from the beads.

Ras peptide lipidation has been extensively surveyed by the Waldmann group (224). There are 3 major choices that scientists have made to synthesize lipidated Ras peptides. The first one involves the use of solid phase support versus solution phase. The second one involves the use lipidated building blocks compared to lipidation post peptide synthesis. And the third one involves a choice between Boc and Fmoc approaches (224). Solution phase chemistry, although feasible, consumes a lot of time and effort. Solid-phase chemistry is believed to be an advance over solution phase yet it requires a sophisticated synthetic chemistry approach that involves multiple protection and deprotection steps. Bmoc and Fmoc strategies also encompass similar complications. It must be noted that the resulting peptides from using these strategies are functionally active (224-226). However, in order to produce a modified peptide in a time-efficient manner and utilizing readily available reagents, we decided to attach farnesyl-cysteine

methyl ester using a crosslinker. The scheme of the reaction is shown in Figure S3. The reaction is extremely time-efficient, and produces significant quantities of stable peptide.

The role of farnesyl modification in lipid binding has received significant attention. Recent progress solving the crystal structure of farnesylated GTP-bound protein Rheb in complex with phosphodiesterase suggests that the farnesyl moiety participates in low specificity protein-protein interactions (227). However, more studies on other proteins are needed to demonstrate the importance of farnesylation in protein-protein interactions.

Generally, protein lipidation is associated with increased binding affinity. There are many literature reports supporting the idea that post-translational lipidation of proteins causes their intracellular trafficking and binding effector molecules (228-230). In certain cases, stability of these proteins is attributed to their post-translational modifications (231).

A majority of small G-proteins undergo requisite post-translational farnesylation at their COOH-terminal cysteine residues. This modification controls subcellular localization and facilitates interactions with effector proteins. One of the prominent targets of farnesylation in humans is a p21 GTPase, K-Ras4B. Our research demonstrates that K-Ras4B farnesylation increases the binding affinity for CaM. This is consistent with previously reported observations. For instance, Lopez-Alcala et al showed that a non-farnesylatable mutant of Ras did not bind CaM (107). In addition to increasing protein binding affinity, we also observe that farnesylation of K-Ras4B alters the mode of protein-protein interactions. We previously reported that the HVR of K-Ras4B constitutes the major binding site for CaM. Unmodified HVR predominantly binds to the C-terminal domain and the linker region of CaM. Surprisingly, post-translational modifications in HVR engage the N-terminal domain of CaM. Thus, when the HVR is modified, all three domains of CaM participate in K-Ras4B binding. This is shown by recording the NMR spectra

of titrations of FM-HVR and CaM. During our experiments with FM-HVR we discovered that the data interpretation is complicated by the fact that FM-HVR aggregates. Nonspecific peptide-protein interactions were observed at peptide concentrations greater than 10 μM.

Protein aggregation often limits the use of NMR for analysis of ligand binding to proteins. Sensitivity issues prevent the use of NMR spectroscopy at physiologically relevant protein concentrations that are often in the nanomolar range. To address this limitation we used reductive methylation of lysine residues in the protein of interest. Given the fact that protein aggregation is a common phenomenon promoted by millimolar protein concentrations required for NMR, reductive methylation provides a viable method to study binding events at physiologically relevant concentrations.

Using reductively methylated CaM, we were able to acquire a ^{13}C HSQC spectrum at a concentration as low as 650 nM. Subsequent NMR titration experiments at 1 and 70 μM CaM with FM-HVR produced different binding interfaces and different binding affinities. At low CaM concentration we observed appearance of new signals in the N- and C-terminal domains as well as the linker region upon addition of FM-HVR. The saturation of the FM-HVR binding site in CaM occurred at 1:1 CaM to peptide molar ratio. The dissociation constant determined by ITC is 350 nM. This value is in similar to the previously published dissociation constant for binding of farnesylated K-Ras to CaM (232). Conversely, when we titrated 70 μM CaM with FM-HVR we observed chemical shift changes in $^{13}CH_3$ (13, 94, 75, 21, 30, 77, 115,148) groups of lysines in CaM. The most dramatic chemical shift perturbations occurred in the linker region of CaM. Although the N- and C-terminal domains and the linker region of CaM were involved in FM-HVR binding, the binding interface was clearly different from that observed at 1 μM CaM. The saturation of CaM with FM-HVR occurred at 1:2 molar ratio of CaM to peptide. This is

indicative of significantly lower binding affinity of CaM to aggregated FM-HVR as compared to the affinity between CaM and FM-HVR monomers. These observations allowed us to conclude that physiologically relevant FM-HVR binding to CaM occurs in the nanomolar range.

The technique of reductive methylation is widely used in x-ray crystallography and is found not to affect protein structure or to introduce spurious protein-protein interactions (233). Reductive methylation does not completely remove the positive charge in lysine epsilon amino groups and, therefore does not induce hydrophobic surfaces in proteins. Enhanced sensitivity is very beneficial for NMR experiments at low protein concentrations. We have used HSQC experiments in our studies. However, the sensitivity can be further improved by the use of experimental schemes like SO-FAST HMQC that relies on standard data sampling in the indirect dimension and allows fast and sensitive NMR data acquisition (234).

Although we believe that reductive methylation has great potential for NMR investigation of protein-protein interactions at physiologically relevant concentrations, we caution that reductive methylation may not be universally applicable to all proteins. Some proteins can be inactivated by reductive methylation. For example, myo-inositol monophospatase has been found to lose its catalytic activity after reductive methylation (235). In our case, reductive methylation of CaM does not affect calcium loading or antagonist binding properties (222). Moreover, we also show that the dissociation constants of the interaction between reductively methylated CaM or unmodified CaM with FM-HVR are similar.

One other possible issue with the use of reductive methylation in NMR is related to the limited chemical shift dispersion for methyl groups (236, 237). This is due to the fact that lysine side chains tend to be solvent exposed. In this state, the methyl groups do not experience significant variation in their electromagnetic environment that is needed for chemical shift dispersion. We

previously found that the uniform influence of the solvent on chemical shifts can be overcome by adjusting the pH closer to the pKa of lysine side chains. Under these conditions, chemical shifts reflect variability in lysine pKa values (222). At the same time, dimethyllsines may exhibit lower spectral dispersion as compared to monomethyllysines (238). Although monomethylated lysines have previously been found to provide improved resolution in comparison with the dimethylated variant, we found signals for dimethylated lysines in CaM sufficiently resolved. Moreover, as we show that the dimethyl lysine modified CaM interacts with FM-HVR in similar manner to non-methylated CaM. Finally, post-translationally introduced ^{13}C methyl groups represent very small spin systems. This property prevents the use of sequential assignment techniques. To address this issue, using CaM we showed that signal assignments in reductively methylated NMR samples can be obtained using site-directed mutagenesis (222). In conclusion, we have uncovered complex binding behavior imparted by post-translational modifications on K-Ras4B. According to our model, farnesylation increases the binding affinity of the protein and alters the way other protein molecules interact with K-Ras4B.

4 PLASMA MEMBRANE REGULATES RAS SIGNALING NETWORKS: A REVIEW

4.1 Introduction

An intriguing phenomenon in biology is the astonishing number of functions some proteins, such as Ras GTPases, tend to perform. Ras activates more than 20 effectors, initiating complex cellular responses to diverse environmental stimuli. Ras signaling is initiated by growth factor, antigen, chemokine and cytokine ligands. The current paradigm states that receptor-ligand interaction activates Ras at the plasma membrane by Guanine exchange factors (GEFs) which promote the displacement of GDP for GTP (63). In its active state Ras interacts with effector proteins to regulate cell proliferation, survival, migration, invasion, and apoptosis (65-67). Of all Ras effectors, Raf and phosphoinositide-3 kinases (PI3-Ks) are the most well studied. Signaling through Ras ceases when its GTPase domain hydrolyses GTP to GDP (Figure 4.1). The intrinsic hydrolysis is a slow process catalyzed by GTPase activating proteins (GAPs) (73). Ras GTPases are small 21 kDa proteins and many of Ras binding partners seem to share the same binding site. This site is a short extension of the Switch I region in the Ras GTPase domain, named the effector binding region (70-72). Binding of multiple effectors to a short stretch of amino acids in a small protein at the same time seems inconceivable. How Ras achieves signaling diversity is a conundrum waiting to be fully resolved. Accumulating evidence suggests that Ras association with the plasma membrane plays a significant role in deciding the number and the type of signaling outputs. Like a circuit board, the plasma membrane has the ability to organize different types of circuits or platforms, through which Ras switches on an intricate network of signals. The principles for the circuit formation are becoming clearer as we discover the complex organization of lipids within the plasma membrane. Lateral segregation of lipids into distinct microdomains within the membrane has led to the hypothesis that these microdomains serve as

signaling platforms (239-241). Accordingly, interaction of Ras with different membrane microdomains can affect its access to different GEFs and effectors. Membrane microdomains may also have distinct effects on Ras structure and orientation. Another possibility is that the oligomerization status of Ras may differ among various microdomains. These are the ideas that the current Ras research is focused on. In this review, we cover the advances in the field of Ras biology leading to deeper understanding of the role the plasma membrane plays in Ras signaling.

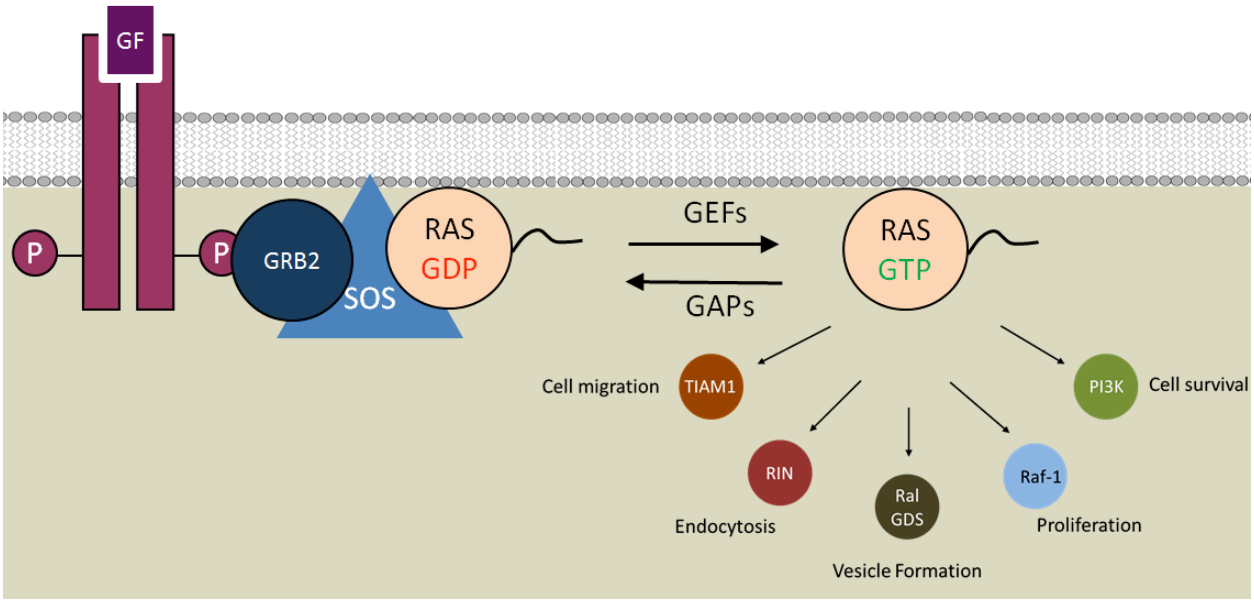

Figure 4.1: Activation of Ras.
Growth factor (GF) binding to its receptor initiates recruitment of GRB2 and SOS to the membrane. SOS is a guanine exchange factor (GEF), which binds Ras-GDP and converts it to active Ras-GTP. GTPase activating proteins (GAPs) catalyze conversion of Ras-GTP to its GDP loaded form. The balance between GEFs and GAPs determines the amount of active Ras in cells. Active Ras proteins bind more than 20 known effectors, which produce various cellular effects.

4.2 Unique microdomains are present in the plasma membrane

The plasma membrane is considered to be a highly heterogeneous and dynamic entity due to the lateral segregation of lipids, localization of proteins and endocytic or exocytic processes. This heterogeneity leads to the formation of several types of microdomains functioning as signaling platforms for membrane proteins (239-241). These microdomains can be either transient or long-lasting and stable assemblies (242). A lipid raft is one such microdomain, which is rich in cholesterol and saturated lipids like sphingolipids. These components are packed tightly together, forming a highly ordered, high density structure that is distinct from the surrounding low density lipids. One example of high density microdomains is caveolae. Caveolae are invaginations present in cells consisting of components similar to those of lipid rafts (243). Several unclassified lipid microdomains have been observed in different studies. Cholesterol-independent non-raft microdomains have been observed using electron microscopy (244). Another such non-raft microdomain contains primarily acidic headgroups present on phosphatidylserine and phosphatidic acid. Positively charged proteins bind to such microdomains through electrostatic interactions (245). Thus, it is becoming evident that the organization of the plasma membrane is complex, as it consists of a number of entities, which differ in lipid composition and physical properties. Membrane associating proteins exploit this heterogeneity to diversify their functions.

4.3 Interaction of Ras GTPases with different membrane microdomains

Ras isoforms, H-Ras, N-Ras, K-Ras4A and K-Ras4B contain a highly conserved N-terminal catalytic domain. The C-terminal 22-25 amino acid-long portion of Ras is termed the hypervariable region (HVR) since it differs significantly across isoforms in its amino acid

sequence (246). Although the N-terminal domains may contribute to membrane binding (247), Ras proteins primarily interact with the membrane through their HVRs (248). The differences in amino acid sequence of Ras HVRs are augmented by different post-translational modifications. For instance, H-Ras, N-Ras and K-Ras4A are modified with farnesyl and palmitoyl lipid groups on their HVRs, which anchor the proteins to the plasma membrane. The palmitoylation-depalmitoylation cycle allows them to shuttle between the plasma membrane and the endomembranes of the Golgi apparatus and Endoplasmic Reticulum (45). K-Ras4B, on the other hand, lacks palmitoyl groups in its HVR. Instead, a polylysine patch in the K-Ras4B HVR in addition to the farnesyl group helps in binding to the membrane. Hence, K-Ras4B has an alternative cycling mechanism. K-Ras4B undergoes protein kinase C (PKC) mediated phosphorylation at a serine residue (S181) on its HVR. This phosphorylation event is believed to dissociate K-Ras4B from the plasma membrane through electrostatic repulsion with the negatively charged phospholipid headgroups (43, 47, 48). However, this view has been recently challenged by a study, claiming that a significant fraction of phosphomimetic oncogenic K-Ras4B stays associated with the membrane (49). In this study, phosphorylation was found to change the distribution of K-Ras4B from low density to high density microdomains in the plasma membrane (49). Another mechanism that allows K-Ras4B to traffic from the membrane to the cytosol is calmodulin binding. Of all Ras isoforms, calmodulin exclusively binds K-Ras4B (103). Upon binding to calmodulin, K-Ras4B dissociates from the membrane to the cytosol in a calcium dependent manner (104). Similarly, other proteins like PDEδ and PRA1 can also dissociate K-Ras from the membrane (249)

So far, evidence for the localization patterns of Ras proteins on lipid rafts is contradictory. While H-Ras is predominantly found on lipid rafts (250-252), K-Ras localization on lipid rafts is a

contentious issue. Some groups have observed K-Ras localization on rafts (253), while others have not (254). The inconsistency may be ascribed to differences in the methods of preparation of lipid rafts or the observational techniques used for protein detection in membrane microdomains. However, recent reports from several groups that use different membrane preparation and detection methods to show K-Ras in lipid rafts lend credibility to this idea (255, 256).

4.4 Membrane microdomains change access of Ras to its binding partners

It has been communicated in several reports that Ras proteins have different degrees of access to GEFs, GAPs, and effectors in different microdomains. This differential access idea (graphically shown in Figure 4.2) has been used to explain isoform specific signaling of Ras (257). For example, H-Ras activates PI3-K to a greater extent than K-Ras4B whereas K-Ras4B is responsible for activation of Raf-1 (211). Although PI3-K membrane localization pattern has not been studied, a substrate of PI3-K, Phosphatidylinositol 4, 5-bisphosphate (PIP2), is found in the inner leaflet membrane microdomains (258). These PIP2 microdomains can be cholesterol independent and distinct from rafts. It is conceivable that PI3-K may co-localize with its substrate PIP2 in these microdomains.

Electrostatic interactions between the HVR of K-Ras4B and the plasma membrane allow for higher affinity binding of K-RasG12V to the membrane as compared to H-RasG12V in BHK cells (48). This causes efficient recruitment and activation of Raf-1 molecules only on the K-Ras clusters in the membrane (259). Moreover, when Raf-1 is directed to H-Ras occupied lipid rafts, the activation is minimal (260). This phenomenon could be attributed to the exposure of Raf-1 to a distinct group of proteins and lipids present on the membrane (260).

Two crucial factors determine the differences in activation by Ras isoforms. The first one is the extent of co-localization of Ras isoforms with their corresponding receptor complexes on the particular membrane microdomains (261). An illustration of this is the fact that K-Ras on disordered microdomains becomes efficiently activated in growth factor dependent cell lines. Conversely, H-Ras or N-Ras bound to lipid rafts are less active in these cells. K-Ras is preferentially activated because epidermal growth factor receptors and components of the activated receptor complex, including GEFs like SOS, also localize on the disordered microdomains (261). The second important factor for isoform specific Ras signaling is the sensitivity of Ras isoforms to different GEFs recruited by activated receptors (261). For example, activation of Ras proteins by B-cell receptor (BCR) is independent of the localization patterns of the isoforms. RasGRP, a GEF protein, is responsible for activation of H-, N- and K-Ras proteins through BCR. Conversely, M-Ras, another Ras superfamily protein, is not activated through BCR. This is because M-Ras is sensitive to a different GEF, namely RasGRF. Thus, the interplay of different receptors and protein complexes that interact with Ras together modify the protein's exact response (261).

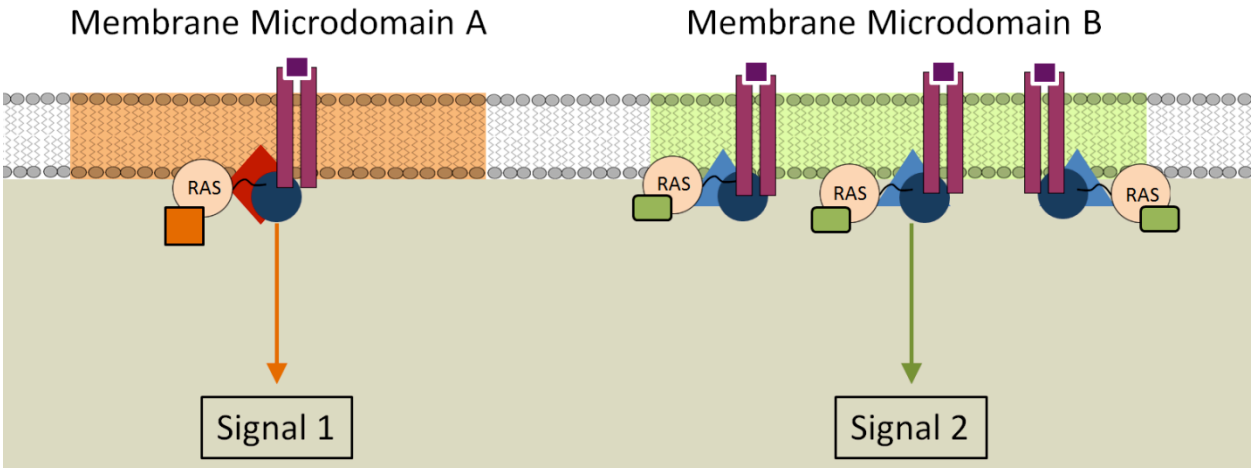

Figure 4.2: Differential access of effectors at distinct mcirodomains.
Binding of Ras proteins to different membrane microdomains can allow differential access to effectors. This causes differential signaling of Ras proteins from different microdomains in the plasma membrane.

4.5 Membrane induces conformational and functional alterations in Ras

Differences in the orientation of Ras proteins on the membrane can also lead to unique signaling mechanisms. This has been predicted to occur through the exposure of different effector interacting surfaces of membrane-bound Ras towards the cytoplasm (Figure 4.3) (262).

Molecular dynamics simulations of Ras proteins, corroborated by fluorescence studies and cell assays, point towards a novel Switch III region involved in reorienting the H-Ras catalytic domain on membrane lipids. The Switch III region is believed to comprise the loop between β-strands 2 and 3, and the α-helix 5 of the catalytic domain. It reorients α-helix 4 of H-Ras upon nucleotide exchange, such that the G-domain in active H-Ras participates in membrane binding. In H-Ras-GDP, however, the HVR plays a more significant role in anchoring the protein in the membrane. This mechanism of orientation-dependent function has been termed the "balance model" (247, 263). Interaction of H-Ras with effectors, PI3K and Ras scaffolding protein galectin are sensitive to H-Ras reorientation at the membrane. For example, while PI3-K and galectin interact better with the α-helix 4 stabilizing R169A/K170A mutant of H-RasG12V, their interaction is abrogated with the α-helix 4 destabilizing R128A/R135A mutant of H-RasG12V (247, 263).

K-Ras, on the other hand, is regulated in a different manner. In K-Ras, the active GTP-bound conformation was stabilized by the HVR binding to the membrane. Although the role of a similar Switch III region has not yet been investigated in other Ras isoforms, its existence cannot be denied (262).

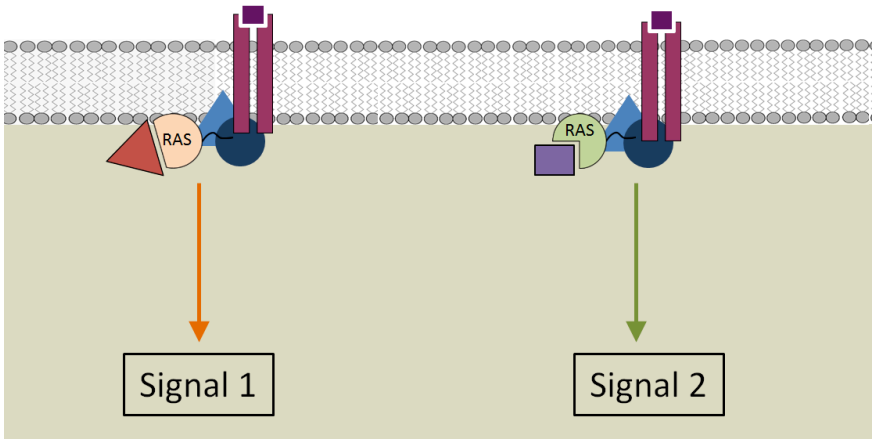

Figure 4.3: Structural differences in Ras isoforms on the membrane.
Different Ras isoforms can adopt distinct conformations on the membrane to allow binding of distinct effectors to elicit diverse downstream signals.

4.6 Ras dimerization, oligomerization and clustering

The possibility of Ras existing in different oligomerization states at the plasma membrane has recently emerged as a new way of regulating Ras function. Ras dimers are frequently found by X-Ray crystallography (264). Inouye et al. used a protein-fragmentation complementation assay to demonstrate that Ras-GTP dimers in HEK293 cells mediate Raf-1 activation (265). Recently, H-Ras dimerization in lipid bilayers has been demonstrated by time-resolved fluorescence spectroscopy and microscopy. In this study, no higher order oligomers of H-Ras were observed (266). Moreover, variations in membrane composition did not affect H-Ras dimerization. N-Ras has also been shown to dimerize in the GDP-bound inactive state in POPC (1-palmitoyl-2-oleoyl-sn-glycero-3-phosphocholine) bilayers. Ras proteins bind the POPC bilayers as dimers or oligomers, in an orientation perpendicular to the membrane surface. Although the computational simulations point towards a dimer, it has been proposed that oligomerization due to diffusion limited partner switching of dimers cannot be excluded (267). K-Ras4B was found to form nanoclusters that are membrane-anchored through a farnesylated HVR. Anchoring stabilizes the Ras dimers, increasing Ras effective local concentration and favorably orienting the catalytic domain (163). To this effect, the formation of large, activated Ras signaling complexes has also been observed by Murakoshi H et. al using single molecule FRET in KB cells (268). These large, activated signaling complexes recruit GAP molecules to the membrane, which then catalyze GTP hydrolysis and cause dissociation of the complexes. These results suggest that GDP-bound Ras is less prone to oligomerization (268). However, several publications propose the formation of Ras-GTP as well as Ras-GDP nanoclusters, which are spatially distinct for each isoform (269). It may be that methodological differences used by different labs lead to alternate conclusions regarding the existence of Ras-GDP oligomers. Murakoshi et al. use FRET to study

the formation of complexes whereas the Hancock group uses EM on immunogold labeled plasma membrane sheets and mathematical models to detect the same. Electron microscopy and single flourophore tracking indicate that Ras proteins are arrayed in nanoclusters on the inner plasma membrane (268, 270-272). These nanoclusters are formed through the assembly of the lipid-anchored Ras proteins into transient dynamic structures. They contain 6–8 Ras proteins with diameter of 12–22 nm, and are highly dynamic structures since each cluster turns over on average every 0.4 s. Each Ras isoform occupies spatially distinct nanoclusters and about 40% of any Ras isoform is arrayed in these nanoclusters (270).

These Ras nanoclusters function as signaling platforms through effector recruitment. As confirmed by single particle tracking, Raf is recruited from the cytosol to immobile Ras clusters (268, 271). The association of MEK with both Raf and ERK ensures the recruitment of the entire MAP kinase cascade to Ras nanoclusters (273-275). Studies confirm the significance of Ras nanoclusters in MAPK activation. Blocking nanocluster formation disrupts Ras-dependent MAPK signaling. MAPK signaling is spatially regulated. Moreover, the propensity of nanoclustering is a direct function of the concentration of EGF upon stimulation. These nanoclusters of Ras have been deemed to be important for signal transmission since their abrogation leads to failure of Raf recruitment in silico (276). The signal output decreases to 3% of its maximal value when Ras proteins function as individual molecules rather than as nanoclusters (272, 276). A decrease in Ras clustering diminishes the target area of the plasma membrane available for Raf-MEK-ERK recruitment, which in turn, decreases the probability of successful recruitment and activation. These combined data reveal that cell signaling relies on the formation of functional Ras nanoclusters at the plasma membrane. Thus, cells can adjust their responsiveness to the stimuli by regulating the degree of Ras clustering (277).

The Ras nanocluster system has an intrinsic capability to maintain its functions despite internal and external perturbations. Activation of the MAP kinase module exclusively at the plasma membrane provides resistance to the pathway against pharmacological inhibitors (278). Experimental studies demonstrate that Ras nanoclusters function as high-gain amplifiers for MEK activity (277). A graphical representation of signaling through Ras oligomers is shown in Figure 4.4.

Thus, the only proposed function of Ras oligomers is to facilitate homo- and heterodimerization of Raf kinases. Homo and heterodimers are required for Raf activation (279). Thus, Ras oligomers are expected to increase the incidence of Raf dimerization. Interactions of Ras GEFs, GAPs, and other effectors with Ras oligomers are possible but have not yet been well investigated.

In conclusion, the diverse plasma membrane microdomains appear to play a decisive role in regulating Ras signaling. Membrane association limits the accessibility of Ras to effectors and alters the conformation of Ras and its oligomerization state. In this way signaling diversity of Ras can be achieved and regulated.

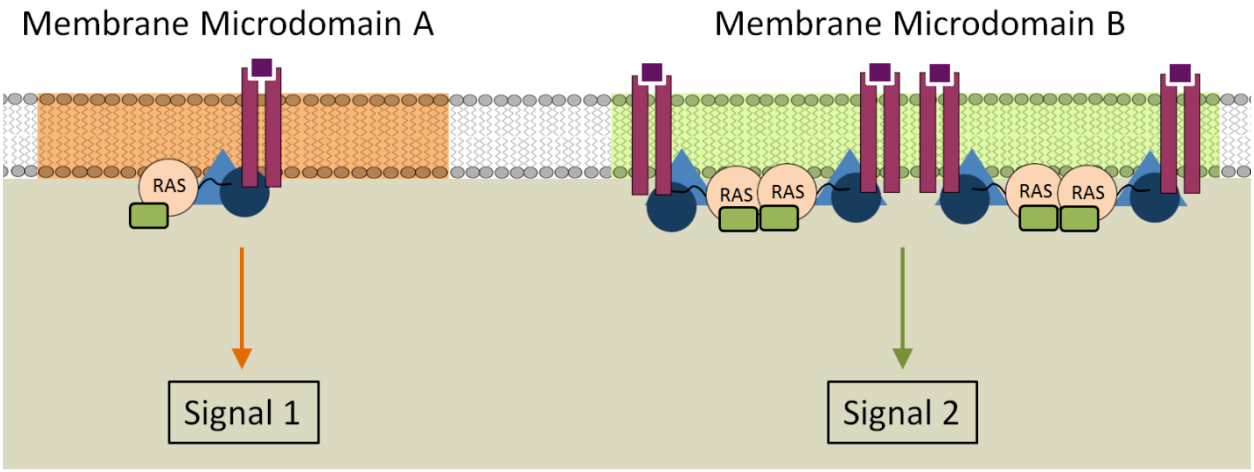

Figure 4.4: Ras oligomerization and signaling outputs.
Ras proteins exist in different oligomeric states on certain membrane microdomains. These states function as signaling platforms that activate distinct effectors to produce different signaling outputs.

5 NUCLEOTIDE DEPENDENT K-RAS4B DIMER AND HIGHER-ORDER ARCHITECTURES

5.1 Introduction

After studying intramolecular interactions of K-Ras4B, we decided to focus on the intermolecular interactions. It is shown that Ras proteins dimerize/oligomerize but the interface involved in these interactions is not known. With the use of biochemical and computational approaches, we focused on uncovering the interface involved in dimerization/oligomerization.

Ras GTPases regulate essential functions including cell survival, proliferation, motility and cytoskeletal organization (171, 280), acting as molecular switches in response to receptor-mediated extracellular signals (281). Ras-GTP activates downstream effectors (228), including Raf kinase (282, 283) and phosphatidylinositol 3-kinase (PI3K) (80, 284-286). Full activation of Raf requires its dimerization (287), which can be facilitated by preformed Ras assemblies (265). The previously accepted concept suggested that Raf dimerization is induced downstream by the dimeric 14-3-3 cofactor protein (288). However, a recent observation that C-Raf exists predominantly as monomers in the cytoplasm under resting conditions but forms dimers, trimers as well as tetramers in the presence of active GTP-bound Ras argues that Ras plays a significant role in Raf dimerization (289). Recent studies suggested that N-Ras-GDP can form dimers in a model membrane (290). Native H-Ras anchors and dimerizes only on the membrane and the Switch II region (residues 60-76) is either a part of, or allosterically linked to, the dimer interface (291). K-Ras4B oligomers are membrane-anchored through a farnesylated HVR. Anchoring stabilizes the Ras dimers, increases Ras effective local concentration and orients the catalytic domain favorably (163). However, how Ras dimerization relates to activation of its effectors has

been unclear. Identification of Ras dimer interfaces and comparing them to the protein surfaces in Ras-effector complexes is a critical step to unveiling the physiological role of Ras dimerization.

Binding of Raf monomers to a Ras dimer has been expected to promote normal Raf dimerization, leading to an overarching community goal to validate and understand Ras dimerization and how it relates to Raf's regulation- activation and inhibition. Raf side-to-side dimer formation (282) is necessary for normal Ras-dependent Raf kinase activation; it also takes place in aberrant, disease-associated mutant Raf proteins and in inhibitor-induced Raf activation, all leading to high intrinsic Raf kinase activity (287). Signal-activated Ras recruits Raf to the cell membrane and activates its kinase domain. Activation takes place by Ras binding, which opens the closed Raf conformation, thereby allosterically altering the kinase domain and promoting its dimerization (292). Through phosphorylation, the active Raf triggers ERK and MEK protein kinases, resulting in cell proliferation and survival (282). The crystal structure of Ras with Raf's Ras binding domain (RBD, PDB code: 4G0N) indicates that the high affinity Raf-Ras interaction involves extension of the Ras β-sheet at the Ras effector binding region.

Here we focus on two key questions: which Ras state (GTP- or GDP-bound) is the preferred dimerization species and what is the dimerization interface. These questions are of fundamental importance to the understanding of Ras and Raf signaling, and for identification of potential surfaces to develop inhibitors against Ras overactivation. We show that the GTP-bound, but not GDP-bound K-Ras4B forms stable homodimers and model the GTP-bound catalytic domain dimer structures. Unexpectedly, we observe two major interface classes; using dynamic light scattering (DLS), microscale thermophoresis (MST), and NMR, we test and confirm the modeled structures. Importantly, the highly populated dimer interface spans the Switch I and effector

binding regions at the effector lobe. It involves β-sheet extension and is very similar to Raf's interaction as well as to other effectors' binding at this surface, such as PI3K. The second homodimer class interaction involves an α-helical interface at the C-terminal allosteric lobe of the G-domain. Our models illustrate how clustering can take place, and provide architectures for Ras oligomers. These results are significant since they suggest a mechanism for how Ras dimerization may regulate Raf dimerization.

5.2 Materials and Methods

5.2.1 Computational prediction of the structures of Ras dimer and tetramer:

We used PRISM (293-295), an accurate template-based protein-protein complex structure prediction algorithm, to predict models for the dimeric and tetrameric structures of the Ras protein. PRISM is based on our observation that protein-protein interface motifs are conserved in nature, similar to single chain architectures. PRISM uses the tertiary structure of proteins of interest to build models. The solutions are optimized by a docking refinement protocol and ranked based on the binding energy scores (BES) computed by FiberDock (296), which has been implemented in PRISM. PRISM has been tested extensively for a range of proteins and pathways. Its accuracy has been demonstrated (297). The structural data for the dimer predictions (target proteins) have been obtained from the PDB. These predictions are then used to build and assess models for Ras tetramers. We used the G-domain (corresponding to Ras residues 4-166) of K-Ras as target proteins. K-Ras catalytic domain has 10 structures in the PDB, respectively. They include GDP- and GTP-bound conformations. We included all K-Ras structures in the prediction. Then, we identified the interface regions of the putative dimers using the HotPoint web server (298), which accounts for conservation, solvent accessibility and the

total contact potential of the interface residues. We compared our results with crystal structures to further affirm our predictions. We used the Evolutionary Protein-Protein Interface Classifier (EPPIC) (299) Server to classify the crystal interfaces in Ras structures. We further built unit cells of Ras crystals using Chimera to check whether the interfaces match.

5.2.2 Protein preparation:

Protein preparation was carried out according to Section 2.2.1.

5.2.3 Dynamic light scattering:

DLS studies were performed on a DynaPro Tytan instrument equipped with a Temperature-Controlled MicroSampler (Wyatt Technology Corp., Santa Barbara, CA) at a laser wavelength of 830 nm, scattering angle of 90° in a 12-µl quartz cuvette at 25°C. Each measurement consisted of sixty 10-second acquisitions (300). All samples were centrifuged at 15000 *g* for 10 min before measurements. To obtain the hydrodynamic radii (R_h) and percentage polydispersity, the intensity autocorrelation functions were fitted with a non-negative least squares algorithm by *Dynamics 7.1.1.3* software (Wyatt Technology Corp., Santa Barbara, CA.)(301).

5.2.4 Microscale thermophoresis:

For labeling the Ras protein with fluorescein, 1.6 mg fluoresceine maleimide (Santa Cruz Biotechnology Inc.) was dissolved in 25 µl DMSO. 5 µl were diluted in 10 µl buffer. The resulting solution was slowly added to 400 µl of 75 µM GTP-γ-S-loaded K-Ras solution in 100 mM HEPES buffer pH 6.5 containing 5 mM $MgCl_2$, 50 mM NaCl and 0.5 M BCEP. The mixture was incubated overnight at 4°C and filtered through NP-5 column (GE) equilibrated with the reaction buffer. LC/MS showed no traces of the maleimide and complete labeling of intact K-

Ras. For MST studies we have prepared 16 2-fold serial dilution of GDP or GTP-γ-S-loaded K-Ras_{1-166} starting from 60 μM. Titration series were prepared that contained 15 μl of 60 nM fluorescein-labeled K-Ras and 15 μl of non-labeled K-Ras. The final buffer composition included 25 mM HEPES pH 7.2, 50 mM NaCl, 2.5 mM $MgCl_2$. MST measurements were taken as per Section 2.2.4.

5.2.5 NMR experiments:

All ^{1}H-^{15}N HSQC NMR spectra were collected on a 900 Mhz Bruker Avance Spectrometer at 25°C. The buffer used for dissolving the proteins contained 50 mM Tris-citrate, pH 6.5, 50 mM NaCl, 5 mM $MgCl_2$, 10 mM β-mercaptoethanol and 10 mM $CaCl_2$ and 10% deuterated water. Data processing and analysis were carried out as per Section 2.2.5.

5.3 Results

5.3.1 GTP-bound, but not GDP-bound K-Ras catalytic domain forms stable dimers.

To evaluate the oligomerization state of K-Ras G-domain, we performed dynamic light scattering (DLS) experiments. DLS of GDP-bound K-Ras_{1-166} showed a broad size distribution of protein particles (Figure 5.1). The predominant species has a radius that corresponds to a globular protein of 18 kDa molecular mass, which is close to the mass of a G-domain monomer (18.8 kDa for K-$Ras4B_{1-166}$). In contrast, GTP-γ-S-bound K-Ras_{1-166} demonstrates narrow particle size distribution (with 9.9% polydispersity) and a radius that corresponds to a globular protein with a molecular mass of 41 kDa. These data suggest that K-Ras_{1-166}-GTP-γ-S forms a stable dimer, while K-Ras_{1-166}-GDP may have a reduced tendency to aggregate, but the dimer is unstable, in good agreement with the modeling data.

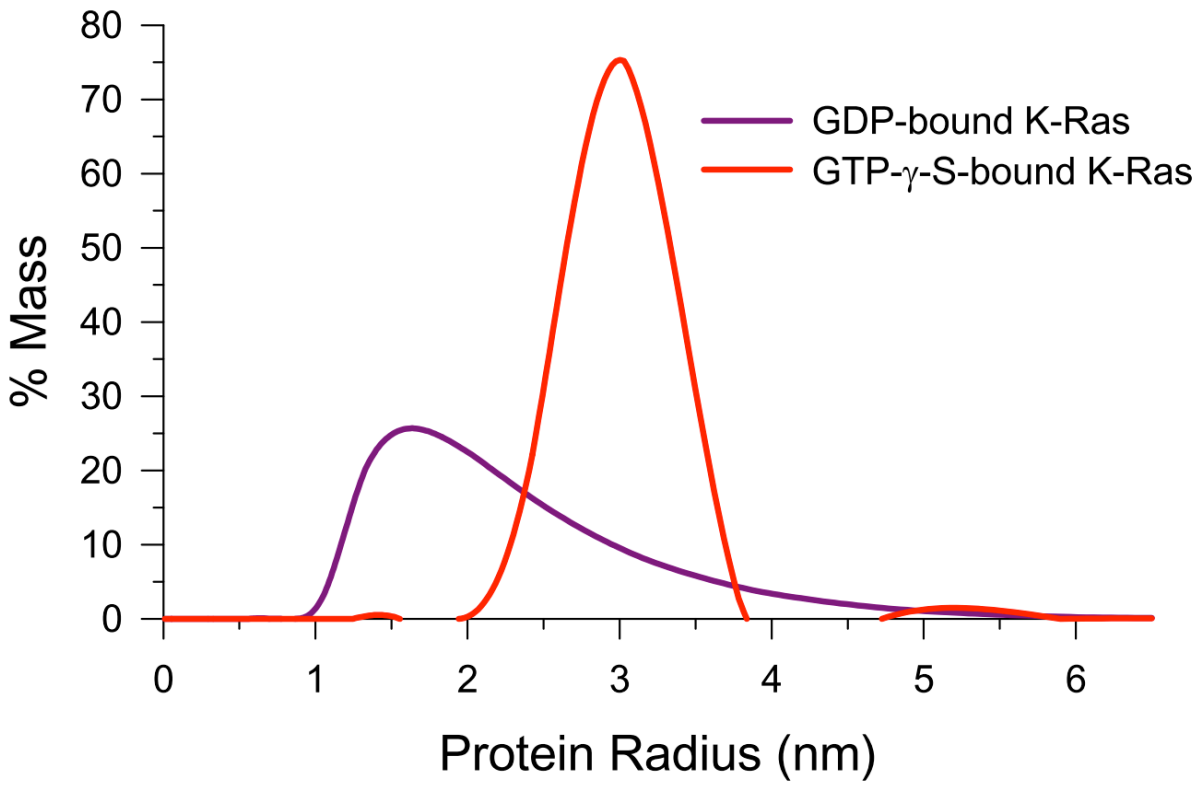

Figure 5.1: Dynamic light scattering (DLS) of active and inactive catalytic domains of K-Ras4B.
DLS shows the formation of a stable dimer (41 kDa) by GTP-γ-S-loaded K-Ras4B G-domain, but not by GDP-loaded protein (18 kDa).

5.3.2 Predictions of K-Ras4B dimer structures.

To evaluate the structural basis for dimer formation by Ras proteins, we exploited a powerful template-based protein-protein complex structure prediction algorithm (PRISM)(293-295). The list of target PDB codes used for the predictions is provided in Table II. Our modeling results suggested that the K-Ras4B-GTP dimer is more stable than its GDP counterpart. The first predicted dimer interface involves a β-sheet extension, forming intermolecular H-bonds between β2 strands. Computations also predict a second dimer interface, involving an α-helical interface in the α3 and α4 regions at the C-terminal allosteric lobe of the G-domain. The enhanced stability is associated with a larger interface and more hot spots in the GTP-bound dimer and thus favored a higher binding energy score (BES) (Figure 5.2). Analysis of atomic interactions showed that the K-Ras4B-GTP dimer interface contains more H-bonds than the K-Ras4B-GDP dimer interface (Appendix C).

Table II: The list of K-Ras PDB structures used in PRISM predictions.

GTP-bound	3GFT, 4DSN, 4DSO
GDP-bound	4EPR, 4EPT, 4EPV, 4EPW, 4EPX, 4EPY, 4DSU

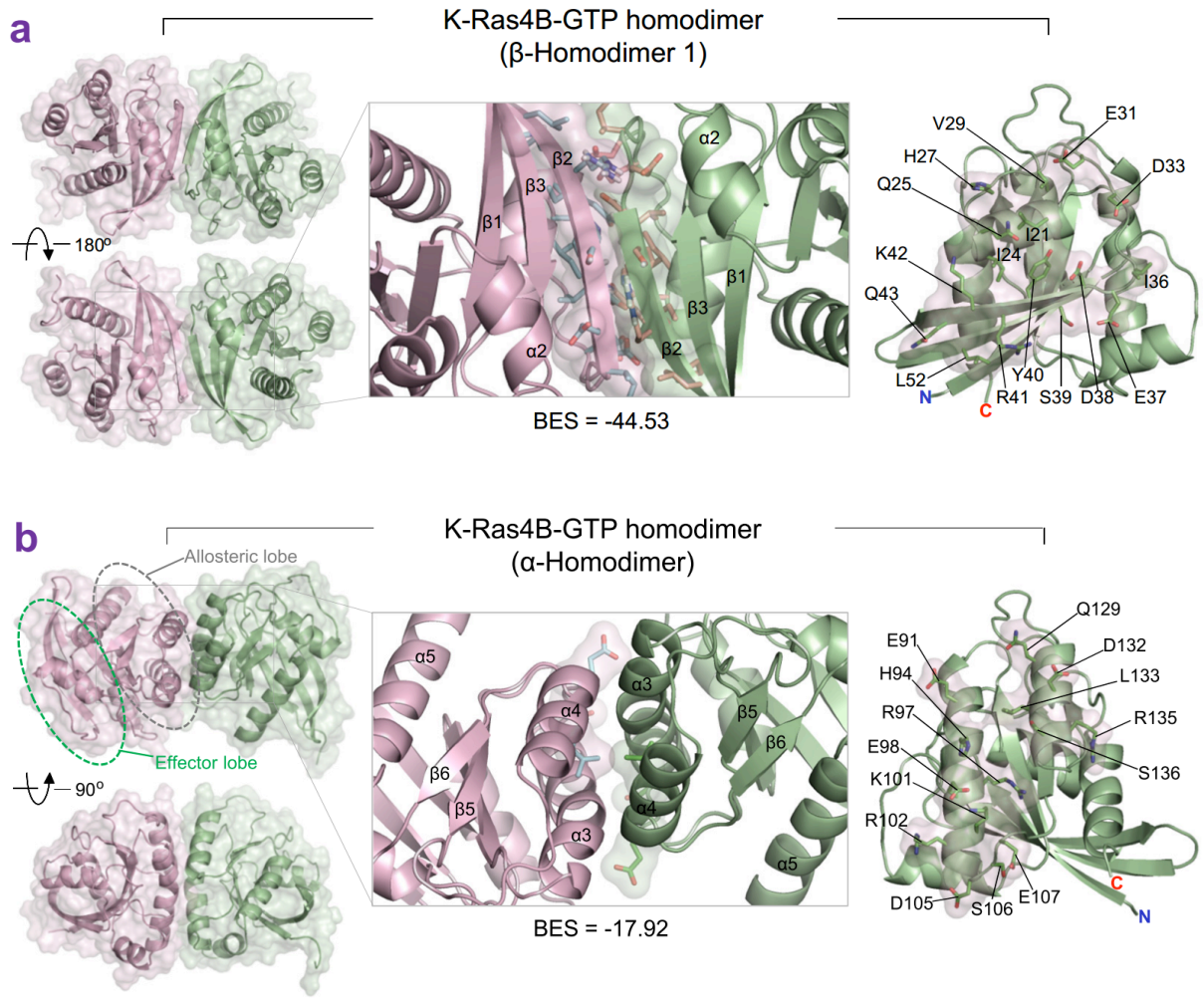

Figure 5.2: Predicted dimer structure of active K-Ras4B.
(A) Predicted dimer structure of GTP-bound K-Ras4B$_{1-180}$ with a β-sheet extension (Target PDB code: 4DSO). Binding energy score (BES) for the prediction is -44.53 and the predicted residues are labeled (B) Predicted dimer structure of GTP-bound K-Ras4B$_{1-167}$ with an α-helical interface (Target PDB code: 3GFT). Dimer interface is found to be at the allosteric lobe with binding energy score (BES) of -17.92. The predicted residues involved in binding are labeled.

5.3.3 Biophysics of K-Ras4B dimers.

To confirm further the high affinity dimerization of K-Ras$_{1-166}$-GTP, we employed microscale thermophoresis (MST)(194). The G-domain was labeled with fluorescein maleimide on Cys118. Substitution of this residue with Ser had no influence on Ras activity. Thus, we assume that addition of fluorescein to this position might have an insignificant effect on dimerization. We titrated the fluorescent protein with unlabeled GTP-γ-S-loaded K-Ras4B$_{1-166}$ for determining the dissociation constant for dimerization. The dissociation constant obtained was 1180 ± 92 nM (Figure. 5.3).

To map the interfaces involved in the association of K-Ras4B molecules in solution, we analyzed NMR chemical shift perturbations (CSPs) induced by dilution of K-Ras4B samples. High protein concentration in NMR samples may simulate the role of the plasma membrane, which increases the local concentration of Ras. Sample dilution can cause dissociation of the protein-protein complexes and reveal the interfaces by changes in the chemical shift values. Earlier we observed that the HVR associates with the catalytic domain of K-Ras4B-GDP primarily via the high affinity β-sheet interface, raising the possibility that this intramolecular interaction influences K-Ras4B dimerization. To address this possibility, we studied the interface of K-Ras4B$_{1-166}$. We compared the spectra of 245 μM and 30 μM K-Ras4B$_{1-166}$-GTP-γ-S. Assuming the dissociation constant for K-Ras4B$_{1-166}$-GTP-γ-S of 1180 nM, the dilution changes the dimer concentration by 8% from 95.4% to 87.4%, making observation of CSPs at 900 MHz possible. In our experiments the catalytic domain of K-Ras4B in its GTP-bound conformation is responsible for dimerization. Hence, for all subsequent NMR experiments we assumed similar or higher dissociation constants producing an at least 8% reduction in dimer concentration upon dilution. Residues in K-Ras4B$_{1-}$

$_{166}$-GTP-γ-S that exhibited dilution-dependent CSPs include K16 and I24 in α1, D30, E31, and E37 in the Switch I region, S39 and V44 in β2. In addition, we observed significant changes in N86, D119, Q131, R135, and K147. All these residues lie in the α3, α4 helices and the G4 loop which is adjacent to α4. These CSPs are shown in Figure 5.4 A.

Spectral overlays of ^{15}N HSQC spectra of 250 μM and 30 μM K-Ras4B$_{1-166}$-GDP indicated dilution-associated chemical shift changes of only five residues, E3 in β1, F28 and D38 in the Switch I region, H94 in α3, and Q129 in α4 as shown in Figure 5.4 B. The average CSP for K-Ras4B-GDP is significantly lower as compared to K-Ras4B-GTP-γ-S. Moreover, the number of statistically significant CSPs observed in GDP loaded K-Ras4B is comparatively fewer. These two observations support the DLS data which points toward a lower affinity interaction in the K-Ras4B-GDP dimer.

In conclusion, we observe the presence of two interfaces, namely a beta sheet interface located mainly on β2 and β1 and an alpha helix interface mainly on α3 and α4 that are involved in the formation of a K-Ras4B dimer.

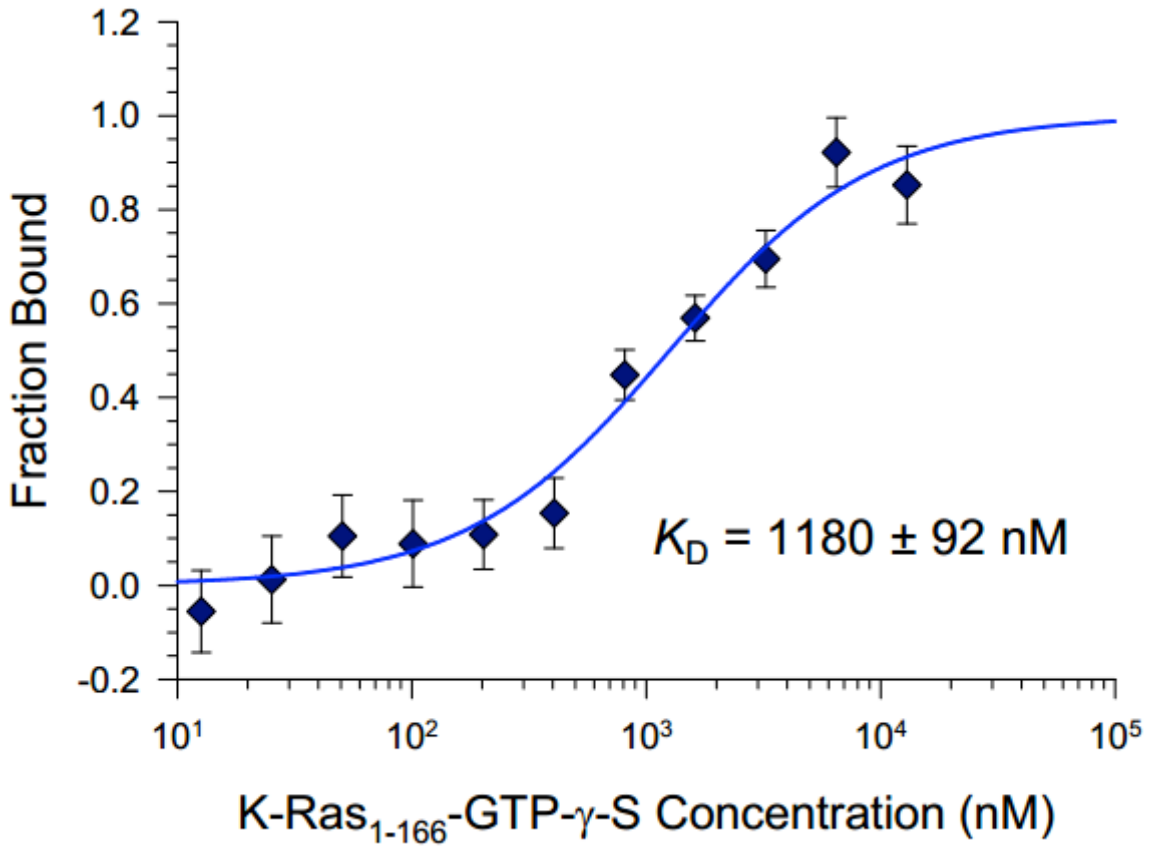

Figure 5.3: Determination of the Dissociation constant of the dimer using Microscale Thermophoresis (MST).

Dissociation constant, K_D, was determined by MST using 30 nM K-Ras$_{1-166}$-GTP-γ-S labeled with fluorescein maleimide on Cys118, which was mixed with increasing concentrations of non-labeled protein.

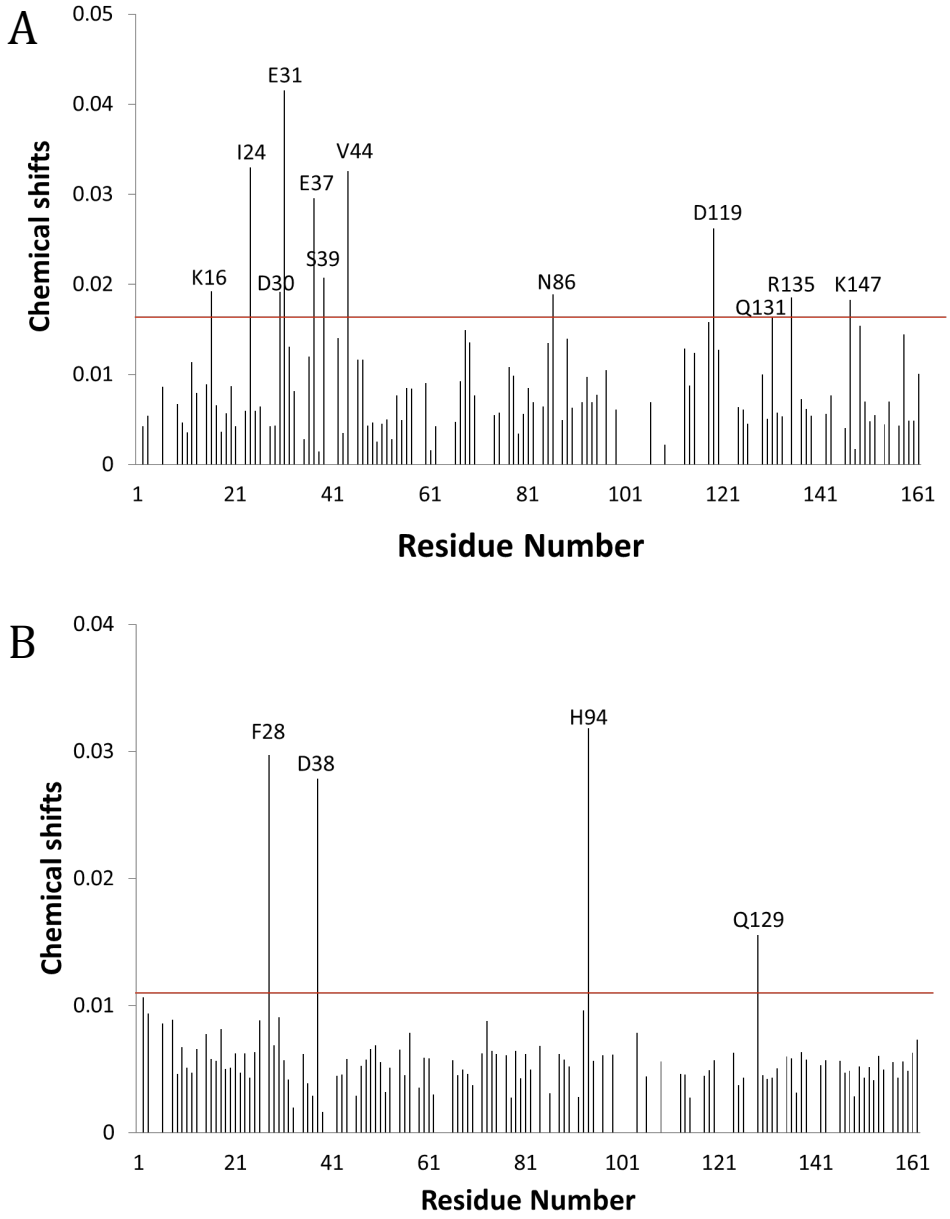

Figure 5.4: Chemical Shift changes obtained upon dilution of K-Ras4B catalytic domain. NMR experiments were run at high and low concentrations of K-Ras4B$_{1\text{-}166}$ in the GTP and GDP states. The perturbed residues of K-Ras4B$_{1\text{-}166}$-GTP-γ-S and K-Ras4B$_{1\text{-}166}$-GDP are mapped on the catalytic domain sequence in (A) and (B), respectively. The concentrations used for GTP-γ-S loaded protein was 245 μM and 30 μM whereas that for GDP loaded protein was 275 μM and 30 μM. The red horizontal lines in the graphs show the sum of average CSP and one standard deviation which represents significant CSPs. The residues showing significant chemical shifts are the ones involved in the dimerization.

5.3.4 Predictions on Ras-effector binding and oligomerization.

We predicted the Raf-Ras interaction interface using PRISM (Figure 5.5 A). We observed that the binding surfaces and interaction modes of Raf (from our predictions), and other Ras effectors important in cell transformation and proliferation such as PI3Kγ, PLCε, and Byr2 (crystal structures of the complexes of these effectors bound to Ras are available), overlap Ras' β-sheet dimer interface. Overlapping interfaces argue for an effective local effector concentration threshold as a regulatory mechanism in activation and signaling. Computations also predict a second, helical interface, supported by NMR chemical shift experiments for K-Ras4B-GTP dimers. PKCα binding interface (from crystal), overlaps this interface. Exploiting PRISM, computations reveal tetrameric architectures are possible for full length proteins. NMR data showed the presence of the beta sheet interface on the effector lobe and the alpha helix interface at the allosteric lobe. According to our predictions, Ras dimerizes and further tetramerizes through these two interfaces observed on the G-domain. We observe two major types of tetramer organizations: linear and curved. K-Ras4B-GTP prefers the linear form, which we observe computationally to form either through the β-sheet extension dimers followed by tetramerization through the helical interface or *vice versa*, which is more stable (Figure 5.5 B). Although K-Ras4B-GDP dimers and tetramers can occur through the same interfaces, their stability is significantly lower and a curved shape is observed (Figure 5.5 C). The two classes of dimers and the higher-order tetrameric organizations further substantiate nanocluster formation. Our interface predictions supported by NMR data suggest that the major nanocluster species is Ras-GTP. Since effector binding overlaps the dimeric interfaces, dynamic cluster reorganization can be expected.

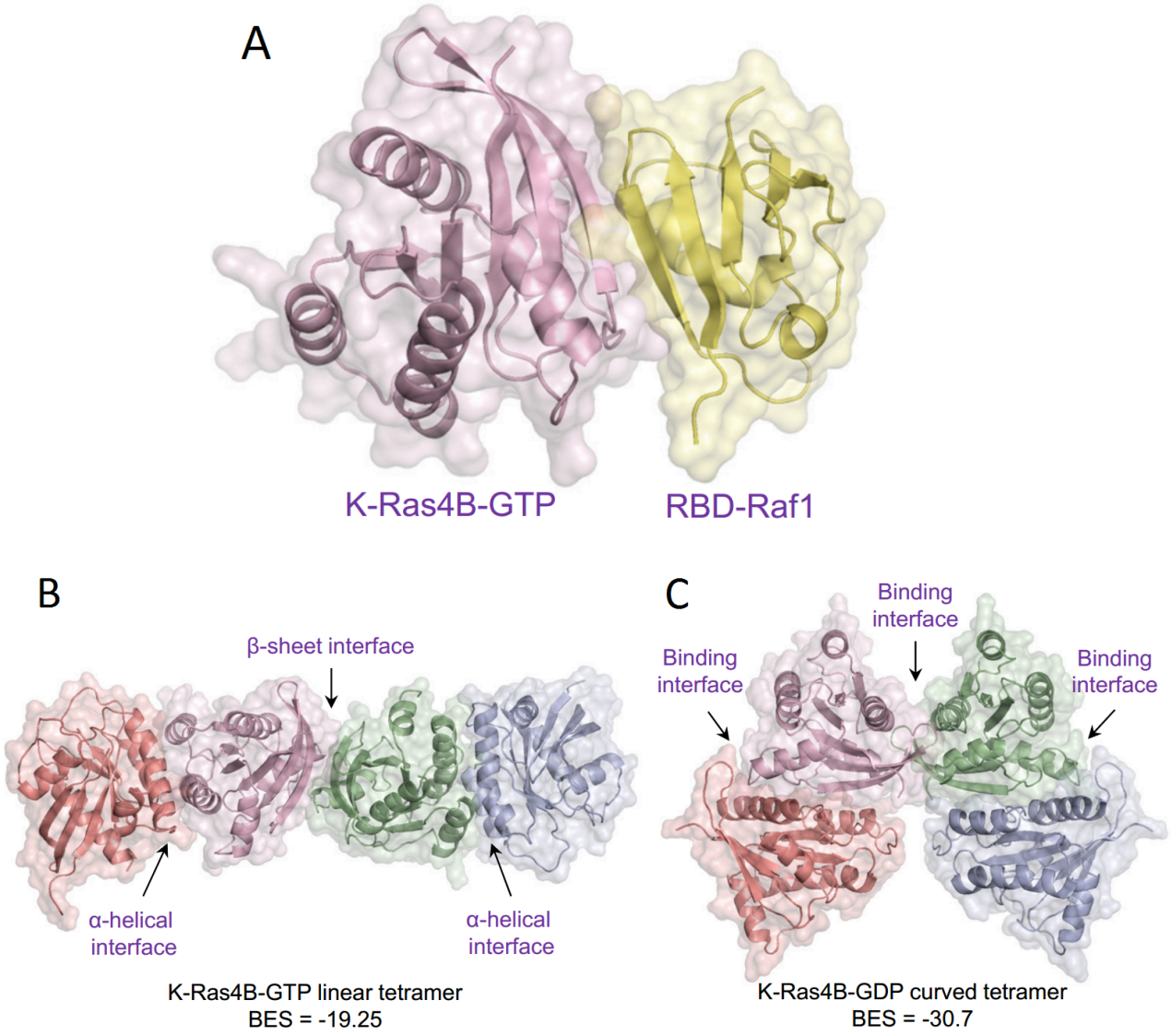

Figure 5.5: K-Ras4B-Raf-1 interaction interface matches one of the dimer interfaces.
(A) Predicted interaction interfaces of the GTP-bound K-Ras4B with Ras-binding-domain (RBD) of Raf1 (Target PDB code: 1C1Y). Predicted dimer, tetramer interface and corresponding binding energy scores for (B) K-Ras4B-GTP and (C) K-Ras4B-GDP.

5.4 Discussion

Application of a powerful structural prediction algorithm confirmed high affinity dimer formation for K-Ras4B-GTP, but only low affinity dimerization for K-Ras4B-GDP. A survey of Ras crystal structures showed that while the functional state of Ras has been identified as a monomer, its predicted membrane-anchored dimeric interface is among its crystal packing interactions. Dilution induced NMR CSPs of K-Ras4B$_{1\text{-}188}$ and K-Ras4B$_{1\text{-}166}$ dimers identify the dimer interfaces. Remarkably, the residues involved in the dimer interactions are in good agreement with those predicted by the computations, pointing to the significance of the dimerization. Collectively, dimerization emerges as a key control mechanism for protection from premature receptor-initiated signal firing.

We also propose formation of tetramers (monomer-dimer-monomer, or possibly dimer-of-dimers), predicted computationally and supported by NMR CSPs. The preferences observed in the Ras tetramer conformations underscore the heterogeneity of the Ras tetramer landscape, whose conformational preferences can be nucleotide-dependent, and shift with isoform sequence, and conditions like effector concentrations and membrane environment. Preferred isoform interactions may be further enhanced by different Ras isoform orientation with respect to the membrane (163). When in a tetramer form, the K-Ras4B-GTP dimer may be more amenable to Raf displacement, posing some possible activation scenarios. Lipid post-translational modifications on Ras proteins may further enhance the dimerization. Farnesylated and methylated HVR of K-Ras4B tends to aggregate at a concentration range as low as 10μM (302).

The dimer interfaces described here suggest a deviation from our current understanding in Ras effector activation. Common view holds that Ras dimerization is involved in Raf's activation,

with each Ras monomer being able to simultaneously dimerize and interact with the Raf's RBD. However, the interfaces of Ras-Raf and Ras dimer share a similar site. Raf, with nanomolar affinity for Ras, can outcompete β-sheet mediated dimerization. Raf dimerization may occur via Ras monomers linked by a less stable helical dimer interface, or by recruiting adjacent membrane-anchored Ras monomers. Nanoclustering may engage the helical interface to reassociate. We propose that both helical and β-sheet dimers are populated in membrane nanoclusters; a single interface type is unlikely to support nanocluster formation.

K-Ras can activate its effectors as a monomer so a drug abolishing dimer formation via β-sheet extension is unlikely to affect Raf activation. The only scenario where it would be useful is if its affinity outcompetes the high affinity Ras-Raf that already challenges drug discovery (303). However, dimerization will make activation robust to the cellular environment, preventing external stimuli from causing repetitive cellular firing. Thus, we propose higher order tetramer organization via the two interfaces revealed in this work, both shared with distinct Ras effectors. Both β-sheet extension and helical organization are common motifs in protein-protein interfaces in nature (304, 305). We reason that tetramerization driven by farnesylated K-Ras4B on the inner plasma membrane via dynamic, concentration- and actin-dependent(306) associations, possibly through IQGAP1(307, 308), confers higher specificity and dynamic cellular control(309). Signaling will be more robust as a higher order oligomer (310), than as a monomer. These heterogeneous oligomeric organizations can form basic membrane nanocluster units (306).

To conclude, it has been proposed that protein multimers play an important role in Raf activation (289). Here, a powerful combination of interdisciplinary techniques allowed us to elucidate the structural basis of Ras dimerization and an elegant mechanism of Raf regulation by Ras oligomerization. Our results substantiate nanocluster formation, and argue that Ras-GDP, with its

interface occupied by HVR, may not form stable dimers, and hence stable nanoclusters, via the β-sheet interface. We observe that Ras' double-interface is nucleotide-dependent, thereby unveiling the structural underpinning of nanocluster formation. Competitive binding at the highly populated interface by Raf can dynamically reorganize the nanocluster. Our results argue that therapeutically abolishing the major β-sheet mediated dimerization may not deter Raf's activation. However, targeting the helical dimer interface by small molecular weight compounds can decrease Raf signaling in cancer.

6 PRODUCTION OF FULLY MODIFIED K-RAS4B

6.1 Introduction

In the prior chapters I have described the structural mechanisms by which K-Ras4B activity is regulated. In this chapter I will describe how we successfully produced fully post-translationally modified K-Ras4B for future biochemical studies.

Protein expression and purification techniques have long been a staple in biochemical research. They often allow for in-depth biochemical analysis of proteins of interest from a structural and/or mechanistic point of view. While some proteins can be easily produced in their wild type forms, others may have properties which necessitate the use of more complex methods. These properties include protein post-translational modifications that often cannot be obtained in bacteria. Approximately 0.5% of all eukaryotic proteins undergo a form of post-translational modification known as prenylation (311). Prenylation is the addition of an isoprenyl lipid moiety, of which there are two known types: farnesyl and geranylgeranyl. The farnesyl group is 15 carbons long; the geranylgeranyl moiety is longer, consisting of 20 carbons. The farnesyl and geranylgeranyl groups are added to proteins by farnesyltransferase (FTase) and geranylgeranyltransferase (GGTase) enzymes, respectively. Prenyl groups are commonly involved in protein-protein and protein-lipid interactions employed by signalling molecules to initiate signal-transduction cascades.

A number of proto-oncogenic proteins are modified with a farnesyl moiety, including members of the Ras subfamily (30). Ras proteins are small GTPases that play an essential role in a number of cellular signalling processes. Several isoforms of classical Ras proteins have been discovered: H-Ras, N-Ras, K-Ras4A and K-Ras4B. Ras proteins share a basic structure, comprising a

GDP/GTP binding catalytic domain and a C-terminal hypervariable region (HVR), at which farnesylation occurs. Ras proteins signal from phospholipid bilayers, with the farnesyl modification thought to be essential for their localisation (41, 312).

While it is possible to produce sizeable amounts of K-Ras in its unmodified form(313), synthesis of fully modified K-Ras is far more problematic. One reason for this is that naturally modified K-Ras binds to effector proteins, with a nanomolar affinity. Consequently, purification of naturally modified K-Ras is extremely challenging. Conversely, unmodified K-Ras can be produced relatively easily using a recombinant approach.

K-Ras4B is a ubiquitously expressed splice variant of K-Ras. Its 3-step process of post-translational modification begins with the addition of a farnesyl group to a C-terminal CAAX sequence in the HVR, after which the AAX peptide is removed by Rcel protease. Finally, the terminal cysteine is methylated by the isoprenylcysteine carboxyl methyltransferase (ICMT enzyme). The methylation step removes the C-terminal negative charge, renders the protein more hydrophobic, and aids in membrane binding (34, 36). To better understand K-Ras4B signalling, a model needs to be established which accurately mimics these modification steps.

Mammalian and insect cell expression systems can produce naturally post-translationally modified K-Ras4B (314). However, the yields of these systems are low and not feasible for extensive biochemical analyses. Recently, progress in solid and solution-phase procedures for preparation of synthetic lipidated peptides has allowed a more practical method to produce modified K-Ras4B (315). In this instance, the lipidated peptide corresponds to the K-Ras4B HVR, and can be attached to truncated K-Ras4B *via* intein-mediated protein splicing or

maleimidocaproyl-controlled ligation. However, this method requires a complex peptide synthesis procedure.

Our method of K-Ras4B synthesis replicates all three stages of post-translational processing. Firstly, a bi-functional cross-linker is used to conjugate S-farnesyl L-cysteine methyl ester to the isolated HVR peptide of K-Ras4B. After this, a bacterial transpeptidase, sortase A, is used to ligate the peptide to truncated K-Ras4B.

We demonstrate that our semi-synthetically modified K-Ras4B bears much of the functionality of the naturally produced protein, through a range of activity assays. This makes it a desirable model upon which to base further biochemical studies, and ultimately design and test novel anti-cancer therapeutics. This method can be carried out using readily available reagents. In addition, this process can potentially be applied to other prenylation targets such as GTP binding proteins Rheb and Rnd3.

6.2 Materials and Methods

6.2.1 Protein Purification:

The protein purification was carried out as per mentioned in Section 2.2.1. The pET42a construct used for the expression of catalytic domain of K-Ras4B contained an additional sortase recognition sequence "LPXTG", where X can be any amino acid (E in our case), followed by a His-Tag on the C-terminus of K-Ras4B$_{1\text{-}166}$ gene.

6.2.2 Modification of the hypervariable region:

The modification of the HVR was carried out as per mentioned in Section 3.2.8. The peptide used for modification contained an additional G on its N-terminus for recognition by sortase.

6.2.3 Purification of Sortase A:

Sortase A cDNA was cloned into the pET42a vector. The restriction sites used were NdeI and XhoI. A His-tag was introduced to aid protein purification. The plasmid was transformed into BL21AI cells and the cells were grown in LB medium with shaking at 250 rpm. The cells were grown at 37 °C until their OD_{600} reached 0.6. Then, the expression of K-Ras4B was induced with 0.2 mM IPTG and 0.2% arabinose. The cells were grown thereon for 4 hrs at 30 °C with shaking at 250 rpm. The cells were harvested by centrifuging and the pellets were stored at -80 °C. The pellets were thawed at room temperature before lysis. The pellets were resuspended in 10 mM Tris-HCl pH 7.6, 20 mM Na-citrate, 50 mM KCl, 5 mM $MgCl_2$, 50 μg/mL DNaseI, and 2 mM β-mercaptoethanol. Lysis was carried out by sonicating the resuspended pellets. The lysate was centrifuged at 14000g at 4 °C and the supernatant was collected. The supernatant was incubated with the His-Bind resin for 2 hrs. Washing was done with the His-Bind Wash buffer and elution was carried out using a gradient from 30 mM to 1 M imidazole. The purity of the protein was assessed using an SDS-PAGE gel and mass spectrometry.

6.2.4 GTPase Activity Assay:

The GTPase activity assay was carried out using the EnzChek® Phosphate Assay Kit manufactured by Life Technologies. Fully modified K-Ras4B was mixed with 0.2 mM 2-amino-6-mercapto-7-methylpurine riboside (MESG), 1 unit/mL purine nucleoside phosphorylase (PNP), 10 mM $(NH_4)_2SO_4$, 0.1 mM EDTA and 0.5 mM GTP. Control mixture was made with the same components of the reaction mixture and replacing fully modified K-Ras4B with remaining volume made up using K-Ras4B storage buffer. After making these reaction mixtures, samples were transferred to quartz cuvettes and the absorbance was measured of the sample

mixture against the control at 360 nM for at least 600 minutes. The same assay was also carried out on the catalytic domain of K-Ras4B. The activity of the catalytic domain was used for comparison since it is responsible for the GTPase activity of K-Ras4B.

6.2.5 Raf-1 Binding assay:

The Raf-1 binding assay was carried out using the Ras Activation Kit manufactured by Millipore. Before carrying out the assay, K-Ras4B in its full length and truncated was freshly loaded with either GTP or GDP as per the nucleotide loading procedure mentioned in Section 2.2.1. The protein samples were then diluted separately to the required concentrations with a buffer containing 25 mM HEPES, 150 mM NaCl, 5 mM $MgCl_2$, 10 mM βME, and 5% glycerol. Raf-1 RBD agarose resin was added to these samples and incubated for 45 minutes at room temperature with intermittent mixing. The beads were then washed three times with the HEPES based buffer. A western blot was run on the pulled down protein and probed with an anti-Ras antibody provided in the kit.

6.2.6 Surface Plasmon Resonance:

SPR experiments were performed as per Section 2.1.8. The affinity wizard was used to test the binding and dissociation of protein samples. Data analysis was performed by plotting baseline corrected response units at equilibrium *versus* concentration.

6.3 Results

6.3.1 Ligation of farnesylated HVR to the K-Ras4B catalytic domain using sortase.

In order to successfully carry out the ligation procedure, we had to start out by producing the catalytic domain of K-Ras4B containing a sortase recognition sequence (LPETG) in addition to the His tag at its C-terminus and a farnesylated HVR peptide containing a glycine at its N-terminus. Purification of the catalytic domain of K-Ras4B containing the LPETG motif was carried out in the exact same manner as before. Also, the farnesylation of the HVR peptide with an N-terminal glycine was carried out as before. Before making the reaction mixture, K-Ras4B, sortase and the farnesylated HVR peptide were dialyzed against 50 mM Tris-citrate pH 9, 50 mM sodium chloride, 5 mM magnesium chloride, 10 mM calcium chloride and 10 mM β-mercaptoethanol. Then all the components were mixed together in a 2 mL Eppendorf tube such that the final concentrations of K-Ras4B, sortase and the farnesylated HVR peptide were 10 μM, 15 μM and 30 μM respectively. The reaction mixture was left at room temperature for 48 hours. When a sample of this reaction mixture is run on an SDS PAGE gel, it indicates the presence of the product which is the fully modified K-Ras4B (Figure 6.1 and 6.2). The reaction was stopped after 48 hours by passing it through nickel beads for separating the unreacted catalytic domain from the product. This step is also essential to separate the sortase, which also contains a His tag, from the product. The fully modified K-Ras4B does not bind to the beads and hence can be immediately collected without the need for elution.

6.3.2 Fully modified K-Ras4B is functionally active.

Functional characterization of the fully modified K-Ras4B was done using the GTP hydrolysis assay. The catalytic domain of K-Ras4B is responsible for binding to nucleotides and hence also

primarily responsible for hydrolysis of GTP to GDP. Hence we decided to compare the GTP hydrolysis rates of the catalytic domain of K-Ras4B with that of the fully modified protein. We found that the hydrolysis rates in both versions of the protein were quite comparable hence suggesting that the fully modified version of K-Ras4B produced using the sortase reaction was functionally active and retains its GTPase activity (Figure 6.3).

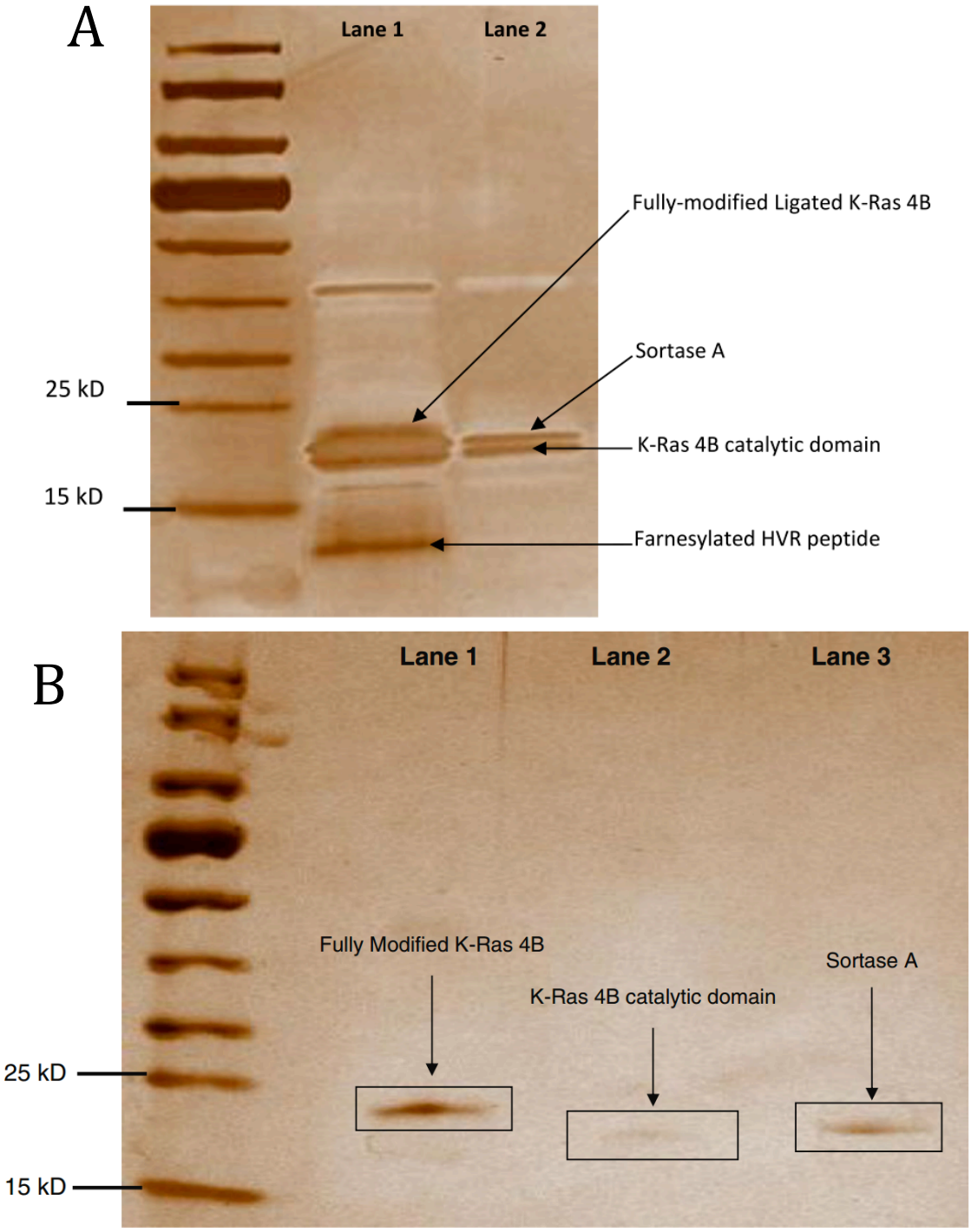

Figure 6.1: Formation of fully-modified K-Ras4B.
(A) SDS PAGE gel showing the protein mixture before (Lane 2) and after the 48 hours (Lane 1). Lane 1 shows the presence of an extra band forming due to sortase mediated ligation. Lane 2 shows K-Ras4B catalytic domain and sortase. (B) SDS PAGE gel showing the purified components individually.

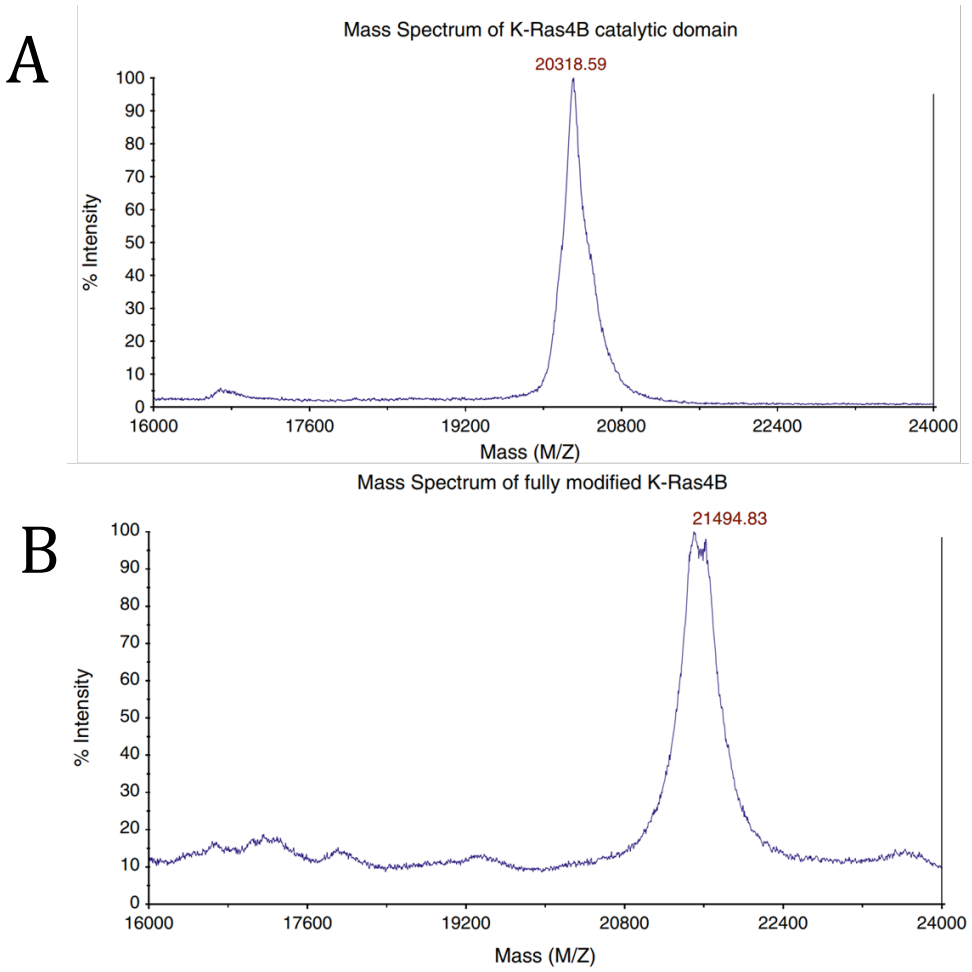

Figure 6.2: Mass spec comparison of modified and unmodified K-Ras4B

(A) Mass spectrum of K-Ras4B catalytic domain appended with N-terminal LPETG sequence and 6(His) tag. Sample analyzed using MALDI-TOF mass spectrometry. (B) The mass spectrum of fully modified ligated K-Ras4B.

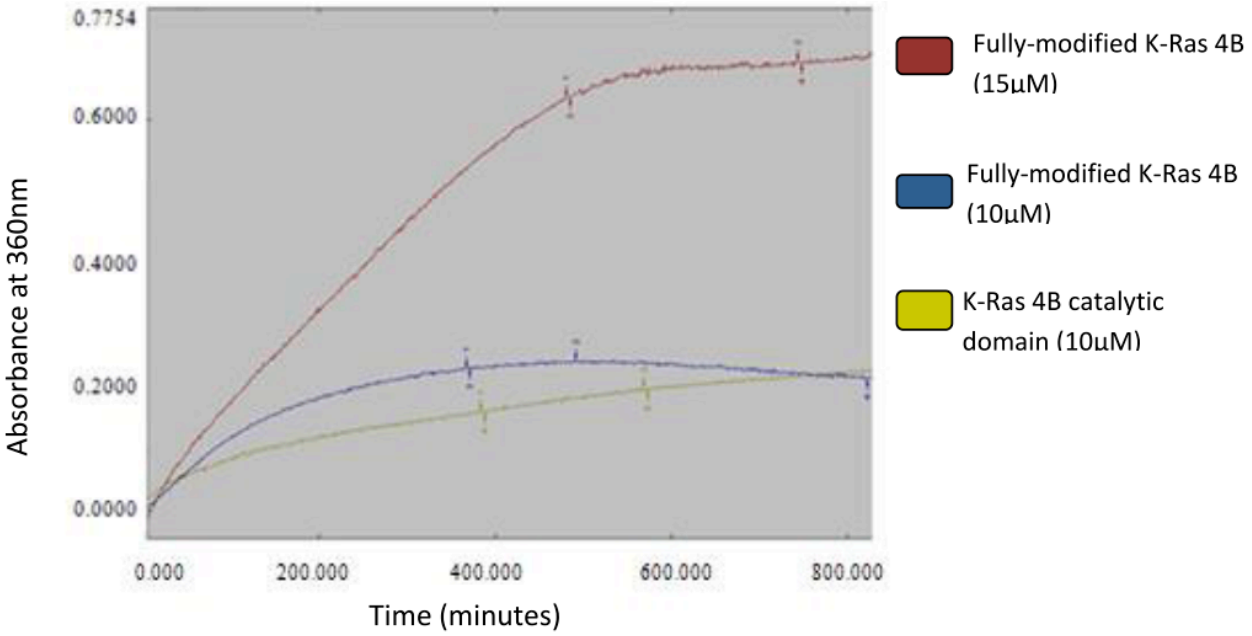

Figure 6.3: Fully-modified K-Ras4B is catalytically active.
GTP hydrolysis assay was carried out using the catalytic domain of K-Ras4B and fully modified K-Ras4B. Spectrophotometric recording of K-Ras4B modified using the sortase-mediated ligation reaction as well as a positive control using the catalytic domain of K-Ras4B is shown.

6.3.3 Fully modified K-Ras4B binds to Raf-1 in a nucleotide dependent manner.

We made use of Raf-1 RBD pulldowns to test whether the functionally active fully modified K-Ras4B binds to its effectors. We used the catalytic domain of K-Ras4B for comparison since the effector binding region is present on it. We carried out the pulldown assay using GDP and GTP loaded forms of both versions of K-Ras4B. We found that the GTP loaded form of K-Ras4B bound the beads better than the GDP loaded form as expected. The western blot performed on these proteins is shown in Figure 6.4. These results suggest that the fully modified K-Ras4B binds to Raf-1 in a nucleotide dependent manner.

6.3.4 Addition of the post-translational modifications increases the membrane binding affinity in K-Ras4B.

Ras proteins are known to bind to the membrane hence we decided to test if the fully modified K-Ras4B interacted with the membrane in the same way. The membrane binding ability of K-Ras4B has been attributed largely to the polylysine patch in its HVR. Hence, we compared the membrane binding activity of the fully modified K-Ras4B with the full length non-farnesylated version of K-Ras4B. Figure 6.5 shows the SPR sensorgram comparing the membrane binding abilities of the modified and unmodified version of K-Ras4B. As seen in the figure, the binding capacity of modified K-Ras4B is a lot higher than compared to unmodified K-Ras4B. This suggests that in addition to the polylysine patch on the HVR, the farnesyl and methyl groups on the HVR play a critical role in the membrane binding ability of K-Ras4B. Moreover, these post-translational modifications increase the affinity of K-Ras4B towards the membrane.

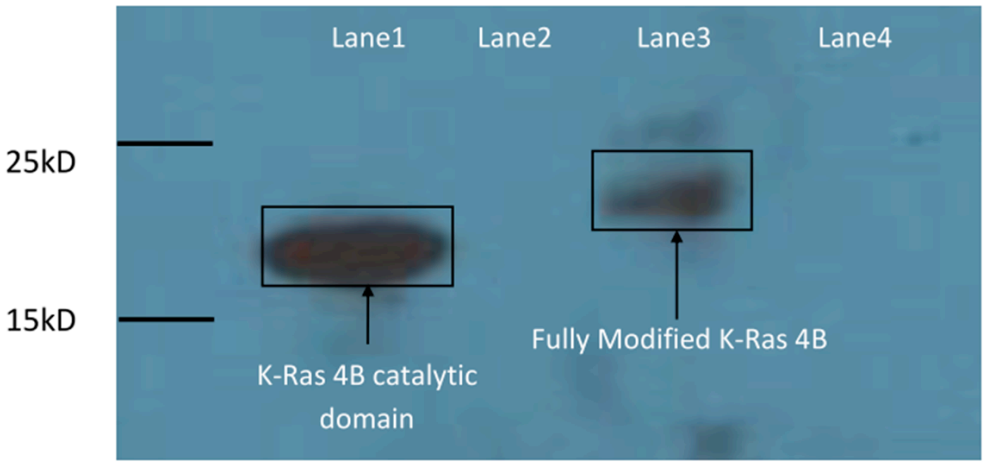

Figure 6.4: Fully modified K-Ras4B-GTP interacts with Raf-1 RBD.
The western blot was run on GTP-γ-S loaded K-Ras4B catalytic domain (Lane 1), GDP-loaded K-Ras4B catalytic domain (Lane 2), GTP-γ-S loaded fully modified K-Ras4B (Lane 3), and GDP-loaded fully modified K-Ras4B (Lane 4) after carrying out the Ras activation assay. Since the GDP-loaded forms of K-Ras4B do not bind to Raf-1, no band is seen in lanes 2 and 4. Since fully modified K-Ras4B has a higher molecular weight as compared to its catalytic domain, it runs higher than the catalytic domain of K-Ras4B.

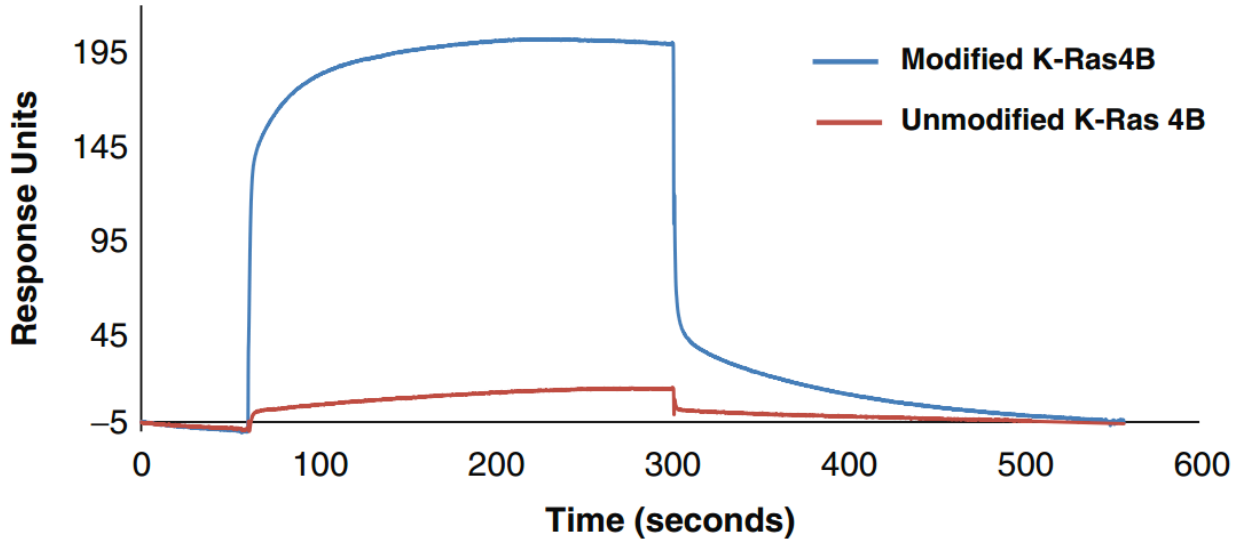

Figure 6.5: SPR sensorgram of modified and unmodified GTP-γ-S K-Ras4B.
Solutions of 2.4 μM fully modified GTP-γ-S loaded K-Ras4B (blue) and 2.4 μM unmodified K-Ras4B (red) were applied to immobilized DPPC nanodiscs at a flow rate of 10 μL/min. Binding of the fully modified version of the protein leads to an increase in response units as compared to the unmodified protein.

6.4 Discussion

Sortase A belongs to the sortase family of transpeptidase enzymes commonly encountered in gram positive bacteria. These enzymes modify surface protein and covalently anchor them to the peptidoglycan layer on the cell wall (316). Transpeptidases identify a recognition sequence in the target protein and cleave a specific amide bond at this recognition site before ligating it to a polyglycine bridge on the peptidoglycan layer. There are 4 isoforms of sortase, namely A, B, C and D, that differ in sequence and recognition site (317-319). Sortase A recognizes an LPXTG (where X can be any amino acid) motif on the target protein and cleaves the bond between the threonine and glycine. Then, it ligates this cleaved target protein to a substrate containing a glycine at its N-terminus (320). The threonine-glycine amide bond in the protein is cleaved by sortase by its active site containing a catalytic cysteine residue. The thiol group engages in a nucleophilic attack to form an acyl intermediate with threonine in the protein. The subsequent protein or peptide containing the glycine residue then resolves the intermediate and regenerates the cysteine in the sortase active site through a nucleophilic attack on the intermediate. This property of sortase A has been exploited by several groups for protein or peptide modifications (321-324). Hence, I used this enzyme to ligate the catalytic domain of K-Ras4B to the modified HVR peptide resulting in full length K-Ras4B containing its post-translational modifications.

The catalytic domain used in this section of my work contained the LPETG motif for sortase recognition. Purification of this catalytic domain was carried out with the His tag which was present after the LPETG motif. Before the ligation step, sortase cleaves the amide bond between the threonine and glycine and thus removes the His tag present. Hence it is desirable to have the His tag after the LPETG. Then, sortase ligates the catalytic domain to the glycine present on the N-terminus of farnesylated HVR.

I have noticed that for dialyzing the proteins in the Tris-citrate buffer, it is better to use dialysis cassettes over buffer exchange columns. These columns have often led to a sizeable loss of protein from my sample. This could be occurring due to the protein sticking onto the matrix of these exchange columns. Since the dialysis cassettes do not contain a matrix surface for non-specific interactions, it gives the best results.

Moreover, I have also noticed that the reaction can be carried out at pH 7.6 with a lesser yield. The maximum yield was obtained when I changed the pH of the sortase reaction buffer to 9. It has been shown in a previous publication that the yield of the reaction was best at 8.2 (324). The pka of cysteine is around 8 hence a higher pH increases the amount of nucleophile for catalyzing the reaction.

Similarly, the reaction can also be carried out at 18^0C or 37^0C but with a lower yield. Room temperature (approximately 25^0C) favored the reaction to give a higher yield. At 18^0C the catalytic activity of sortase is not optimum. At 25^0C, sortase exhibits a higher catalytic activity thus giving better yields. Admittedly, at 37^0C, sortase exhibits much better catalytic activity but K-Ras4B is not stable for a long time at this temperature.

Concentrations of K-Ras4B and the modified HVR peptide are also very important. A higher concentration of the modified HVR peptide is always needed. This is because sortase mediated ligation is an equilibrium process and the products of this reaction can be potential reactants. Accordingly, I have also found the product to decrease in amount if kept for more than 2 days. Hence, to improve the yield of product it is advisable to provide a significant excess of the ligation partner over the target protein and optimize the reaction time.

Use of higher concentrations of K-Ras4B has led to precipitation over the course of the reaction period. Hence I have optimized the protocol to start with a low concentration of protein and peptide. As a result of this, the concentration of the product is also low and needs to be concentrated before using for other studies.

Silver staining of gels is helpful during low concentration detection of product or reaction mixture. I have consistently produced the product with a yield between 10 to 30% as compared to the starting protein concentrations. I have also noted that the yields are best when individual reactions of 1 mL volume are used. Upon increasing the total volume of the reaction sample, there is an increase in precipitation of K-Ras4B and thus the yield. Hence I have carried out individual 1mL sortase ligation reaction mixtures and then pooled these samples together before passing them through nickel beads.

To my knowledge, the sortase ligation procedure has not been previously used to ligate a modified peptide to a protein for creating a post-translationally modified protein. Hence, this research study can serve as an example for ligating different modified peptides to protein domains in order to produce a fully post-translationally modified protein. Such post-translationally modified proteins are more physiologically relevant for conducting biochemical analyses.

However, there is a caveat before using the sortase ligated protein. This protein is not completely natural since it contains an additional LPETG sequence which is not found in naturally occurring protein and hence may introduce certain errors in protein function. Hence, I caution against the use of such proteins if they are not validated functionally. I have conducted several assays in this section to support the functional relevance of fully modified K-Ras4B. Ideally, comparing the

sortase ligated protein to naturally post-translationally modified protein will be the best validation study. But, the unavailability of such naturally post-translationally modified protein has forced me to use K-Ras4B catalytic domain for comparison. Moreover, the catalytic domain contains all the functional regions of the protein hence this comparison is important. Addition of the HVR is more important for membrane binding hence we see a higher membrane binding using SPR experiments.

In the future, I would like to validate my previous results on HVR autoinhibition using the fully post-translationally modified K-Ras4B. It has to be noted that when we carried out mutational studies on the full-length unmodified protein, we did not observe the HVR sequestration in the D173P mutant. This was attributed to the presence of proline in the beta strand region of HVR that was extremely essential for the interaction. Although the sequence of the fully modified K-Ras4B produced by sortase ligation contains a proline in the HVR, the position of this proline does not lie in the putative beta strand in the HVR. This may or may not affect the HVR autoinhibition mechanism in the GDP loaded form of K-Ras4B. If we observe an effect in the autoinhibition mechanism then we may not be able to use this protein to study fully modified K-Ras4B-GDP but we can still make use of it for studying the GTP loaded form of K-Ras4B. K-Ras4B-GTP is not autoinhibited and hence presence of the proline may not be a problem at all.

This post-translationally modified K-Ras4B protein that I have produced can have numerous applications in future studies. For example, this protein can be of tremendous use for structural studies either by NMR or crystallography. Though the structure of the catalytic domain of K-Ras4B is known, the structure of the full-length protein is still to be determined. Moreover, the autoinhibition mechanism can potentially stabilize the full length protein and allow for better crystallization results. Moreover, given the importance of K-Ras4B in several cancers,

production of fully modified protein is the need of the hour. Hence, any step taken in this direction can prove to be helpful. Production of a more physiologically relevant form of K-Ras4B can not only help us understand its relevant binding modes to effectors but also prove important in developing strategies to inhibit this protein.

REFERENCES

1. Rous P (1911) A Sarcoma of the Fowl Transmissible by an Agent Separable from the Tumor Cells. *The Journal of experimental medicine* 13(4):397-411.

2. Rous P (1910) A Transmissible Avian Neoplasm. (Sarcoma of the Common Fowl.). *The Journal of experimental medicine* 12(5):696-705.

3. Duesberg PH & Vogt PK (1970) Differences between the ribonucleic acids of transforming and nontransforming avian tumor viruses. *Proceedings of the National Academy of Sciences of the United States of America* 67(4):1673-1680.

4. Malumbres M & Barbacid M (2003) RAS oncogenes: the first 30 years. *Nature reviews. Cancer* 3(6):459-465.

5. Harvey JJ (1964) An Unidentified Virus Which Causes the Rapid Production of Tumours in Mice. *Nature* 204:1104-1105.

6. Kirsten WH & Mayer LA (1967) Morphologic responses to a murine erythroblastosis virus. *Journal of the National Cancer Institute* 39(2):311-335.

7. Peters RL, Spahn GJ, Rabstein LS, Huebner RJ, & Kelloff GJ (1974) Sensitive in vivo assay for detection of murine leukemia viruses. *Applied microbiology* 28(4):614-617.

8. Rasheed S, Gardner MB, & Huebner RJ (1978) In vitro isolation of stable rat sarcoma viruses. *Proceedings of the National Academy of Sciences of the United States of America* 75(6):2972-2976.

9. Scolnick EM, Rands E, Williams D, & Parks WP (1973) Studies on the nucleic acid sequences of Kirsten sarcoma virus: a model for formation of a mammalian RNA-containing sarcoma virus. *Journal of virology* 12(3):458-463.

10. Stehelin D, Varmus HE, Bishop JM, & Vogt PK (1976) DNA related to the transforming gene(s) of avian sarcoma viruses is present in normal avian DNA. *Nature* 260(5547):170-173.

11. Shih TY, Weeks MO, Young HA, & Scolnick EM (1979) p21 of Kirsten murine sarcoma virus is thermolabile in a viral mutant temperature sensitive for the maintenance of transformation. *Journal of virology* 31(2):546-546.

12. Shih TY, Weeks MO, Young HA, & Scholnick EM (1979) Identification of a sarcoma virus-coded phosphoprotein in nonproducer cells transformed by Kirsten or Harvey murine sarcoma virus. *Virology* 96(1):64-79.

13. Scolnick EM, Papageorge AG, & Shih TY (1979) Guanine nucleotide-binding activity as an assay for src protein of rat-derived murine sarcoma viruses. *Proceedings of the National Academy of Sciences of the United States of America* 76(10):5355-5359.

14. Willingham MC, Pastan I, Shih TY, & Scolnick EM (1980) Localization of the src gene product of the Harvey strain of MSV to plasma membrane of transformed cells by electron microscopic immunocytochemistry. *Cell* 19(4):1005-1014.

15. DeFeo D*, et al.* (1981) Analysis of two divergent rat genomic clones homologous to the transforming gene of Harvey murine sarcoma virus. *Proceedings of the National Academy of Sciences of the United States of America* 78(6):3328-3332.

16. Ellis RW*, et al.* (1981) The p21 src genes of Harvey and Kirsten sarcoma viruses originate from divergent members of a family of normal vertebrate genes. *Nature* 292(5823):506-511.

17. Chang EH, Furth ME, Scolnick EM, & Lowy DR (1982) Tumorigenic transformation of mammalian cells induced by a normal human gene homologous to the oncogene of Harvey murine sarcoma virus. *Nature* 297(5866):479-483.

18. Gibbs JB, Sigal IS, Poe M, & Scolnick EM (1984) Intrinsic GTPase activity distinguishes normal and oncogenic ras p21 molecules. *Proceedings of the National Academy of Sciences of the United States of America* 81(18):5704-5708.

19. Barbacid M (1987) ras genes. *Annual review of biochemistry* 56:779-827.

20. Lowy DR & Willumsen BM (1993) Function and regulation of ras. *Annual review of biochemistry* 62:851-891.

21. Dykes DC*, et al.* (1992) Activated conformations of the ras-gene-encoded p21 protein. 1. An energy-refined structure for the normal p21 protein complexed with GDP. *Journal of biomolecular structure & dynamics* 9(6):1025-1044.

22. Pai EF*, et al.* (1990) Refined crystal structure of the triphosphate conformation of H-ras p21 at 1.35 A resolution: implications for the mechanism of GTP hydrolysis. *Embo J* 9(8):2351-2359.

23. Pai EF*, et al.* (1989) Structure of the guanine-nucleotide-binding domain of the Ha-ras oncogene product p21 in the triphosphate conformation. *Nature* 341(6239):209-214.

24. Schlichting I*, et al.* (1989) Biochemical and crystallographic characterization of a complex of c-Ha-ras p21 and caged GTP with flash photolysis. *Proceedings of the National Academy of Sciences of the United States of America* 86(20):7687-7690.

25. Orengo CA*, et al.* (1997) CATH - a hierarchic classification of protein domain structures. *Structure* 5(8):1093-1108.

26. Buhrman G*, et al.* (2011) Analysis of binding site hot spots on the surface of Ras GTPase. *Journal of molecular biology* 413(4):773-789.

27. Gorfe AA, Grant BJ, & McCammon JA (2008) Mapping the nucleotide and isoform-dependent structural and dynamical features of Ras proteins. *Structure* 16(6):885-896.

28. Gorfe AA, Hanzal-Bayer M, Abankwa D, Hancock JF, & McCammon JA (2007) Structure and dynamics of the full-length lipid-modified H-Ras protein in a 1,2-dimyristoylglycero-3-phosphocholine bilayer. *Journal of medicinal chemistry* 50(4):674-684.

29. Schaber MD*, et al.* (1990) Polyisoprenylation of Ras in vitro by a farnesyl-protein transferase. *The Journal of biological chemistry* 265(25):14701-14704.

30. Casey PJ, Solski PA, Der CJ, & Buss JE (1989) p21ras is modified by a farnesyl isoprenoid. *Proceedings of the National Academy of Sciences of the United States of America* 86(21):8323-8327.

31. Gutierrez L, Magee AI, Marshall CJ, & Hancock JF (1989) Post-translational processing of p21ras is two-step and involves carboxyl-methylation and carboxy-terminal proteolysis. *The EMBO journal* 8(4):1093-1098.

32. Fiordalisi JJ*, et al.* (2003) High affinity for farnesyltransferase and alternative prenylation contribute individually to K-Ras4B resistance to farnesyltransferase inhibitors. *The Journal of biological chemistry* 278(43):41718-41727.

33. Hancock JF, Magee AI, Childs JE, & Marshall CJ (1989) All ras proteins are polyisoprenylated but only some are palmitoylated. *Cell* 57(7):1167-1177.

34. Trueblood CE*, et al.* (2000) The CaaX proteases, Afc1p and Rce1p, have overlapping but distinct substrate specificities. *Molecular and cellular biology* 20(12):4381-4392.

35. Dai Q*, et al.* (1998) Mammalian prenylcysteine carboxyl methyltransferase is in the endoplasmic reticulum. *The Journal of biological chemistry* 273(24):15030-15034.

36. Clarke S, Vogel JP, Deschenes RJ, & Stock J (1988) Posttranslational modification of the Ha-ras oncogene protein: evidence for a third class of protein carboxyl methyltransferases. *Proceedings of the National Academy of Sciences of the United States of America* 85(13):4643-4647.

37. Hrycyna CA, Sapperstein SK, Clarke S, & Michaelis S (1991) The Saccharomyces cerevisiae STE14 gene encodes a methyltransferase that mediates C-terminal methylation of a-factor and RAS proteins. *The EMBO journal* 10(7):1699-1709.

38. Li Z & Stock JB (2009) Protein carboxyl methylation and the biochemistry of memory. *Biological chemistry* 390(11):1087-1096.

39. Gysin S, Salt M, Young A, & McCormick F (2011) Therapeutic strategies for targeting ras proteins. *Genes & cancer* 2(3):359-372.

40. Hancock JF & Parton RG (2005) Ras plasma membrane signalling platforms. *The Biochemical journal* 389(Pt 1):1-11.

41. Hancock JF, Paterson H, & Marshall CJ (1990) A polybasic domain or palmitoylation is required in addition to the CAAX motif to localize p21ras to the plasma membrane. *Cell* 63(1):133-139.

42. Jackson JH, Li JW, Buss JE, Der CJ, & Cochrane CG (1994) Polylysine domain of K-ras 4B protein is crucial for malignant transformation. *Proceedings of the National Academy of Sciences of the United States of America* 91(26):12730-12734.

43. Ghomashchi F, Zhang X, Liu L, & Gelb MH (1995) Binding of prenylated and polybasic peptides to membranes: affinities and intervesicle exchange. *Biochemistry* 34(37):11910-11918.

44. Hancock JF, Cadwallader K, & Marshall CJ (1991) Methylation and proteolysis are essential for efficient membrane binding of prenylated p21K-ras(B). *The EMBO journal* 10(3):641-646.

45. Goodwin JS*, et al.* (2005) Depalmitoylated Ras traffics to and from the Golgi complex via a nonvesicular pathway. *The Journal of cell biology* 170(2):261-272.

46. Mitchell DA, Vasudevan A, Linder ME, & Deschenes RJ (2006) Protein palmitoylation by a family of DHHC protein S-acyltransferases. *Journal of lipid research* 47(6):1118-1127.

47. Ashery U, Yizhar O, Rotblat B, & Kloog Y (2006) Nonconventional trafficking of Ras associated with Ras signal organization. *Traffic* 7(9):119-126.

48. Plowman SJ, Ariotti N, Goodall A, Parton RG, & Hancock JF (2008) Electrostatic interactions positively regulate K-Ras nanocluster formation and function. *Molecular and cellular biology* 28(13):4377-4385.

49. Barcelo C*, et al.* (2013) Oncogenic K-ras segregates at spatially distinct plasma membrane signaling platforms according to its phosphorylation status. *Journal of cell science* 126(Pt 20):4553-4559.

50. Yang MH*, et al.* (2012) Regulation of RAS oncogenicity by acetylation. *Proceedings of the National Academy of Sciences of the United States of America* 109(27):10843-10848.

51. Lander HM*, et al.* (1996) Redox regulation of cell signalling. *Nature* 381(6581):380-381.

52. Lander HM, Ogiste JS, Pearce SF, Levi R, & Novogrodsky A (1995) Nitric oxide-stimulated guanine nucleotide exchange on p21ras. *The Journal of biological chemistry* 270(13):7017-7020.

53. Ahearn IM, Haigis K, Bar-Sagi D, & Philips MR (2012) Regulating the regulator: post-translational modification of RAS. *Nature reviews. Molecular cell biology* 13(1):39-51.

54. Ganesan AK, Vincent TS, Olson JC, & Barbieri JT (1999) Pseudomonas aeruginosa exoenzyme S disrupts Ras-mediated signal transduction by inhibiting guanine nucleotide exchange factor-catalyzed nucleotide exchange. *The Journal of biological chemistry* 274(31):21823-21829.

55. Just I, Selzer J, Hofmann F, Green GA, & Aktories K (1996) Inactivation of Ras by Clostridium sordellii lethal toxin-catalyzed glucosylation. *The Journal of biological chemistry* 271(17):10149-10153.

56. Adachi T, *et al.* (2004) S-glutathiolation of Ras mediates redox-sensitive signaling by angiotensin II in vascular smooth muscle cells. *The Journal of biological chemistry* 279(28):29857-29862.

57. Jura N, Scotto-Lavino E, Sobczyk A, & Bar-Sagi D (2006) Differential modification of Ras proteins by ubiquitination. *Molecular cell* 21(5):679-687.

58. Xu L, Lubkov V, Taylor LJ, & Bar-Sagi D (2010) Feedback regulation of Ras signaling by Rabex-5-mediated ubiquitination. *Current biology : CB* 20(15):1372-1377.

59. Kim SE, *et al.* (2009) H-Ras is degraded by Wnt/beta-catenin signaling via beta-TrCP-mediated polyubiquitylation. *Journal of cell science* 122(Pt 6):842-848.

60. Colicelli J (2010) Signal transduction: RABGEF1 fingers RAS for ubiquitination. *Current biology : CB* 20(15):R630-632.

61. Sasaki AT, *et al.* (2011) Ubiquitination of K-Ras enhances activation and facilitates binding to select downstream effectors. *Science signaling* 4(163):ra13.

62. Baker R, *et al.* (2013) Site-specific monoubiquitination activates Ras by impeding GTPase-activating protein function. *Nature structural & molecular biology* 20(1):46-52.

63. Boriack-Sjodin PA, Margarit SM, Bar-Sagi D, & Kuriyan J (1998) The structural basis of the activation of Ras by Sos. *Nature* 394(6691):337-343.

64. Goody RS, Frech M, & Wittinghofer A (1991) Affinity of guanine nucleotide binding proteins for their ligands: facts and artefacts. *Trends in biochemical sciences* 16(9):327-328.

65. Nassar N, *et al.* (1996) Ras/Rap effector specificity determined by charge reversal. *Nature structural biology* 3(8):723-729.

66. Huang L, Hofer F, Martin GS, & Kim SH (1998) Structural basis for the interaction of Ras with RalGDS. *Nature structural biology* 5(6):422-426.

67. Pacold ME, *et al.* (2000) Crystal structure and functional analysis of Ras binding to its effector phosphoinositide 3-kinase gamma. *Cell* 103(6):931-943.

68. Friday BB & Adjei AA (2005) K-ras as a target for cancer therapy. *Biochim Biophys Acta* 1756(2):127-144.

69. Stieglitz B, *et al.* (2008) Novel type of Ras effector interaction established between tumour suppressor NORE1A and Ras switch II. *The EMBO journal* 27(14):1995-2005.

70. Ito Y, *et al.* (1997) Regional polysterism in the GTP-bound form of the human c-Ha-Ras protein. *Biochemistry* 36(30):9109-9119.

71. Buhrman G, de Serrano V, & Mattos C (2003) Organic solvents order the dynamic switch II in Ras crystals. *Structure* 11(7):747-751.

72. Spoerner M*, et al.* (2010) Conformational states of human rat sarcoma (Ras) protein complexed with its natural ligand GTP and their role for effector interaction and GTP hydrolysis. *The Journal of biological chemistry* 285(51):39768-39778.

73. Scheffzek K*, et al.* (1997) The Ras-RasGAP complex: structural basis for GTPase activation and its loss in oncogenic Ras mutants. *Science* 277(5324):333-338.

74. John J, Frech M, & Wittinghofer A (1988) Biochemical properties of Ha-ras encoded p21 mutants and mechanism of the autophosphorylation reaction. *The Journal of biological chemistry* 263(24):11792-11799.

75. Buhrman G, Kumar VS, Cirit M, Haugh JM, & Mattos C (2011) Allosteric modulation of Ras-GTP is linked to signal transduction through RAF kinase. *The Journal of biological chemistry* 286(5):3323-3331.

76. Romero F, Martinez AC, Camonis J, & Rebollo A (1999) Aiolos transcription factor controls cell death in T cells by regulating Bcl-2 expression and its cellular localization. *The EMBO journal* 18(12):3419-3430.

77. Herrmann C, Martin GA, & Wittinghofer A (1995) Quantitative analysis of the complex between p21ras and the Ras-binding domain of the human Raf-1 protein kinase. *The Journal of biological chemistry* 270(7):2901-2905.

78. Brtva TR*, et al.* (1995) Two distinct Raf domains mediate interaction with Ras. *The Journal of biological chemistry* 270(17):9809-9812.

79. Moodie SA*, et al.* (1995) Different structural requirements within the switch II region of the Ras protein for interactions with specific downstream targets. *Oncogene* 11(3):447-454.

80. Repasky GA, Chenette EJ, & Der CJ (2004) Renewing the conspiracy theory debate: does Raf function alone to mediate Ras oncogenesis? *Trends in cell biology* 14(11):639-647.

81. Campbell SL, Khosravi-Far R, Rossman KL, Clark GJ, & Der CJ (1998) Increasing complexity of Ras signaling. *Oncogene* 17(11 Reviews):1395-1413.

82. Katz ME & McCormick F (1997) Signal transduction from multiple Ras effectors. *Current opinion in genetics & development* 7(1):75-79.

83. Malumbres M & Pellicer A (1998) RAS pathways to cell cycle control and cell transformation. *Front Biosci* 3:d887-912.

84. Hanahan D & Weinberg RA (2011) Hallmarks of cancer: the next generation. *Cell* 144(5):646-674.

85. Dent P*, et al.* (1992) Activation of mitogen-activated protein kinase kinase by v-Raf in NIH 3T3 cells and in vitro. *Science* 257(5075):1404-1407.

86. Moodie SA & Wolfman A (1994) The 3Rs of life: Ras, Raf and growth regulation. *Trends in genetics : TIG* 10(2):44-48.

87. Moodie SA, Willumsen BM, Weber MJ, & Wolfman A (1993) Complexes of Ras.GTP with Raf-1 and mitogen-activated protein kinase kinase. *Science* 260(5114):1658-1661.

88. Drugan JK*, et al.* (1996) Ras interaction with two distinct binding domains in Raf-1 may be required for Ras transformation. *The Journal of biological chemistry* 271(1):233-237.

89. Hatzivassiliou G*, et al.* (2010) RAF inhibitors prime wild-type RAF to activate the MAPK pathway and enhance growth. *Nature* 464(7287):431-435.

90. Poulikakos PI, Zhang C, Bollag G, Shokat KM, & Rosen N (2010) RAF inhibitors transactivate RAF dimers and ERK signalling in cells with wild-type BRAF. *Nature* 464(7287):427-430.

91. Garnett MJ, Rana S, Paterson H, Barford D, & Marais R (2005) Wild-type and mutant B-RAF activate C-RAF through distinct mechanisms involving heterodimerization. *Molecular cell* 20(6):963-969.

92. Rushworth LK, Hindley AD, O'Neill E, & Kolch W (2006) Regulation and role of Raf-1/B-Raf heterodimerization. *Molecular and cellular biology* 26(6):2262-2272.

93. Dougherty MK*, et al.* (2005) Regulation of Raf-1 by direct feedback phosphorylation. *Molecular cell* 17(2):215-224.

94. Freeman AK, Ritt DA, & Morrison DK (2013) The importance of Raf dimerization in cell signaling. *Small GTPases* 4(3):180-185.

95. Vanhaesebroeck B*, et al.* (2001) Synthesis and function of 3-phosphorylated inositol lipids. *Annual review of biochemistry* 70:535-602.

96. Cully M, You H, Levine AJ, & Mak TW (2006) Beyond PTEN mutations: the PI3K pathway as an integrator of multiple inputs during tumorigenesis. *Nature reviews. Cancer* 6(3):184-192.

97. Rajalingam K, Schreck R, Rapp UR, & Albert S (2007) Ras oncogenes and their downstream targets. *Biochimica et biophysica acta* 1773(8):1177-1195.

98. Scheid MP & Woodgett JR (2001) Phosphatidylinositol 3' kinase signaling in mammary tumorigenesis. *Journal of mammary gland biology and neoplasia* 6(1):83-99.

99. Song G, Ouyang G, & Bao S (2005) The activation of Akt/PKB signaling pathway and cell survival. *Journal of cellular and molecular medicine* 9(1):59-71.

100. Russell M, Lange-Carter CA, & Johnson GL (1995) Direct interaction between Ras and the kinase domain of mitogen-activated protein kinase kinase kinase (MEKK1). *The Journal of biological chemistry* 270(20):11757-11760.

101. Karandikar M, Xu S, & Cobb MH (2000) MEKK1 binds raf-1 and the ERK2 cascade components. *The Journal of biological chemistry* 275(51):40120-40127.

102. Boldt S, Weidle UH, & Kolch W (2003) The kinase domain of MEKK1 induces apoptosis by dysregulation of MAP kinase pathways. *Experimental cell research* 283(1):80-90.

103. Villalonga P*, et al.* (2001) Calmodulin binds to K-Ras, but not to H- or N-Ras, and modulates its downstream signaling. *Molecular and cellular biology* 21(21):7345-7354.

104. Sidhu RS, Clough RR, & Bhullar RP (2003) Ca2+/calmodulin binds and dissociates K-RasB from membrane. *Biochemical and biophysical research communications* 304(4):655-660.

105. Fivaz M & Meyer T (2005) Reversible intracellular translocation of KRas but not HRas in hippocampal neurons regulated by Ca2+/calmodulin. *The Journal of cell biology* 170(3):429-441.

106. Abraham SJ, Nolet RP, Calvert RJ, Anderson LM, & Gaponenko V (2009) The hypervariable region of K-Ras4B is responsible for its specific interactions with calmodulin. *Biochemistry* 48(32):7575-7583.

107. Lopez-Alcala C*, et al.* (2008) Identification of essential interacting elements in K-Ras/calmodulin binding and its role in K-Ras localization. *The Journal of biological chemistry* 283(16):10621-10631.

108. Liao J, Planchon SM, Wolfman JC, & Wolfman A (2006) Growth factor-dependent AKT activation and cell migration requires the function of c-K(B)-Ras versus other cellular ras isoforms. *The Journal of biological chemistry* 281(40):29730-29738.

109. Bosch M, Gil J, Bachs O, & Agell N (1998) Calmodulin inhibitor W13 induces sustained activation of ERK2 and expression of p21(cip1). *The Journal of biological chemistry* 273(34):22145-22150.

110. Villalonga P*, et al.* (2002) Calmodulin prevents activation of Ras by PKC in 3T3 fibroblasts. *The Journal of biological chemistry* 277(40):37929-37935.

111. Razzaque MA*, et al.* (2012) Characterization of a novel KRAS mutation identified in Noonan syndrome. *American journal of medical genetics. Part A* 158A(3):524-532.

112. Gelb BD & Tartaglia M (2006) Noonan syndrome and related disorders: dysregulated RAS-mitogen activated protein kinase signal transduction. *Human molecular genetics* 15 Spec No 2:R220-226.

113. Niihori T*, et al.* (2006) Germline KRAS and BRAF mutations in cardio-facio-cutaneous syndrome. *Nature genetics* 38(3):294-296.

114. Aoki Y*, et al.* (2005) Germline mutations in HRAS proto-oncogene cause Costello syndrome. *Nature genetics* 37(10):1038-1040.

115. Gripp KW*, et al.* (2006) HRAS mutation analysis in Costello syndrome: genotype and phenotype correlation. *American journal of medical genetics. Part A* 140(1):1-7.

116. Forbes SA, *et al.* (2011) COSMIC: mining complete cancer genomes in the Catalogue of Somatic Mutations in Cancer. *Nucleic acids research* 39(Database issue):D945-950.

117. Fernandez-Medarde A & Santos E (2011) Ras in cancer and developmental diseases. *Genes & cancer* 2(3):344-358.

118. Fujita J, *et al.* (1984) Ha-ras oncogenes are activated by somatic alterations in human urinary tract tumours. *Nature* 309(5967):464-466.

119. Visvanathan KV, Pocock RD, & Summerhayes IC (1988) Preferential and novel activation of H-ras in human bladder carcinomas. *Oncogene research* 3(1):77-86.

120. Bos JL, *et al.* (1987) Prevalence of ras gene mutations in human colorectal cancers. *Nature* 327(6120):293-297.

121. McCarthy SA, Samuels ML, Pritchard CA, Abraham JA, & McMahon M (1995) Rapid induction of heparin-binding epidermal growth factor/diphtheria toxin receptor expression by Raf and Ras oncogenes. *Genes & development* 9(16):1953-1964.

122. Gangarosa LM, *et al.* (1997) A raf-independent epidermal growth factor receptor autocrine loop is necessary for Ras transformation of rat intestinal epithelial cells. *The Journal of biological chemistry* 272(30):18926-18931.

123. Schulze A, Lehmann K, Jefferies HB, McMahon M, & Downward J (2001) Analysis of the transcriptional program induced by Raf in epithelial cells. *Genes & development* 15(8):981-994.

124. Woods D, *et al.* (2001) Induction of beta3-integrin gene expression by sustained activation of the Ras-regulated Raf-MEK-extracellular signal-regulated kinase signaling pathway. *Molecular and cellular biology* 21(9):3192-3205.

125. Dajee M, Tarutani M, Deng H, Cai T, & Khavari PA (2002) Epidermal Ras blockade demonstrates spatially localized Ras promotion of proliferation and inhibition of differentiation. *Oncogene* 21(10):1527-1538.

126. Nalca A, Qiu SG, El-Guendy N, Krishnan S, & Rangnekar VM (1999) Oncogenic Ras sensitizes cells to apoptosis by Par-4. *The Journal of biological chemistry* 274(42):29976-29983.

127. Ahmed MM, *et al.* (2008) Downregulation of PAR-4, a pro-apoptotic gene, in pancreatic tumors harboring K-ras mutation. *International journal of cancer. Journal international du cancer* 122(1):63-70.

128. Kinoshita T, Yokota T, Arai K, & Miyajima A (1995) Regulation of Bcl-2 expression by oncogenic Ras protein in hematopoietic cells. *Oncogene* 10(11):2207-2212.

129. Wu L, Nam YJ, Kung G, Crow MT, & Kitsis RN (2010) Induction of the apoptosis inhibitor ARC by Ras in human cancers. *The Journal of biological chemistry* 285(25):19235-19245.

130. Fisher DE (1994) Apoptosis in cancer therapy: crossing the threshold. *Cell* 78(4):539-542.

131. Kozma R, Ahmed S, Best A, & Lim L (1995) The Ras-related protein Cdc42Hs and bradykinin promote formation of peripheral actin microspikes and filopodia in Swiss 3T3 fibroblasts. *Molecular and cellular biology* 15(4):1942-1952.

132. Nobes CD & Hall A (1995) Rho, rac, and cdc42 GTPases regulate the assembly of multimolecular focal complexes associated with actin stress fibers, lamellipodia, and filopodia. *Cell* 81(1):53-62.

133. Klemke RL*, et al.* (1997) Regulation of cell motility by mitogen-activated protein kinase. *The Journal of cell biology* 137(2):481-492.

134. Himelstein BP, Canete-Soler R, Bernhard EJ, & Muschel RJ (1994) Induction of fibroblast 92 kDa gelatinase/type IV collagenase expression by direct contact with metastatic tumor cells. *Journal of cell science* 107 (Pt 2):477-486.

135. Warburg O (1956) On the origin of cancer cells. *Science* 123(3191):309-314.

136. Mathupala SP, Heese C, & Pedersen PL (1997) Glucose catabolism in cancer cells. The type II hexokinase promoter contains functionally active response elements for the tumor suppressor p53. *The Journal of biological chemistry* 272(36):22776-22780.

137. Blum R, Jacob-Hirsch J, Amariglio N, Rechavi G, & Kloog Y (2005) Ras inhibition in glioblastoma down-regulates hypoxia-inducible factor-1alpha, causing glycolysis shutdown and cell death. *Cancer research* 65(3):999-1006.

138. Shaw RJ (2006) Glucose metabolism and cancer. *Current opinion in cell biology* 18(6):598-608.

139. Semenza GL (2007) Hypoxia and cancer. *Cancer metastasis reviews* 26(2):223-224.

140. Kole HK, Resnick RJ, Van Doren M, & Racker E (1991) Regulation of 6-phosphofructo-1-kinase activity in ras-transformed rat-1 fibroblasts. *Archives of biochemistry and biophysics* 286(2):586-590.

141. Jones RG & Thompson CB (2009) Tumor suppressors and cell metabolism: a recipe for cancer growth. *Genes & development* 23(5):537-548.

142. Dergham ST*, et al.* (1997) Prevalence and clinical significance of combined K-ras mutation and p53 aberration in pancreatic adenocarcinoma. *Int J Pancreatol* 21(2):127-143.

143. Shibata D*, et al.* (1990) Detection of c-K-ras mutations in fine needle aspirates from human pancreatic adenocarcinomas. *Cancer research* 50(4):1279-1283.

144. Tabernero J*, et al.* (2004) Targeted therapy in advanced colon cancer: the role of new therapies. *Ann Oncol* 15 Suppl 4:iv55-62.

145. Der CJ, Krontiris TG, & Cooper GM (1982) Transforming genes of human bladder and lung carcinoma cell lines are homologous to the ras genes of Harvey and Kirsten sarcoma viruses. *Proceedings of the National Academy of Sciences of the United States of America* 79(11):3637-3640.

146. Zhang M & Vogel HJ (1993) Determination of the side chain pKa values of the lysine residues in calmodulin. *J Biol Chem* 268(30):22420-22428.

147. Plowman SJ*, et al.* (2006) K-ras 4A and 4B are co-expressed widely in human tissues, and their ratio is altered in sporadic colorectal cancer. *J Exp Clin Cancer Res* 25(2):259-267.

148. Esteban LM*, et al.* (2001) Targeted genomic disruption of H-ras and N-ras, individually or in combination, reveals the dispensability of both loci for mouse growth and development. *Molecular and cellular biology* 21(5):1444-1452.

149. Johnson L*, et al.* (1997) K-ras is an essential gene in the mouse with partial functional overlap with N-ras. *Genes Dev* 11(19):2468-2481.

150. Sieburth DS, Sun Q, & Han M (1998) SUR-8, a conserved Ras-binding protein with leucine-rich repeats, positively regulates Ras-mediated signaling in C. elegans. *Cell* 94(1):119-130.

151. Vos MD*, et al.* (2003) RASSF2 is a novel K-Ras-specific effector and potential tumor suppressor. *The Journal of biological chemistry* 278(30):28045-28051.

152. Duursma AM & Agami R (2003) Ras interference as cancer therapy. *Seminars in cancer biology* 13(4):267-273.

153. Zhang Y, Mukhopadhyay T, Donehower LA, Georges RN, & Roth JA (1993) Retroviral vector-mediated transduction of K-ras antisense RNA into human lung cancer cells inhibits expression of the malignant phenotype. *Human gene therapy* 4(4):451-460.

154. Adjei AA (2005) Farnesyltransferase inhibitors. *Cancer chemotherapy and biological response modifiers* 22:123-133.

155. Sun J, Qian Y, Hamilton AD, & Sebti SM (1998) Both farnesyltransferase and geranylgeranyltransferase I inhibitors are required for inhibition of oncogenic K-Ras prenylation but each alone is sufficient to suppress human tumor growth in nude mouse xenografts. *Oncogene* 16(11):1467-1473.

156. Winter-Vann AM*, et al.* (2005) A small-molecule inhibitor of isoprenylcysteine carboxyl methyltransferase with antitumor activity in cancer cells. *Proceedings of the National Academy of Sciences of the United States of America* 102(12):4336-4341.

157. Sridhar SS, Hedley D, & Siu LL (2005) Raf kinase as a target for anticancer therapeutics. *Molecular cancer therapeutics* 4(4):677-685.

158. Sebolt-Leopold JS*, et al.* (1999) Blockade of the MAP kinase pathway suppresses growth of colon tumors in vivo. *Nature medicine* 5(7):810-816.

159. Wu L, Birle DC, & Tannock IF (2005) Effects of the mammalian target of rapamycin inhibitor CCI-779 used alone or with chemotherapy on human prostate cancer cells and xenografts. *Cancer research* 65(7):2825-2831.

160. Ellis CA & Clark G (2000) The importance of being K-Ras. *Cellular signalling* 12(7):425-434.

161. Nussinov R, Tsai CJ, & Mattos C (2013) 'Pathway drug cocktail': targeting Ras signaling based on structural pathways. *Trends in molecular medicine* 19(11):695-704.

162. Ahearn IM, Haigis K, Bar-Sagi D, & Philips MR (2012) Regulating the regulator: post-translational modification of RAS. *Nat Rev Mol Cell Biol* 13(1):39-51.

163. Abankwa D, Gorfe AA, Inder K, & Hancock JF (2010) Ras membrane orientation and nanodomain localization generate isoform diversity. *Proceedings of the National Academy of Sciences of the United States of America* 107(3):1130-1135.

164. Quinlan MP & Settleman J (2009) Isoform-specific ras functions in development and cancer. *Future Oncol* 5(1):105-116.

165. Castellano E & Santos E (2011) Functional specificity of ras isoforms: so similar but so different. *Genes Cancer* 2(3):216-231.

166. Pleasance ED*, et al.* (2010) A comprehensive catalogue of somatic mutations from a human cancer genome. *Nature* 463(7278):191-196.

167. Prior IA, Lewis PD, & Mattos C (2012) A comprehensive survey of Ras mutations in cancer. *Cancer Res* 72(10):2457-2467.

168. Schlichting I*, et al.* (1990) Time-resolved X-ray crystallographic study of the conformational change in Ha-Ras p21 protein on GTP hydrolysis. *Nature* 345(6273):309-315.

169. Wittinghofer A & Vetter IR (2011) Structure-function relationships of the G domain, a canonical switch motif. *Annual review of biochemistry* 80:943-971.

170. Resh MD (2004) Membrane targeting of lipid modified signal transduction proteins. *Subcell Biochem* 37:217-232.

171. Karnoub AE & Weinberg RA (2008) Ras oncogenes: split personalities. *Nat Rev Mol Cell Biol* 9(7):517-531.

172. Saxena N, Lahiri SS, Hambarde S, & Tripathi RP (2008) RAS: target for cancer therapy. *Cancer Invest* 26(9):948-955.

173. Sun Q*, et al.* (2012) Discovery of small molecules that bind to K-Ras and inhibit Sos-mediated activation. *Angew Chem Int Ed Engl* 51(25):6140-6143.

174. Maurer T*, et al.* (2012) Small-molecule ligands bind to a distinct pocket in Ras and inhibit SOS-mediated nucleotide exchange activity. *Proc Natl Acad Sci U S A* 109(14):5299-5304.

175. Ostrem JM, Peters U, Sos ML, Wells JA, & Shokat KM (2013) K-Ras(G12C) inhibitors allosterically control GTP affinity and effector interactions. *Nature* 503(7477):548-551.

176. Wang W, Fang G, & Rudolph J (2012) Ras inhibition via direct Ras binding--is there a path forward? *Bioorg Med Chem Lett* 22(18):5766-5776.

177. Nussinov R, Tsai CJ, & Mattos C (2013) 'Pathway drug cocktail': targeting Ras signaling based on structural pathways. *Trends Mol Med* 19(11):695-704.

178. Gysin S, Salt M, Young A, & McCormick F (2011) Therapeutic strategies for targeting ras proteins. *Genes Cancer* 2(3):359-372.

179. Sun K*, et al.* (2013) High-dose sodium selenite toxicity cannot be prevented by the co-administration of pharmacological levels of epigallocatechin-3-gallate which in turn aggravates the toxicity. *Food and chemical toxicology : an international journal published for the British Industrial Biological Research Association* 52:36-41.

180. Iwig JS & Kuriyan J (2013) Fixing a hole where the Ras gets in. *Cell* 153(6):1191-1193.

181. Abraham SJ, Muhamed I, Nolet R, Yeung F, & Gaponenko V (2010) Expression, purification, and characterization of soluble K-Ras4B for structural analysis. *Protein Expr Purif* 73(2):125-131.

182. Neidhardt FC, Bloch PL, & Smith DF (1974) Culture medium for enterobacteria. *J Bacteriol* 119(3):736-747.

183. Tanigawa S*, et al.* (2011) Wnt4 induces nephronic tubules in metanephric mesenchyme by a non-canonical mechanism. *Developmental biology* 352(1):58-69.

184. Delaglio F*, et al.* (1995) NMRPipe: a multidimensional spectral processing system based on UNIX pipes. *J Biomol NMR* 6(3):277-293.

185. Brooks BR*, et al.* (1983) Charmm - a program for macromolecular energy, minimization, and dynamics calculations. *J. Comp. Chem.* 4(2):187-217.

186. Grayson P, Tajkhorshid E, & Schulten K (2003) Mechanisms of selectivity in channels and enzymes studied with interactive molecular dynamics. *Biophys J* 85(1):36-48.

187. Humphrey W, Dalke A, & Schulten K (1996) VMD: visual molecular dynamics. *J Mol Graph* 14(1):33-38, 27-38.

188. Phillips JC*, et al.* (2005) Scalable molecular dynamics with NAMD. *J. Comp. Chem.* 26:1781-1802.

189. Durell SR, Brooks BR, & Bennaim A (1994) Solvent-induced forces between two hydrophilic groups. *J. Phys. Chem.* 98:2198–2202.

190. Jang H*, et al.* (2013) Familial Alzheimer's disease Osaka mutant (DeltaE22) beta-barrels suggest an explanation for the different Abeta1-40/42 preferred conformational states observed by experiment. *The journal of physical chemistry. B* 117(39):11518-11529.

191. Chavan TS, Meyer JO, Chisholm L, Dobosz-Bartoszek M, & Gaponenko V (2014) A novel method for the production of fully modified K-Ras 4B. *Methods in molecular biology* 1120:19-32.

192. Denisov IG, Grinkova YV, Lazarides AA, & Sligar SG (2004) Directed self-assembly of monodisperse phospholipid bilayer Nanodiscs with controlled size. *Journal of the American Chemical Society* 126(11):3477-3487.

193. Ritchie TK*, et al.* (2009) Chapter 11 - Reconstitution of membrane proteins in phospholipid bilayer nanodiscs. *Methods in enzymology* 464:211-231.

194. Jerabek-Willemsen M, Wienken CJ, Braun D, Baaske P, & Duhr S (2011) Molecular interaction studies using microscale thermophoresis. *Assay Drug Dev Technol* 9(4):342-353.

195. Seidel SA*, et al.* (2013) Microscale thermophoresis quantifies biomolecular interactions under previously challenging conditions. *Methods* 59(3):301-315.

196. Alvarez-Moya B, Barcelo C, Tebar F, Jaumot M, & Agell N (2011) CaM interaction and Ser181 phosphorylation as new K-Ras signaling modulators. *Small GTPases* 2(2):99-103.

197. Alvarez-Moya B, Lopez-Alcala C, Drosten M, Bachs O, & Agell N (2010) K-Ras4B phosphorylation at Ser181 is inhibited by calmodulin and modulates K-Ras activity and function. *Oncogene* 29(44):5911-5922.

198. Das R*, et al.* (2007) cAMP activation of PKA defines an ancient signaling mechanism. *Proc Natl Acad Sci U S A* 104(1):93-98.

199. Masterson LR, Mascioni A, Traaseth NJ, Taylor SS, & Veglia G (2008) Allosteric cooperativity in protein kinase A. *Proc Natl Acad Sci U S A* 105(2):506-511.

200. Frishman D & Argos P (1995) Knowledge-based protein secondary structure assignment. *Proteins* 23(4):566-579.

201. Neal S, Nip AM, Zhang H, & Wishart DS (2003) Rapid and accurate calculation of protein 1H, 13C and 15N chemical shifts. *J Biomol NMR* 26(3):215-240.

202. Tochio H, Hung F, Li M, Bredt DS, & Zhang M (2000) Solution structure and backbone dynamics of the second PDZ domain of postsynaptic density-95. *J Mol Biol* 295(2):225-237.

203. Pylayeva-Gupta Y, Grabocka E, & Bar-Sagi D (2011) RAS oncogenes: weaving a tumorigenic web. *Nature reviews. Cancer* 11(11):761-774.

204. Abraham SJ, Muhamed I, Nolet R, Yeung F, & Gaponenko V (2010) Expression, purification, and characterization of soluble K-Ras4B for structural analysis. *Protein expression and purification* 73(2):125-131.

205. Williams JG*, et al.* (2000) Elucidation of binding determinants and functional consequences of Ras/Raf-cysteine-rich domain interactions. *The Journal of biological chemistry* 275(29):22172-22179.

206. Thapar R, Williams JG, & Campbell SL (2004) NMR characterization of full-length farnesylated and non-farnesylated H-Ras and its implications for Raf activation. *J Mol Biol* 343(5):1391-1408.

207. Arozarena I, Calvo F, & Crespo P (2011) Ras, an actor on many stages: posttranslational modifications, localization, and site-specified events. *Genes Cancer* 2(3):182-194.

208. Holderfield M*, et al.* (2013) RAF inhibitors activate the MAPK pathway by relieving inhibitory autophosphorylation. *Cancer cell* 23(5):594-602.

209. Hubbard SR (2004) Juxtamembrane autoinhibition in receptor tyrosine kinases. *Nature reviews. Molecular cell biology* 5(6):464-471.

210. Jones MK & Jackson JH (1998) Ras-GRF activates Ha-Ras, but not N-Ras or K-Ras 4B, protein in vivo. *The Journal of biological chemistry* 273(3):1782-1787.

211. Yan J, Roy S, Apolloni A, Lane A, & Hancock JF (1998) Ras isoforms vary in their ability to activate Raf-1 and phosphoinositide 3-kinase. *The Journal of biological chemistry* 273(37):24052-24056.

212. Thapar R, Williams JG, & Campbell SL (2004) NMR characterization of full-length farnesylated and non-farnesylated H-Ras and its implications for Raf activation. *Journal of molecular biology* 343(5):1391-1408.

213. Yong HY*, et al.* (2011) Identification of H-Ras-specific motif for the activation of invasive signaling program in human breast epithelial cells. *Neoplasia* 13(2):98-107.

214. Castellano E & Downward J (2011) RAS Interaction with PI3K: More Than Just Another Effector Pathway. *Genes & cancer* 2(3):261-274.

215. Gomes AV, Barnes JA, & Vogel HJ (2000) Spectroscopic characterization of the interaction between calmodulin-dependent protein kinase I and calmodulin. *Archives of biochemistry and biophysics* 379(1):28-36.

216. Chin D, Sloan DJ, Quiocho FA, & Means AR (1997) Functional consequences of truncating amino acid side chains located at a calmodulin-peptide interface. *The Journal of biological chemistry* 272(9):5510-5513.

217. Kranz JK, Lee EK, Nairn AC, & Wand AJ (2002) A direct test of the reductionist approach to structural studies of calmodulin activity: relevance of peptide models of target proteins. *The Journal of biological chemistry* 277(19):16351-16354.

218. Abraham SJ, Hoheisel S, & Gaponenko V (2008) Detection of protein-ligand interactions by NMR using reductive methylation of lysine residues. *Journal of biomolecular NMR* 42(2):143-148.

219. Wilhelm M*, et al.* (1991) Polymer Micelle Formation .3. Poly(Styrene-Ethylene Oxide) Block Copolymer Micelle Formation in Water - a Fluorescence Probe Study. *Macromolecules* 24(5):1033-1040.

220. Chabbert M, Lukas TJ, Watterson DM, Axelsen PH, & Prendergast FG (1991) Fluorescence analysis of calmodulin mutants containing tryptophan: conformational changes induced by calmodulin-binding peptides from myosin light chain kinase and protein kinase II. *Biochemistry* 30(30):7615-7630.

221. Means GE & Feeney RE (1968) Reductive alkylation of amino groups in proteins. *Biochemistry* 7(6):2192-2201.

222. Abraham SJ, Kobayashi T, Solaro RJ, & Gaponenko V (2009) Differences in lysine pKa values may be used to improve NMR signal dispersion in reductively methylated proteins. *Journal of biomolecular NMR* 43(4):239-246.

223. Waddell WJ (1956) A simple ultraviolet spectrophotometric method for the determination of protein. *The Journal of laboratory and clinical medicine* 48(2):311-314.

224. Brunsveld L*, et al.* (2006) Lipidated ras and rab peptides and proteins--synthesis, structure, and function. *Angewandte Chemie* 45(40):6622-6646.

225. Meister A*, et al.* (2006) Insertion of lipidated Ras proteins into lipid monolayers studied by infrared reflection absorption spectroscopy (IRRAS). *Biophysical journal* 91(4):1388-1401.

226. Weise K, Triola G, Brunsveld L, Waldmann H, & Winter R (2009) Influence of the lipidation motif on the partitioning and association of N-Ras in model membrane subdomains. *Journal of the American Chemical Society* 131(4):1557-1564.

227. Ismail SA*, et al.* (2011) Arl2-GTP and Arl3-GTP regulate a GDI-like transport system for farnesylated cargo. *Nature chemical biology* 7(12):942-949.

228. Takai Y, Sasaki T, & Matozaki T (2001) Small GTP-binding proteins. *Physiological reviews* 81(1):153-208.

229. Kowluru A (2010) Small G proteins in islet beta-cell function. *Endocrine reviews* 31(1):52-78.

230. Kowluru A (2008) Protein prenylation in glucose-induced insulin secretion from the pancreatic islet beta cell: a perspective. *Journal of cellular and molecular medicine* 12(1):164-173.

231. Linder ME & Deschenes RJ (2007) Palmitoylation: policing protein stability and traffic. *Nature reviews. Molecular cell biology* 8(1):74-84.

232. Wu LJ, Xu LR, Liao JM, Chen J, & Liang Y (2011) Both the C-terminal polylysine region and the farnesylation of K-RasB are important for its specific interaction with calmodulin. *PloS one* 6(7):e21929.

233. Rayment I (1997) Reductive alkylation of lysine residues to alter crystallization properties of proteins. *Methods in enzymology* 276:171-179.

234. Schanda P & Brutscher B (2005) Very fast two-dimensional NMR spectroscopy for real-time investigation of dynamic events in proteins on the time scale of seconds. *Journal of the American Chemical Society* 127(22):8014-8015.

235. Ganzhorn AJ*, et al.* (1996) The contribution of lysine-36 to catalysis by human myo-inositol monophosphatase. *Biochemistry* 35(33):10957-10966.

236. Gao G*, et al.* (2006) Determination of lysine pK values using [5-13C]lysine: application to the lyase domain of DNA Pol beta. *Journal of the American Chemical Society* 128(25):8104-8105.

237. Iwahara J, Jung YS, & Clore GM (2007) Heteronuclear NMR spectroscopy for lysine NH(3) groups in proteins: unique effect of water exchange on (15)N transverse relaxation. *Journal of the American Chemical Society* 129(10):2971-2980.

238. Larda ST, Bokoch MP, Evanics F, & Prosser RS (2012) Lysine methylation strategies for characterizing protein conformations by NMR. *Journal of biomolecular NMR* 54(2):199-209.

239. Simons K & Vaz WL (2004) Model systems, lipid rafts, and cell membranes. *Annual review of biophysics and biomolecular structure* 33:269-295.

240. Fujiwara T, Ritchie K, Murakoshi H, Jacobson K, & Kusumi A (2002) Phospholipids undergo hop diffusion in compartmentalized cell membrane. *The Journal of cell biology* 157(6):1071-1081.

241. Murase K*, et al.* (2004) Ultrafine membrane compartments for molecular diffusion as revealed by single molecule techniques. *Biophysical journal* 86(6):4075-4093.

242. Hancock JF & Prior IA (2005) Electron microscopic imaging of Ras signaling domains. *Methods* 37(2):165-172.

243. Laude AJ & Prior IA (2004) Plasma membrane microdomains: organization, function and trafficking. *Molecular membrane biology* 21(3):193-205.

244. Prior IA, Parton RG, & Hancock JF (2003) Observing cell surface signaling domains using electron microscopy. *Science's STKE : signal transduction knowledge environment* 2003(177):PL9.

245. Murray D, Ben-Tal N, Honig B, & McLaughlin S (1997) Electrostatic interaction of myristoylated proteins with membranes: simple physics, complicated biology. *Structure* 5(8):985-989.

246. Reuther GW & Der CJ (2000) The Ras branch of small GTPases: Ras family members don't fall far from the tree. *Current opinion in cell biology* 12(2):157-165.

247. Abankwa D*, et al.* (2008) A novel switch region regulates H-ras membrane orientation and signal output. *The EMBO journal* 27(5):727-735.

248. Eisenberg S & Henis YI (2008) Interactions of Ras proteins with the plasma membrane and their roles in signaling. *Cellular signalling* 20(1):31-39.

249. Bhagatji P, Leventis R, Rich R, Lin CJ, & Silvius JR (2010) Multiple cellular proteins modulate the dynamics of K-ras association with the plasma membrane. *Biophysical journal* 99(10):3327-3335.

250. Rizzo MA, Kraft CA, Watkins SC, Levitan ES, & Romero G (2001) Agonist-dependent traffic of raft-associated Ras and Raf-1 is required for activation of the mitogen-activated protein kinase cascade. *The Journal of biological chemistry* 276(37):34928-34933.

251. Roy S*, et al.* (1999) Dominant-negative caveolin inhibits H-Ras function by disrupting cholesterol-rich plasma membrane domains. *Nature cell biology* 1(2):98-105.

252. Mineo C, James GL, Smart EJ, & Anderson RG (1996) Localization of epidermal growth factor-stimulated Ras/Raf-1 interaction to caveolae membrane. *The Journal of biological chemistry* 271(20):11930-11935.

253. Kranenburg O, Verlaan I, & Moolenaar WH (2001) Regulating c-Ras function. cholesterol depletion affects caveolin association, GTP loading, and signaling. *Current biology : CB* 11(23):1880-1884.

254. Prior IA*, et al.* (2001) GTP-dependent segregation of H-ras from lipid rafts is required for biological activity. *Nature cell biology* 3(4):368-375.

255. Parmryd I, Adler J, Patel R, & Magee AI (2003) Imaging metabolism of phosphatidylinositol 4,5-bisphosphate in T-cell GM1-enriched domains containing Ras proteins. *Experimental cell research* 285(1):27-38.

256. White MA & Anderson RG (2001) Which Ras rides the raft? *Nature cell biology* 3(8):E172.

257. Plowman SJ & Hancock JF (2005) Ras signaling from plasma membrane and endomembrane microdomains. *Biochimica et biophysica acta* 1746(3):274-283.

258. van den Bogaart G*, et al.* (2011) Membrane protein sequestering by ionic protein-lipid interactions. *Nature* 479(7374):552-555.

259. Stokoe D, Macdonald SG, Cadwallader K, Symons M, & Hancock JF (1994) Activation of Raf as a result of recruitment to the plasma membrane. *Science* 264(5164):1463-1467.

260. Carey KD, Watson RT, Pessin JE, & Stork PJ (2003) The requirement of specific membrane domains for Raf-1 phosphorylation and activation. *The Journal of biological chemistry* 278(5):3185-3196.

261. Ehrhardt A, David MD, Ehrhardt GR, & Schrader JW (2004) Distinct mechanisms determine the patterns of differential activation of H-Ras, N-Ras, K-Ras 4B, and M-Ras

by receptors for growth factors or antigen. *Molecular and cellular biology* 24(14):6311-6323.

262. Abankwa D, Gorfe AA, & Hancock JF (2008) Mechanisms of Ras membrane organization and signalling: Ras on a rocker. *Cell cycle* 7(17):2667-2673.

263. Abankwa D, Gorfe AA, Inder K, & Hancock JF (2010) Ras membrane orientation and nanodomain localization generate isoform diversity. *Proceedings of the National Academy of Sciences of the United States of America* 107(3):1130-1135.

264. Guldenhaupt J*, et al.* (2012) N-Ras forms dimers at POPC membranes. *Biophysical journal* 103(7):1585-1593.

265. Inouye K, Mizutani S, Koide H, & Kaziro Y (2000) Formation of the Ras dimer is essential for Raf-1 activation. *The Journal of biological chemistry* 275(6):3737-3740.

266. Lin WC*, et al.* (2014) H-Ras forms dimers on membrane surfaces via a protein-protein interface. *Proceedings of the National Academy of Sciences of the United States of America* 111(8):2996-3001.

267. Woolf PJ & Linderman JJ (2003) Self organization of membrane proteins via dimerization. *Biophysical chemistry* 104(1):217-227.

268. Murakoshi H*, et al.* (2004) Single-molecule imaging analysis of Ras activation in living cells. *Proceedings of the National Academy of Sciences of the United States of America* 101(19):7317-7322.

269. Zhou Y*, et al.* (2014) Signal integration by lipid-mediated spatial cross talk between Ras nanoclusters. *Molecular and cellular biology* 34(5):862-876.

270. Prior IA, Muncke C, Parton RG, & Hancock JF (2003) Direct visualization of Ras proteins in spatially distinct cell surface microdomains. *The Journal of cell biology* 160(2):165-170.

271. Hibino K*, et al.* (2003) Single- and multiple-molecule dynamics of the signaling from H-Ras to cRaf-1 visualized on the plasma membrane of living cells. *Chemphyschem : a European journal of chemical physics and physical chemistry* 4(7):748-753.

272. Plowman SJ, Muncke C, Parton RG, & Hancock JF (2005) H-ras, K-ras, and inner plasma membrane raft proteins operate in nanoclusters with differential dependence on the actin cytoskeleton. *Proceedings of the National Academy of Sciences of the United States of America* 102(43):15500-15505.

273. Harding A, Hsu V, Kornfeld K, & Hancock JF (2003) Identification of residues and domains of Raf important for function in vivo and in vitro. *The Journal of biological chemistry* 278(46):45519-45527.

274. Zhu J*, et al.* (2005) Identification of Raf-1 S471 as a novel phosphorylation site critical for Raf-1 and B-Raf kinase activities and for MEK binding. *Molecular biology of the cell* 16(10):4733-4744.

275. Terai K & Matsuda M (2005) Ras binding opens c-Raf to expose the docking site for mitogen-activated protein kinase kinase. *EMBO reports* 6(3):251-255.

276. Tian T*, et al.* (2007) Plasma membrane nanoswitches generate high-fidelity Ras signal transduction. *Nature cell biology* 9(8):905-914.

277. Harding A & Hancock JF (2008) Ras nanoclusters: combining digital and analog signaling. *Cell cycle* 7(2):127-134.

278. Harding A, Tian T, Westbury E, Frische E, & Hancock JF (2005) Subcellular localization determines MAP kinase signal output. *Current biology : CB* 15(9):869-873.

279. Roskoski R, Jr. (2010) RAF protein-serine/threonine kinases: structure and regulation. *Biochemical and biophysical research communications* 399(3):313-317.

280. Schubbert S, Shannon K, & Bollag G (2007) Hyperactive Ras in developmental disorders and cancer. *Nature reviews. Cancer* 7(4):295-308.

281. Cebecauer M, Spitaler M, Serge A, & Magee AI (2010) Signalling complexes and clusters: functional advantages and methodological hurdles. *J Cell Sci* 123(Pt 3):309-320.

282. Rajakulendran T, Sahmi M, Lefrancois M, Sicheri F, & Therrien M (2009) A dimerization-dependent mechanism drives RAF catalytic activation. *Nature* 461(7263):542-545.

283. Brennan DF*, et al.* (2011) A Raf-induced allosteric transition of KSR stimulates phosphorylation of MEK. *Nature* 472(7343):366-369.

284. Castellano E & Downward J (2011) RAS Interaction with PI3K: More Than Just Another Effector Pathway. *Genes Cancer* 2(3):261-274.

285. Mitin N, Rossman KL, & Der CJ (2005) Signaling interplay in Ras superfamily function. *Current biology : CB* 15(14):R563-574.

286. Castellano E*, et al.* (2013) Requirement for interaction of PI3-kinase p110alpha with RAS in lung tumor maintenance. *Cancer Cell* 24(5):617-630.

287. Lavoie H*, et al.* (2013) Inhibitors that stabilize a closed RAF kinase domain conformation induce dimerization. *Nat Chem Biol* 9(7):428-436.

288. Tzivion G, Luo Z, & Avruch J (1998) A dimeric 14-3-3 protein is an essential cofactor for Raf kinase activity. *Nature* 394(6688):88-92.

289. Nan X*, et al.* (2013) Single-molecule superresolution imaging allows quantitative analysis of RAF multimer formation and signaling. *Proceedings of the National Academy of Sciences of the United States of America* 110(46):18519-18524.

290. Guldenhaupt J*, et al.* (2012) N-Ras forms dimers at POPC membranes. *Biophys J* 103(7):1585-1593.

291. Lin WC*, et al.* (2014) H-Ras forms dimers on membrane surfaces via a protein-protein interface. *Proceedings of the National Academy of Sciences of the United States of America*:DOI: 10.1073/pnas.1321155111.

292. Tsai CJ & Nussinov R (2014) The free energy landscape in translational science: how can somatic mutations result in constitutive oncogenic activation? *Phys Chem Chem Phys*:DOI: 10.1039/c1033cp54253j.

293. Aytuna AS, Gursoy A, & Keskin O (2005) Prediction of protein-protein interactions by combining structure and sequence conservation in protein interfaces. *Bioinformatics* 21(12):2850-2855.

294. Ogmen U, Keskin O, Aytuna AS, Nussinov R, & Gursoy A (2005) PRISM: protein interactions by structural matching. *Nucleic acids research* 33(Web Server issue):W331-336.

295. Tuncbag N, Gursoy A, Nussinov R, & Keskin O (2011) Predicting protein-protein interactions on a proteome scale by matching evolutionary and structural similarities at interfaces using PRISM. *Nature protocols* 6(9):1341-1354.

296. Mashiach E, Nussinov R, & Wolfson HJ (2010) FiberDock: Flexible induced-fit backbone refinement in molecular docking. *Proteins* 78(6):1503-1519.

297. Tuncbag N, Keskin O, Nussinov R, & Gursoy A (2012) Fast and accurate modeling of protein-protein interactions by combining template-interface-based docking with flexible refinement. *Proteins* 80(4):1239-1249.

298. Tuncbag N, Keskin O, & Gursoy A (2010) HotPoint: hot spot prediction server for protein interfaces. *Nucleic acids research* 38(Web Server issue):W402-406.

299. Duarte JM, Srebniak A, Scharer MA, & Capitani G (2012) Protein interface classification by evolutionary analysis. *BMC bioinformatics* 13:334.

300. Wang J*, et al.* (2009) Determination of multicomponent protein structures in solution using global orientation and shape restraints. *Journal of the American Chemical Society* 131(30):10507-10515.

301. Brinas RP*, et al.* (2012) Design and synthesis of multifunctional gold nanoparticles bearing tumor-associated glycopeptide antigens as potential cancer vaccines. *Bioconjugate chemistry* 23(8):1513-1523.

302. Chavan TS, Abraham S, & Gaponenko V (2013) Application of reductive (1)(3)C-methylation of lysines to enhance the sensitivity of conventional NMR methods. *Molecules* 18(6):7103-7119.

303. Shima F*, et al.* (2013) In silico discovery of small-molecule Ras inhibitors that display antitumor activity by blocking the Ras-effector interaction. *Proceedings of the National Academy of Sciences of the United States of America* 110(20):8182-8187.

304. Keskin O, Gursoy A, Ma B, & Nussinov R (2008) Principles of protein-protein interactions: what are the preferred ways for proteins to interact? *Chem Rev* 108(4):1225-1244.

305. Keskin O & Nussinov R (2005) Favorable scaffolds: proteins with different sequence, structure and function may associate in similar ways. *Protein Eng Des Sel* 18(1):11-24.

306. Plowman SJ, Muncke C, Parton RG, & Hancock JF (2005) H-ras, K-ras, and inner plasma membrane raft proteins operate in nanoclusters with differential dependence on the actin cytoskeleton. *Proceedings of the National Academy of Sciences of the United States of America* 102(43):15500-15505.

307. Jang H*, et al.* (2013) Alzheimer's disease: which type of amyloid-preventing drug agents to employ? *Physical chemistry chemical physics : PCCP* 15(23):8868-8877.

308. Osman MA, Sarkar FH, & Rodriguez-Boulan E (2013) A molecular rheostat at the interface of cancer and diabetes. *Biochimica et biophysica acta* 1836(1):166-176.

309. Marsh JA & Teichmann SA (2014) Parallel dynamics and evolution: Protein conformational fluctuations and assembly reflect evolutionary changes in sequence and structure. *Bioessays* 36(2):209-218.

310. Groves JT & Kuriyan J (2010) Molecular mechanisms in signal transduction at the membrane. *Nat Struct Mol Biol* 17(6):659-665.

311. Cox AD & Der CJ (1992) Protein prenylation: more than just glue? *Current opinion in cell biology* 4(6):1008-1016.

312. Resh MD (2006) Trafficking and signaling by fatty-acylated and prenylated proteins. *Nature chemical biology* 2(11):584-590.

313. Campbell-Burk SL & Carpenter JW (1995) Refolding and purification of Ras proteins. *Methods Enzymol* 255:3-13.

314. Porfiri E, Evans T, Bollag G, Clark R, & Hancock JF (1995) Purification of baculovirus-expressed recombinant Ras and Rap proteins. *Methods in enzymology* 255:13-21.

315. Chen YX*, et al.* (2010) Synthesis of the Rheb and K-Ras4B GTPases. *Angewandte Chemie* 49(35):6090-6095.

316. Marraffini LA, Dedent AC, & Schneewind O (2006) Sortases and the art of anchoring proteins to the envelopes of gram-positive bacteria. *Microbiology and molecular biology reviews : MMBR* 70(1):192-221.

317. Bierne H*, et al.* (2004) Sortase B, a new class of sortase in Listeria monocytogenes. *Journal of bacteriology* 186(7):1972-1982.

318. Conners SB*, et al.* (2005) An expression-driven approach to the prediction of carbohydrate transport and utilization regulons in the hyperthermophilic bacterium Thermotoga maritima. *Journal of bacteriology* 187(21):7267-7282.

319. Dramsi S, Trieu-Cuot P, & Bierne H (2005) Sorting sortases: a nomenclature proposal for the various sortases of Gram-positive bacteria. *Research in microbiology* 156(3):289-297.

320. Ritzefeld M (2014) Sortagging: A Robust and Efficient Chemoenzymatic Ligation Strategy. *Chemistry* 20(28):8516-8529.

321. Mao H (2004) A self-cleavable sortase fusion for one-step purification of free recombinant proteins. *Protein expression and purification* 37(1):253-263.

322. Mao H, Hart SA, Schink A, & Pollok BA (2004) Sortase-mediated protein ligation: a new method for protein engineering. *Journal of the American Chemical Society* 126(9):2670-2671.

323. Parthasarathy R, Subramanian S, & Boder ET (2007) Sortase A as a novel molecular "stapler" for sequence-specific protein conjugation. *Bioconjugate chemistry* 18(2):469-476.

324. Levary DA, Parthasarathy R, Boder ET, & Ackerman ME (2011) Protein-protein fusion catalyzed by sortase A. *PloS one* 6(4):e18342.

APPENDICES

APPENDIX A: Timeline of Ras discoveries

Year	Discovery
1964	An unidentified virus isolated from leukemic rats found to responsible for causing tumors when injected in mice. (Ha-MSV)
1967	Yet another virus isolated from mice found responsible for lymphomas in rats. (Ki-MSV)
1973	Ha-MSV genome found to contain rat gene sequences
1979	Viral Ras protein found to be 21kDa proteins that bind nucleotides
1981	Viral H- and K-Ras genes have normal cellular counterparts.
1982	Overexpression of Ha-MSV homologus sequences in rats induces tumorigenic transformation in mammalian cells.
	Human tumors have active Ras mutations.
1983	N-Ras discovered.
1984	Oncogenic Ras shows loss of GTP hydrolysis.
	Active Ras is membrane bound.
1985	Normal Ras required for cell proliferation.
1987	RasGAP discovered and oncogenic Ras shown to be GAP insensitive.
	Ras transgenic mice generated.
1988	Ras structure solved.
	Ras proteins are carboxyl methylated.
1989	Ras is isoprenylated.
1990	Ftase discovered.
	First RasGEF discovered.
1992	Ras activates MEK1 and MEK2.
1993	Ras is activated by EGFR through Grb2 and SOS.
	Raf is a Ras effector.
1994	PI3K is a Ras effector.
	RalGDS is a Ras effector.
1995	FTIs block Ras induced tumors.
	N-Ras deficient mice found to be viable.
1996	RasGAP structure solved.
	Raf-RBD pulldown developed for measuring Ras activity.
1997	K-Ras found indispensible for development.
	K- and N-Ras prenylate alternatively in presence of FTIs.
1998	NORE1 is a Ras effector.
	RasGEF structure solved (SOS).

APPENDIX A (Continued)

1999	Ras genes shown to be essential for tumor maintenance.
	H- and N-Ras traffic to plasma membrane through endomembranes.
2000	Formation of Ras dimer essential for Raf-1 activation.
2001	H- and N-Ras double knockout mice found to be viable.
	Calmodulin binds and modulates K-Ras signaling but not H- or N-Ras.
2002	Tiam1 is a Ras effector.
2004	PLC required for Ras tumorigenesis.
2005	H- and N-Ras undergo acylation-deacylation.
	H- and K-Ras operate in nanoclusters.
2006	H-Ras undergoes ubiquitination.
	K-Ras localizes to mitochondria after phosphorylation by PKC.
2008	Active K-Ras but not N-Ras stimulates colonic epithelium proliferation.
	K-Ras most frequently mutated oncogene in pancreatic cancer.

APPENDIX B: Plasmids used

K-Ras full length wild type plasmid

```
   atgactgaatataaacttgtggtagttggagctggtggcgtaggcaagagtgccttg
    M  T  E  Y  K  L  V  V  V  G  A  G  G  V  G  K  S  A  L
acgatacagctaattcagaatcattttgtggacgaatatgatccaacaatagaggattcc
 T  I  Q  L  I  Q  N  H  F  V  D  E  Y  D  P  T  I  E  D  S
tacaggaagcaagtagtaattgatggagaaacctgtctcttggatattctcgacacagca
 Y  R  K  Q  V  V  I  D  G  E  T  C  L  L  D  I  L  D  T  A
ggtcaagaggagtacagtgcaatgagggaccagtacatgaggactggggagggctttctt
 G  Q  E  E  Y  S  A  M  R  D  Q  Y  M  R  T  G  E  G  F  L
tgtgtatttgccataaataatactaaatcatttgaagatattcaccattatagagaacaa
 C  V  F  A  I  N  N  T  K  S  F  E  D  I  H  H  Y  R  E  Q
attaaaagagttaaggactctgaagatgtacctatggtcctagtaggaaataaatgtgat
 I  K  R  V  K  D  S  E  D  V  P  M  V  L  V  G  N  K  C  D
ttgccttctagaacagtagacacaaaacaggctcaggacttagcaagaagttatggaatt
 L  P  S  R  T  V  D  T  K  Q  A  Q  D  L  A  R  S  Y  G  I
ccttttattgaaacatcagcaaagacaagacagggtgttgatgatgccttctatacatta
 P  F  I  E  T  S  A  K  T  R  Q  G  V  D  D  A  F  Y  T  L
gttcgagaaattcgaaaacataaagaaaagatgagcaaagatggtaaaaagaagaaaaag
 V  R  E  I  R  K  H  K  E  K  M  S  K  D  G  K  K  K  K  K
aagtcaaagacaaagtgtgtaattatg
 K  S  K  T  K  C  V  I  M
```

K-Ras catalytic domain wild type plasmid

```
  atgactgaatataaacttgtggtagttggagctggtggcgtaggcaagagtgccttg
    M  T  E  Y  K  L  V  V  V  G  A  G  G  V  G  K  S  A  L
acgatacagctaattcagaatcattttgtggacgaatatgatccaacaatagaggattcc
 T  I  Q  L  I  Q  N  H  F  V  D  E  Y  D  P  T  I  E  D  S
tacaggaagcaagtagtaattgatggagaaacctgtctcttggatattctcgacacagca
 Y  R  K  Q  V  V  I  D  G  E  T  C  L  L  D  I  L  D  T  A
ggtcaagaggagtacagtgcaatgagggaccagtacatgaggactggggagggctttctt
 G  Q  E  E  Y  S  A  M  R  D  Q  Y  M  R  T  G  E  G  F  L
tgtgtatttgccataaataatactaaatcatttgaagatattcaccattatagagaacaa
 C  V  F  A  I  N  N  T  K  S  F  E  D  I  H  H  Y  R  E  Q
attaaaagagttaaggactctgaagatgtacctatggtcctagtaggaaataaatgtgat
 I  K  R  V  K  D  S  E  D  V  P  M  V  L  V  G  N  K  C  D
ttgccttctagaacagtagacacaaaacaggctcaggacttagcaagaagttatggaatt
 L  P  S  R  T  V  D  T  K  Q  A  Q  D  L  A  R  S  Y  G  I
ccttttattgaaacatcagcaaagacaagacagggtgttgatgatgccttctatacatta
 P  F  I  E  T  S  A  K  T  R  Q  G  V  D  D  A  F  Y  T  L
gttcgagaaattcgaaaacatctcgag
 V  R  E  I  R  K  H  L  E
```

APPENDIX B (continued)

Calmodulin

```
atggctgatcagctgaccgaagaacagattgctgaattcaaggaagccttctccctattt
 M  A  D  Q  L  T  E  E  Q  I  A  E  F  K  E  A  F  S  L  F
gataaagatggcgatggcaccatcacaacaaaggaacttggaactgtcatgaggtcactg
 D  K  D  G  D  G  T  I  T  T  K  E  L  G  T  V  M  R  S  L
ggtcagaacccaacagaagctgaattgcaggatatgatcaatgaagtggatgctgatggt
 G  Q  N  P  T  E  A  E  L  Q  D  M  I  N  E  V  D  A  D  G
aatggcaccattgacttccccgaatttttgactatgatggctagaaaaatgaaagataca
 N  G  T  I  D  F  P  E  F  L  T  M  M  A  R  K  M  K  D  T
gatagtgaagaagaaatccgtgaggcattccgagtctttgacaaggatggcaatggttat
 D  S  E  E  E  I  R  E  A  F  R  V  F  D  K  D  G  N  G  Y
atcagtgcagcagaactacgtcacgtcatgacaaacttaggagaaaaactaacagatgaa
 I  S  A  A  E  L  R  H  V  M  T  N  L  G  E  K  L  T  D  E
gaagtagatgaaatgatcagagaagcagatattgatggagacggacaagtcaactatgaa
 E  V  D  E  M  I  R  E  A  D  I  D  G  D  G  Q  V  N  Y  E
gaattcgtacagatgatgactgcaaaactcgagcaccaccaccaccaccaccaccactaa
 E  F  V  Q  M  M  T  A  K  L  E
```

The histags were attached to these plasmids at C- or N-termini depending on the experiments. Point mutations have also been carried out in some experiments. This is mentioned in the procedures.

APPENDIX C

Types of atomic interactions in the GTP-bound K-Ras4B dimer. Data here are shown for β-sheet interface dimer.

Hydrogen bonds			
No	**Chain 1**	**Distance (Å)**	**Chain 2**
1	A:ILE 36 [H]	2.20	K:ARG 41 [O]
2	A:SER 39 [H]	1.57	K:SER 39 [O]
3	A:SER 39 [OG]	3.55	K:GLU 37 [O]
4	A:ARG 41 [H]	2.44	K:GLU 37 [O]
6	A:LYS 42 [NZ]	3.36	K:ASP 33 [OD1]
7	A:ARG 41 [O]	2.19	K:ILE 36 [H]
8	A:SER 39 [O]	1.48	K:SER 39 [H]
9	A:GLU 37 [O]	3.49	K:SER 39 [OG]
10	A:ASP 38 [OD1]	1.77	K:ARG 41 [H]
11	A:ASP 33 [OD1]	3.30	K:LYS 42 [NZ]
Salt Bridges			
No	**Chain 1**	**Distance (Å)**	**Chain 2**
1	A:GLU 37 [OE2]	3.05	K:ARG 41 [NE]
2	A:GLU 37 [OE2]	3.09	K:ARG 41 [NH2]

APPENDIX C (continued)

Types of atomic interactions in the GTP-bound K-Ras4B dimer. Data here are shown for the α-helical interface dimer.

Hydrogen bonds			
No	**Chain 1**	**Distance (Å)**	**Chain 2**
1	A:ASP 105 [OD1]	2.37	B:ARG 102 [NH2]
2	A:GLU 107 [OE1]	3.74	B:GLN 99 [NE2]
3	A:LEU 133 [O]	3.89	B:HIS 94 [ND1]
Salt Bridges			
No	**Chain 1**	**Distance (Å)**	**Chain 2**
1	A:ASP 105 [OD1]	3.75	B:ARG 102 [NH1]
2	A:ASP 105 [OD1]	2.37	B:ARG 102 [NH2]
3	A:ASP 105 [OD1]	3.79	B:ARG 102 [NE]
4	A:GLU 107 [OE1]	2.69	B:HIS 95 [NE2]

APPENDIX C (continued)

Types of atomic interactions in the GDP-bound K-Ras4B dimer.

Hydrogen bonds			
No	Chain 1	Distance (Å)	Chain 2
1	A:GLN 25 [NE2]	3.46	K:ASP 38 [OD2]
2	A:SER 39 [H]	1.95	K:SER 39 [O]
3	A:SER 39 [OG]	3.84	K:SER 39 [O]
4	A:ARG 41 [HE]	2.36	K:GLU 37 [O]
5	A:ARG 41 [NH2]	3.23	K:SER 39 [OG]
6	A:ARG 41 [NH2]	2.84	K:GLU 37 [O]
7	A:ASP 38 [OD2]	3.52	K:GLN 25 [NE2]
8	A:SER 39 [O]	1.95	K:SER 39 [H]
9	A:GLU 37 [O]	2.27	K:ARG 41 [HE]
10	A:GLU 37 [O]	2.80	K:ARG 41 [NH2]

APPENDIX D

Declaration of Authenticity and Publishing License Agreements

This thesis is a presentation of my original research work done under the guidance of Dr Vadim Gaponenko. The material described in chapter 3 has been published in MDPI Molecules and is cited as follows: Chavan TS, Abraham S, & Gaponenko V (2013) Application of reductive ^{13}C-methylation of lysines to enhance the sensitivity of conventional NMR methods. *Molecules* 18(6):7103-7119. The material described in chapter 6 has been published in Springer Protocols, Methods in Molecular Biology and is cited as follows: Chavan TS, Meyer JO, Chisholm L, Dobosz-Bartoszek M, & Gaponenko V (2014) A novel method for the production of fully modified K-Ras 4B. *Methods in molecular biology* 1120:19-32.

Myself (first author) and Dr Vadim Gaponenko (corresponding author) are responsible for writing, editing, collecting, and analyzing the results for the majority of the paper content. Contributions of others involved in the work have been duly acknowledged. A license agreement for both these chapters is provided in the following pages that allows the author the full usage of the contents in these papers.

All the computational studies mentioned in chapters 2 and 5 were done in the lab of Dr. Ruth Nussinov at the National Cancer Institute, Frederick MD. All the Microscale thermophoresis and Dynamic Light Scattering experiments mentioned in chapters 2 and 5 were done in the lab of Dr Nadya Tarasova at the National Cancer Institute, Frederick, MD.

We would like to mention that the dissertation research was funded by ACS Grant RGS-09-057-01-GMC and the NIH Grants R01 CA135341 and R21HL118588 to Vadim Gaponenko. A part

of the research done was funded with Federal funds from the Frederick National Laboratory for Cancer Research, NIH to Ruth Nussinov and Nadya Tarasova.

MDPI Open Access Information and Policy

All articles published by MDPI are made immediately available worldwide under an open access license. This means:

- everyone has free and unlimited access to the full-text of *all* articles published in MDPI journals, and
- everyone is free to re-use the published material if proper accreditation/citation of the original publication is given.
- open access publication is supported by the authors' institutes or research funding agencies by payment of a comparatively low Article Processing Charge (APC) for accepted articles.

SPRINGER LICENSE
TERMS AND CONDITIONS

Aug 01, 2014

This is a License Agreement between Tanmay S Chavan ("You") and Springer ("Springer") provided by Copyright Clearance Center ("CCC"). The license consists of your order details, the terms and conditions provided by Springer, and the payment terms and conditions.

All payments must be made in full to CCC. For payment instructions, please see information listed at the bottom of this form.

License Number	3440230861269
License date	Aug 01, 2014
Licensed content publisher	Springer
Licensed content publication	Springer eBook
Licensed content title	A Novel Method for the Production of Fully Modified K-Ras 4B
Licensed content author	Tanmay S. Chavan
Licensed content date	Jan 1, 2014
Type of Use	Thesis/Dissertation
Portion	Full text
Number of copies	1
Author of this Springer article	Yes and you are a contributor of the new work
Order reference number	None
Title of your thesis / dissertation	Intra and Intermolecular Interactions of K-Ras4B: From Structure to Function
Expected completion date	Aug 2014
Estimated size(pages)	180

VITA
TANMAY CHAVAN

tchava2@uic.edu

Education:

- PhD Candidate (Medicinal Chemistry)
  University of Illinois at Chicago
  Fall 2010 – Present

- Bachelor of Pharmacy
  University of Pune, India
  July 2006 – 2010

Experience:

Teaching Assistant for Dr. Constance Jeffery (Biological Sciences Department)
Spring 2011

- Directed discussion sessions, graded exams and corrected homework for a 400-level Biochemistry course (BioS 454).

Research Assistant for Dr. Vadim Gaponenko (Department of Biochemistry and Molecular Genetics)
Fall 2011 – Present

- Research project focused on studying the intra and intermolecular interactions of Ras proteins

Publications:

1. **Chavan TS**, Meyer J, Dobosz-Bartoszek M, Chisholm L, Gaponenko V; A Novel Method for the Production of Fully modified K-Ras4B, *Methods in Molecular Biology, 1120, 2014, 19-34.*

2. **Chavan TS**, Abraham S, Gaponenko V; Application of reductive 13C-methylation of lysine to enhance the sensitivity of conventional NMR methods, *Molecules, 18(6), 2013, 7103-19*.

3. Halasi M, Wang M, **Chavan TS**, Gaponenko V, Hay N, Gartel AL; ROS inhibitor N-acetyl-L-cysteine antagonizes the activity of proteasome inhibitors, *Biochemical Jounral, 454(2), 2013, 201-8.*

4. **Chavan TS**, Jang H, Khavrutskii L, Abraham SJ, Freed BC, Tarasov SG, Gaponenko V, Nussinov R, Tarasov NI; High affinity interaction of K-Ras4B hypervariable region with Ras active site, *manuscript under preparation.*

5. **Chavan TS**, Muratcioglu, Freed BC, Jang H, Khavrutskii L, Dyba M, Tarasova SG, Gursoy A, Keskin O, Tarasova NI, Gaponenko V, Nussinov R; Nucleotide-dependent K-Ras4B dimer and higher order architechture; *manuscript under preparation.*

6. Bore V, Gangurde PR, Bandewar RP, **Chavan TS**, Harle UN; Mediation of melatonin in ethanol withdrawal induced depression and muscle incoordination in rats, *Advances in Pharmacology and Toxicology 10(3) 2009, 45-52.*

Honors and Awards:

- Received **WE van Doren Scholar Award** from the **Department of Medicinal Chemistry, UIC** in March 2014.

- Received **Charles Bell Award** from the **Department of Medicinal Chemistry, UIC** in February 2013.

- Third rank in Poster Presentation organized by the **Indian Pharmaceutical Association**, Pune, India in November 2006.

- **S**econd Prize in Inter collegiate Competition on "Invention Project of Young Pharmaceutical Scientists" organized by **Saraswathi Vidya Bhavan's College of Pharmacy**, Thane, India in January 2007.

Selected Conference Presentations:

- Poster presentation on *Elucidating Mechanisms of CXCR4 Inhibitors using Reductive Methylation* at the **14th Annual GPCR Retreat 2013** at Cleveland, Ohio and at the **Chicago Biomedical Consortium 2013** at University of Chicago.

- Oral and poster presentation on *Modes of binding between the fully post-translationally modifies hypervariable region of K-Ras and Calmodulin* at the **Keystone Symposia in Molecular and Cellular Biology (Frontiers of NMR in Biology)** in January 2013 at Snowbird, Utah.

- Oral presentation on *Modes of binding between the fully post-translationally modified hypervariable region of K-Ras and Calmodulin* at the **7th Midwest Conference on Protein Folding** in April 2012 at the University of Notre Dame, South Bend, Indiana.

- Poster presentation on *Modes of binding between the fully post-translationally modified hypervariable region of K-Ras and Calmodulin* at the **MIKI conference 2012** held at University of Kansas and at the **UIC Cancer Centre Forum 2012**.

- Poster Presentation on *RP HPLC Determination of Artesunate and Amodiaquine Hydrochloride in Pharmaceutical Dosage Form*, at the **20th International Symposium on Pharmaceutical and Biomedical Analysis** in March 2009 at Agra, India.

- Poster presentation on *Simultaneous Spectrophotometric Methods of Determination of Nitazoxanide and Ofloxacin in Combined Dosage Form* at the **60th Indian Pharmaceutical Congress** in December 2008 at New Delhi, India.